A Qualitative and Quantitative Magnetic Resonance Diffusion Study investigating the pathogenesis of Cryptococcal-induced visual loss

by

Anandan A Moodley

Submitted in fulfillment of the academic requirements for the degree of

Doctor of Philosophy in the discipline of Neurology,

Nelson Mandela School of Medicine,

University of KwaZulu-Natal,

Durban

2013

PREFACE

The experimental work described in this thesis was carried out at Greys and Edendale Hospitals, Pietermaritzburg, South Africa.

The data acquisition was conducted from January 2007 to December 2011 and post processing analysis of MRI data was done from January 2011 to June 2012 under the supervision of Professor Ahmed I. Bhigjee and Professor William I.D. Rae.

These studies represent original work by the author and have not otherwise been submitted in any form for any degree or diploma to any university. Where use has been made of the work of others it is duly acknowledged in the text.

Signed: Anandan A Moodley (candidate)

Signed: Professor William I.D.Rae (co-supervisor)

Signed: Professor Ahmed I Bhigjee (supervisor)

Plagiarism:

DECLARATION

I Dr Anandan A. Moodley declare that

(i) The research reported in this dissertation, except where otherwise indicated, is my original work.

(ii) This dissertation has not been submitted for any degree or examination at any other university.

(iii) This dissertation does not contain other persons' data, pictures, graphs or other information, unless specifically acknowledged as being sourced from other persons.

(iv) This dissertation does not contain other persons' writing, unless specifically acknowledged as being sourced from other researchers. Where other written sources have been quoted, then:

a) their words have been re-written but the general information attributed to them has been referenced;

b) where their exact words have been used, their writing has been placed inside quotation marks, and referenced.

(v) Where I have reproduced a publication of which I am an author, co-author or editor, I have indicated in detail which part of the publication was actually written by myself alone and have fully referenced such publications.

(vi) This dissertation does not contain text, graphics or tables copied and pasted from the Internet, unless specifically acknowledged, and the source being detailed in the dissertation and in the References sections.

Signed: _____ Date: 14 FEBRUARY 2013

ABSTRACT

Background: Cryptococcal induced visual loss is common and increasingly becoming a debilitating consequence in survivors of cryptococcal meningitis (CM). Conflicting reports of the optic neuritis and papilloedema models of visual loss have delayed the introduction of effective interventional strategies for prevention and treatment of visual loss in CM. Qualitative and quantitative diffusion-weighted imaging (DWI) and diffusion tensor imaging (DTI) of the optic nerves have proven useful in the examination of the microstructure of the optic nerve especially in optic neuritis. Its application has been extrapolated to other optic nerve disorders such as ischaemic optic neuropathy and glaucoma. The aim of this study is to elucidate the pathogenesis of cryptococcal-induced visual loss using diffusion imaging of the optic nerve as an investigational tool.

Method: Full ethical approval was obtained from the Greys Hospital, Department of Health and University of KwaZulu Natal Ethics Committees. Reliable and reproducible optic nerve diffusion techniques were first developed and optimized on 29 healthy volunteers at Greys Hospital, Neurology and Radiology departments using a Philips 1.5 Tesla Gyroscan. Informed consent was also obtained from 95 patients suffering from CM (≥18 yrs. of age), 14 patients with papilloedema and 14 patients with optic neuritis from other causes, recruited from Greys and Edendale Hospitals. Patients underwent full neuro-ophthalmological assessments, CSF examination, haematological workup, CD4 count, (viral load for some), electrophysiological assessment of vision [Visual evoked potential (VEP) and Humphreys visual fields (HVF)], Magnetic Resonance Imaging (MRI) scan of the brain and orbits and DWI and DTI of the optic nerves.

Results and Discussion: Visual loss is common in CM, occurring in 34.6-48%. Optic neuritis was uncommon as evidenced by a lack of signal change and lack of enhancement within the optic nerve in all patients scanned. The peri-optic CSF space was not dilated and the optic nerve diameter was not increased regardless of CSF pressure and visual status. Swollen optic discs occurred in only 25% of patients whereas raised intracranial pressure (> 20cmCSF) was demonstrated in 69-71% of patients. Therefore visual loss could not be explained by papilloedema alone. The VEP P100 latency was shown to be a useful screening test for subclinical optic nerve disease in CM, but HVF was not.

The optic nerve diffusion imaging used was reliable and reproducible and produced diffusion parameters equivalent to other investigators in the field. Neither optic nerve movement nor the CSF signal was demonstrated to impact significantly on optic nerve diffusion parameters. Optic nerve diffusion imaging did not demonstrate similarities between CM and papilloedema or optic neuritis regardless of CSF pressure or vision.

Conclusion: The rarity of optic neuritis in CM and the disparity between papilloedema and visual loss together with the lack of support from diffusion studies suggest a 3rd mechanism of visual loss viz. the optic nerve compartment syndrome. Good clinical support is provided by a case report for this hypothesis that shows re-opening of the peri-optic CSF space and return of the peri-optic CSF signal on MRI with lowering of intracranial pressure and antifungal treatment.

Dedication

To

My son, Aidan Moodley and

My parents, Mr A and Mrs M Mudly

Acknowledgements

I am deeply grateful to

1. All volunteers and patients who participated in the study. I am also grateful to Greys Hospital, Edendale Hospital and The Department of Health for permission granted to conduct this study.

2. Drs Andrew Michowicz, Lalitha Govender and Angela Loyse for assistance in patient recruitment.

3. Mrs Shereen Matthews and Mrs Garcia Andrews for all radiographic assistance and the many hours of post processing analysis. Their willingness to help even over weekends was much appreciated.

4. Miss Nontokozo Hlatshwayo and Miss Natasha Devparsad for all visual field testing and visual evoked potential recording of patients and volunteers.

5. The neurology registrars and medical officers who assisted with patient clerking and lumbar punctures during patient recruitment.

6. Mrs Cathy Connolly and Dr Noleen Loubser for all statistical services rendered.

7. Prof Ahmed Bhigjee for supervision and guidance during the study.

8. Prof William Rae, for supervision, guidance and insightful comments on all the papers written and thesis write up. I am most grateful for his continuous support and motivation when needed most.

9. The Medical Research Council for part sponsorship of the study.

10. My partner, Ms Keshnee Naidoo for all the emotional support and encouragement. This would not have been possible without her.

TABLE OF CONTENTS

	Page
Title	i
Preface	ii
Plagiarism Statement	iii
Abstract	iv
Dedication	vi
Acknowledgements	vii
Table of Contents	viii
List of Abbreviations	xiii
Congress presentations, Abstracts and Publications	xvi
CHAPTER 1 INTRODUCTION	1
CHAPTER 2 LITERATURE REVIEW	6
2.1. Cryptococcal meningitis	6
2.2 Epidemiology of Cryptococcal meningitis in South Africa and other developing countries	7
2.3 Neuro-imaging of Cryptococcal Meningitis	7
2.4 Visual loss in Cryptococcal Meningitis	10
2.4.1 The Papilloedema Model	11
2.4.2 The Optic Neuritis Model	12
2.5 In vivo examination of Optic Nerve structure and function	13
2.5.1 Anatomy of the optic nerve and the perioptic space	14
2.5.2 Clinical evaluation of Optic nerve functioning	20
2.5.3 Electrophysiological testing of optic nerve function	22

2.5.3.1 Visual Evoked Potential (VEP) 22

2.5.3.2 Humphrey's Visual Field 23

2.6 Imaging of the optic nerve 24

2.6.1 Diffusion 26

2.6.2 Diffusion Weighted Imaging 27

2.6.2.1 Signal strength, Apparent Diffusion Coefficient (ADC) and b value 28

2.6.3 Diffusion Tensor Imaging 30

2.6.4 Anisotropic Parameters 32

2.6.4.1 Axis ratio 33

2.6.4.2 Anisotropic Index 33

2.6.4.3 Fractional Anisotropy 34

2.6.4.4 Relative Anisotropy 34

2.6.4.5 Volume Ratio 34

2.6.4.6 Other Scalar Anisotropic Parameters 34

2.6.5 Optic nerve diffusion imaging 35

2.6.5.1 CSF suppressed ZOOM-EPI technique of Wheeler-Kingshott 36

2.6.5.2 Intravoxel Incoherent Motion (IVIM) technique of Iwasawa 38

2.6.5.3 The Non-CPMG FSE technique of Chabert 39

2.7 Optic neuritis

2.7.1 Pathophysiology of Optic neuritis 42

2.7.2 Optic nerve diffusion imaging in Optic Neuritis 43

2.7.3 Other applications of optic nerve diffusion 45

2.8 Papilloedema

2.8.1 Pathophysiology of Papilloedema 47

2.8.2 Predicted diffusion parameters of Papilloedema 48

2.9 The Optic Nerve Compartment Syndrome

2.9.1 Pathophysiology of the Compartment Syndrome 48

2.9.2 The Compartment Syndrome and Cryptococcal Meningitis 52

CHAPTER 3 AIMS 54

CHAPTER 4 PAPER 1

New insights into the pathogenesis of Cryptococcal-induced visual loss using Diffusion-Weighted Imaging of the optic nerve

4.1 Overview 56

4.2 Full Paper 58

CHAPTER 5 PAPER 2

The impact of optic nerve movement on optic nerve and peri-optic CSF diffusion parameters

5.1 Overview 65

5.2 Full Paper 66

CHAPTER 6 PAPER 3

Neurological, visual, and MRI brain scan findings in 87 South African patients with HIV-associated cryptococcal meningoencephalitis.

6.1 Overview 83

6.2 Full Paper 85

CHAPTER 7 PAPER 4

Early Clinical and Subclinical Visual Evoked Potential and Humphrey's Visual Field Defects in Cryptococcal Meningitis

7.1 Overview 109

7.2 Full Paper 111

CHAPTER 8 PAPER 5

Optic nerve and Peri-optic CSF diffusion in Cryptococcal Meningitis, Optic Neuritis and Papilloedema

8.1 Overview 117

8.2 Full Paper 119

CHAPTER 9 PAPER 6

The Optic Nerve Compartment Syndrome in Cryptococcal-induced Visual Loss

9.1 Overview 144

9.2 Full Paper 145

CHAPTER 10 DISCUSSION 155

CHAPTER 11 CONCLUSION 169

CHAPTER 12 LIMITATIONS AND FUTURE RESEARCH 170

CHAPTER 13 REFERENCES 172

APPENDIX

A. Study Proposal 184

B. Ethics Approval and Recertification 191

List of Abbreviations

ADC - Apparent Diffusion Coefficient

ADEM- Acute disseminated encephalo-myelitis

AI - Anisotropy Index

AION - Anterior ischaemic optic neuropathy

ARV - Anti-retroviral

BCVA - Best corrected Visual Acuity

CF - Counting fingers

CLCSF- Contrast loaded Cerebrospinal Fluid

cmCSF- centimeter Cerebrospinal Fluid

CM - Cryptococcal Meningitis

CN - Cranial nerves

CSF - Cerebrospinal Fluid

CT - Computerized Tomography

DWI - Diffusion Weighted Imaging

DTI - Diffusion Tensor Imaging

EPI - Echo Planar Imaging

FA - Fractional Anisotropy

FLAIR- Fluid attenuated inversion recovery

FOV - Field of view

FSE - Fast spin echo

GE - General Electric

HIV - Human immunodeficiency virus

HM	-	Hand movements
HVF	-	Humphreys Visual Field
IIH	-	Idiopathic Intracranial Hypertension
IVI-EPI	-	Inner Volume Imaging – Echo-planar Imaging
IVIM	-	Intravoxel incoherent motion
LED	-	Light-emitting diode
LogMAR	-	Logarithm of the Minimum angle of Resolution
LP	-	Light perception
LP Shunt	-	Lumbo-peritoneal Shunt
L-PGDS	-	Lipocalin-like prostaglandin D synthase
MD	-	Mean Diffusivity
MRI	-	Magnetic Resonance Imaging
MS	-	Multiple Sclerosis
ms	-	milliseconds
MTR	-	Magnetic Transfer Ratio
NLP	-	No light perception
NMO	-	Neuromyelitis Optica
Non-CPMG	-	Non-Carr-Purcell-Meiboom-Gill
ON	-	Optic nerve
ONTT	-	Optic Neuritis Treatment Trial
RA	-	Relative anisotropy
SAS	-	Subarachnoid space
SD	-	Standard deviation
SENSE	-	Sensitivity encoding
SITA	-	Swedish interactive threshold algorithm
SPIR	-	Selective partial inversion recovery

STIR	-	Short *tau* inversion recovery
TE	-	Echo time
TR	-	Repetition time
TSE	-	Turbo spin echo
μL	-	Microlitre
VA	-	Visual Acuity
VEP	-	Visual Evoked Potential
VP Shunt	-	Ventriculo-peritoneal Shunt
VR	-	Volume Ratio
VRS	-	Virchow Robin Space
WHO	-	World Health Organisation
ZOOM-EPI	-	Zonal oblique multislice-Echo Planar Imaging

Congress presentations

1. **Moodley AA,** Rae WID, Bhigjee AI, Loubser ND, Michowicz A. Cerebrospinal fluid pressure effects on optic nerve diffusion in cryptococcal meningitis. Neurological Association of SA Congress. Durban. March **2011**

2. **Moodley AA,** Rae WID, Bhigjee AI, Loubser ND, Michowicz A. Optic nerve diffusion in cryptococcal meningitis. 10th EUNOS Meeting, Barcelona, Spain. June **2011**

3. Loyse A, **Moodley AA**, Rich P, Rae WID, Bhigjee AI, Loubser ND, Michowicz AJ, Bishop L,Wilson D, Harrison TS. Neurological, visual, and MRI brain scan findings in 87 South African patients with HIV-associated cryptococcal meningoencephalitis (CM). 52nd ICAAC Interscience Conference on. Antimicrobial Agents and Chemotherapy September, **2012**, San Francisco.

4. **Moodley AA,** Naidoo N, Reitz D, Chetty N, Rae WID. The Optic Nerve Compartment syndrome in Cryptococcal Induced Visual loss. Neurological Association of SA Congress. Stellenbosch. March **2013**

Abstracts and Publications

1. **Moodley AA,** Rae W, Bhigjee A, Loubser N, Michowicz A. Cerebrospinal fluid (CSF) pressure effects on optic nerve diffusion in patients with cryptococcal meningitis. *Neuro-ophthalmology* Jun **2011**, Vol. 35, p17. Abstract

2. **Moodley AA**, Rae W, Bhigjee A, Loubser N, Michowicz A. New Insights into the Pathogenesis of Cryptococcal Induced Visual Loss Using Diffusion-Weighted Imaging of the Optic Nerve. *Neuro-Ophthalmology* Oct **2012**, Vol. 36, No. 5: 186–192.

3. **Moodley AA**, Rae W, Bhigjee A, Connolly C, Devparsad N, et al. (**2012**) Early Clinical and Subclinical Visual Evoked Potential and Humphrey's Visual Field Defects in Cryptococcal Meningitis. *PLoS ONE* 7(12): e52895.doi:10.1371/journal.pone.0052895

4. **Moodley AA,** Naidoo N, Reitz D, Chetty N, Rae W. The Optic Nerve Compartment Syndrome in Cryptococcus induced visual loss. *Neuro-Ophthalmology* Jun 2013, Vol. 37, No. 3: 1-5.

CHAPTER 1 INTRODUCTION

In developing countries, cryptococcal meningitis (CM) is a common opportunistic infection in severely immunocompromised human immunodeficiency virus (HIV) - infected patients [1]. In South Africa, the antiretroviral (ARV) rollout program has not yet had an impact on the incidence of CM due to limited access to ARV rollout sites, poor compliance and restrictions imposed on the number of patients eligible for treatment [2-4]. The result is that CM presents as an AIDS - defining illness in 5-10% of patients and in 50% of these patients, with neurological complications (visual loss, cranial nerve palsies such as 6th , 7th and 8th, papilloedema, depressed level of consciousness) [5, 6]. One such devastating complication viz. visual loss from optic nerve disease is reported in 35- 52.6% of patients with CM [3, 7, 8]. Visual loss continues to progress in 17.3% despite antifungal therapy and in 3.7% of patients follows commencement of antifungal therapy [9]. So despite antifungal therapy vision may continue to deteriorate and recovery is unpredictable. Early and effective adjunctive therapy is therefore of paramount importance to prevent or reverse the frequent and sometimes catastrophic loss of vision.

Effective interventional therapy can only be advocated when the pathophysiology of vision loss in CM is well understood. Unfortunately, there are conflicting reports regarding its pathophysiology and standard treatment protocols are disappointingly lacking. The landmark study by Rex et al in 1993 proposed 2 main pathophysiological mechanisms viz. early optic neuritis and late papilloedema [10].

The inflammatory (optic neuritis) model was supported by work done by various authors. Seaton et al in 1997 showed visual improvement with corticosteroid therapy in cryptococcal induced vision loss suggesting the benefit of its anti-inflammatory action [11]. Their patients

were immunocompetent and infected with *Cryptococcus gattii.* The inflammatory response was therefore excessive and response to steroids understandable. Cohen et al in 1993 showed histopathologically the findings of active inflammation and necrosis of the optic nerve without vascular infiltration but florid infiltration of the surrounding meninges by the cryptococcal organism [12]. Such evidence for nerve infiltration was irrefutable. Lipson BK's visual field work and demonstration of centrocaecal scotomata was also overwhelming evidence of primary optic nerve pathology [13]. On the other hand, the raised intracranial pressure (papilloedema) model was suggested by various reports of the beneficial response to lowering of intracranial pressure either by serial lumbar punctures, ventriculoperitoneal shunts, lumbar drains, lumbar peritoneal shunts or optic nerve sheath fenestration on cryptococcal induced vision loss [14-18]. The co-occurrence of raised intracranial pressure in cryptococcal meningitis is well documented. The pathophysiology of which is most likely due to plugging of the arachnoid granulations by whole cryptococci and fragments of the polysaccharide capsule which Loyse et al have pathologically demonstrated [19].

The mechanism by which patients with cryptococcal meningitis develop visual loss continues to be unclear with anecdotal evidence supporting opposing theories of papilloedema and optic neuritis. These theories may not be mutually exclusive and a mechanism that incorporates both theories is conceivable. The possibility of a third mechanism, viz. the compartment syndrome also needs exploration and in this study evidence for such a mechanism will be presented. Pathological studies are scanty and can be misleading due to the loss of the effects of raised pressure on the optic nerves post mortem. An *in vivo* study that investigates the pathogenesis of optic nerve dysfunction in cryptococcal induced visual loss was therefore necessary.

Diffusion weighted imaging (DWI) and Diffusion tensor imaging (DTI) of the optic nerve has been shown to be of benefit in imaging the microstructure of the optic nerve and detecting pathology at a microscopic level. Most recent studies have involved demonstrating the effects of acute and chronic optic neuritis in multiple sclerosis [20-23]. Additional use for this investigational tool has been in disorders such as acute ischaemic optic neuropathy and glaucoma [24, 25]. The apparent diffusion coefficient (ADC) varies with direction if the diffusion is anisotropic. Mean diffusivity (MD) is a scalar index of diffusion that can be reported in the different orthogonal axes [26]. Both qualitative mapping and quantitative data can be obtained on diffusion imaging [27].

Diffusion of protons within optic nerves is anisotropic due to the orientation of fibres. Hence diffusion that occurs parallel to the axons is greater than that which occurs perpendicular [28]. This parallel to perpendicular ratio is dependent on the presence of intact myelin and axons. Where disruption of the myelin and axons occur as with inflammation of the optic nerve, demyelination and secondary axonal degeneration occur resulting in the optic nerve becoming less anisotropic or more isotropic. The Fractional anisotropy (FA) and anisotropic index (AI) are indices of anisotropy that are measured on DTI and DWI and are lowered in diseases that disrupt the integrity of the optic nerve [29].

In optic neuritis, there is perivascular lymphocytic infiltration, multifocal demyelination, and reactive astrocytosis [30]. Various authors have demonstrated increased ADC and increased MD and decreased FA in chronic optic neuritis due to myelin and axonal loss [20-23]. In acute optic neuritis due to the intact axon cylinders diffusion in the parallel direction (axial/longitudinal) is decreased or unaffected but perpendicular (radial) diffusion increases. One may hypothesize a similar diffusion abnormality in acute optic neuritis to that of the

optic nerves in cryptococcal induced visual loss if the predominant disorder is optic nerve infiltration. In the optic neuritis model of CM, the ADC and MD values along the parallel plane will be decreased and FA values will also be reduced due to the presence of inflammatory cells and fungi within the optic nerve that disrupt optic nerve microstructure. The mean ADC and MD will be decreased in the parallel axis. One may also expect a decrease in the parallel (axial) to perpendicular (radial) diffusion ratios such as the AI due to greater isotropic diffusion.

In papilloedema from any cause of elevated intracranial pressure, disc swelling results from axoplasmic flow stasis [7]. There is entrapment of the optic nerve axons at the lamina cribrosa due to elevated intracranial pressure transmitted along the subarachnoid space to the junction of the globe and retrobulbar optic nerve. Axoplasm and metabolic products accumulate at the optic disc resulting in hyperaemia and elevation of the disc [31]. The retrobulbar optic nerve is structurally normal in papilloedema but little is known about its functional status. In any liquid medium, diffusion of molecules is dependent on the thermal energy of the medium. When thermal energy increases, there is increased kinetic energy and increased diffusion of molecules. Therefore one may speculate that the effect of elevated pressure on the optic nerve as occurs in papilloedema, will result in increased thermal motion of the water molecules and therefore increased diffusion in the parallel axis along the intact axons. Higher ADC values will occur more in the parallel than perpendicular direction. The ratio of parallel (axial) to perpendicular (radial) diffusion should be higher since diffusion will be increased in the parallel/longitudinal axis. AI should be higher. One may also speculate that the FA along the optic nerve should be higher.

Hence, DWI and DTI could theoretically be useful measuring instruments to differentiate between the effects of raised pressure and infiltration on optic nerve functioning. The possibility of dual mechanisms will also be entertained and explored.

The aim of this study was to investigate the pathogenesis of cryptococcal induced visual loss by the use of DWI and DTI *in vivo.* The initial goal was to clinically and electrophysiologically describe visual loss in patients with cryptococcal meningitis. Concurrently, the techniques of DWI and DTI of the optic nerve were optimized and made reproducible for reliable testing of subjects and controls. Techniques that have already been employed were modified to accommodate the restricted resources available and imaging of mildly encephalopathic patients [32-34]. The modifiable parameters that were considered were the amount of eye movement, fat suppression, fluid attenuation, 'b' values etc to optimize signal to noise ratio (SNR).

Comparisons were made to normal controls, patients without visual loss, and to patients with pathophysiologically established causes of papilloedema and optic neuritis with the goal of confirming or refuting the optic neuritis and papilloedema models. Early recognition and prevention of blindness in survivors of CM are the primary objective of this study. The results will show that visual loss in CM is common and electrophysiological testing will confirm subclinical disease. The possibility of a compartment syndrome at the optic canal level, secondary to raised intracranial pressure will be discussed and evidence presented to support such a model.

CHAPTER 2 LITERATURE REVIEW

2.1 Cryptococcal meningitis

Meningitis caused by *Cryptococcus neoformans* continues to be a common HIV related opportunistic infection in developing countries, largely due to the unavailability of anti-retroviral therapy and poor compliance when available[1, 2, 6, 35]. A CD4 count of <100 cells/µL predisposes to CM [36, 37]. Patients present with subacute onset of fever, headaches, altered mental state, malaise, nausea, vomiting and photophobia followed by diplopia which is usually from 6th nerve palsies [38]. The headaches are due to raised intracranial pressure and are worse when lying down, are aggravated by Valsalva maneuvers and awaken the patient in the early hours of the morning when severity is worst.[5] Typical signs of meningitis are usually evident at presentation and papilloedema is a common clinical finding on eye examination. The 6th nerve palsies result from raised intracranial pressure (> 20cmCSF) as false localizing signs rather than from ischaemia or inflammation.

The cerebrospinal fluid (CSF) findings of CM include elevated pressure, paucity of inflammatory cells, low CSF glucose and elevated CSF protein. India ink staining is positive in 60% of patients and cryptococcal antigen in >99% of patients [38, 39]. While the gold standard is fungal culture, most clinicians rely on the clinical findings, India ink stain and cryptococcal antigen to make the diagnosis. Induction therapy includes intravenous amphotericin B at 0.7 – 1 mg/kg/d plus oral flucytosine (100mg/kg/d) for the first 2 weeks. Where flucytosine is not available, amphotericin B in combination with fluconazole 800mg/d is found to be adequate as induction therapy as recommended by World Health Organisation (WHO) guidelines in 2011 and [40]. Consolidation therapy follows with oral Fluconazole 400mg – 800mg daily for 8 weeks or until the CSF becomes sterile [38]. Fluconazole is

thereafter continued as maintenance therapy at 200mg daily for life in HIV infected patients or until there is immune reconstitution of CD4 count > 200cells/µL for 12 months.

2.2 Epidemiology of Cryptococcal meningitis in South Africa and other developing countries

While the incidence of CM has declined in developed countries, it continues to be a major opportunistic infection in HIV-infected patients in developing countries [1-3]. CM accounts for 26.5% of cases in a series from Malawi [41], 31% of cases in a series from Central African Republic [42]and 45% from Zimbabwe [43]. CM accounts for 13-44% of all deaths in HIV-infected patients [36, 44, 45]. Moosa et al have shown neurological complications in 50% of their cases with mortality as high as 64% for in-patients [6]. Late presentation for treatment, poor compliance and the lack of anti-fungal and anti-retroviral therapy are reasons for the poorer prognosis in developing countries [46]. A median survival of 19 days is quoted in a Zambian case series recruited in the pre-ARV era with low dose fluconazole monotherapy [47].

2.3 Neuro-imaging of Cryptococcal Meningitis

Data on the neuro-radiological findings of CM are scanty and limited to case reports and small case series. The largest reported series is by Charlier et al and comprised 62 cases of whom 24 had magnetic resonance imaging (MRI) scans and 38 had computerized tomography (CT) scans [48]. Ninety-two percent of MRI scans performed were abnormal compared to 53% of CT scans. MRI was also more sensitive than CT in detecting abnormalities (78 % vs. 24%) in 17 patients who had both modalities. In the multivariate analysis, patients with high serum cryptococcal antigen titres and neurological abnormalities were more likely to have cryptococcal related lesions on imaging. The neuro-radiological

lesions related to CM included: dilated perivascular space, pseudocysts, cryptococcoma, basal meningitis and hydrocephalus. Hydrocephalus is an infrequent finding possibly due to equivalent pressure over the surface of the brain and within the ventricles. When hydrocephalus is present it is usually very mild. The frequency and type of radiological lesions from CM have not been documented in South Africa. Paper 3 in Chapter 5 will endeavor to address this and correlate clinical features with radiological abnormalities detected. Table 1 from Charlier et al [48] and Figure 1 show the published series from 1982-2009 of the frequencies of radiological abnormalities in HIV associated cerebral cryptococcosis. MRI is more sensitive in detecting dilated Virchow Robin Spaces (VRS) and meningitis.

Table 1: Reported series of radiological findings in HIV associated cerebral cryptococcosis from 1982 – 2007. The 2007 series refers to the Charlier et al series [48].

References	Year	Country	HIV-status	No. of patients w CT[a] or MR[b]	Main findings, n (%)						
					Normal	Dilated VR spaces	Pseudocysts	Mass(es)	Hydrocephalus	Radiological meningitis	Other lesions
[28]	1985	USA	HIV+	10 CT	8 (80%)	-	-	-	-	-	2 (20%)
[32]	1986	USA	HIV+	13 CT	9 (69%)	-	-	2 (15%)	1 (8%)	-	1 (8%)
[31]	1990	USA	28 HIV+	35 CT	15 (29%)	-	2 (6%)	2 (6%)	3 (9%)	-	13 (37%)
			7 ID HIV−								
[4]	1990	USA	HIV+	29 CT	9 (31%)	-	-	5 (17%)	-	-	15 (52%)
[4]	1990	USA	HIV+	10 MR*	0	6 (60%)	-	6 (60%)	-	-	-
[5]	1992	USA	HIV+	8 CT	1 (12.5%)	-	-	3 (37.5%)	-	-	3 (37.5%)
[5]	1992	USA	HIV+	5 MR	0	5 (100%)	-	1 (20%)	-	1 (20%)	2 (40%)
[6]	1993	Italy	HIV+	9 MR	0	5 (56%)	1 (11%)	1 (11%)	-	7 (78%)	-
[29]	1994	Germany	HIV+	8 CT	5 (62.5%)	-	-	-	-	-	3 (37.5%)
[29]	1994	Germany	HIV+	6 MR	3 (50%)	-	-	1 (17%)	-	1 (17%)	1 (17%)
[30]	1996	France	HIV+	48 CT	33 (69%)	-	-	4 (8%)	4 (8%)	2 (4%)	5 (10%)
[33]	1997	Spain	HIV+	17 CT	8 (41%)	-	-	2 (12%)	-	-	8 (47%)
[34]	1997	South Africa	HIV+	15 CT	12 (80%)	-	-	-	-	-	3 (20%)
[26]	1997	USA	HIV+	10 CT	4 (40%)	-	4 (40%)	-	2 (20%)	-	-
Our study	2007	France	HIV+	55 CT	26 (47%)	3 (5%)	2 (4%)	5 (9%)	2 (4%)	2 (4%)	20 (36%)
Our study	2007	France	HIV+	24 MR	2 (8%)	11 (46%)	2 (8%)	5 (21%)	-	2 (8%)	11 (46%)

[a]CT: computed tomography.
[b]MR: magnetic resonance image.
doi:10.1371/journal.pone.0001950.t003

Figure 1: Pie graph of meta-analysis in Table 1 demonstrating relative frequency of CT and MRI abnormalities in CM

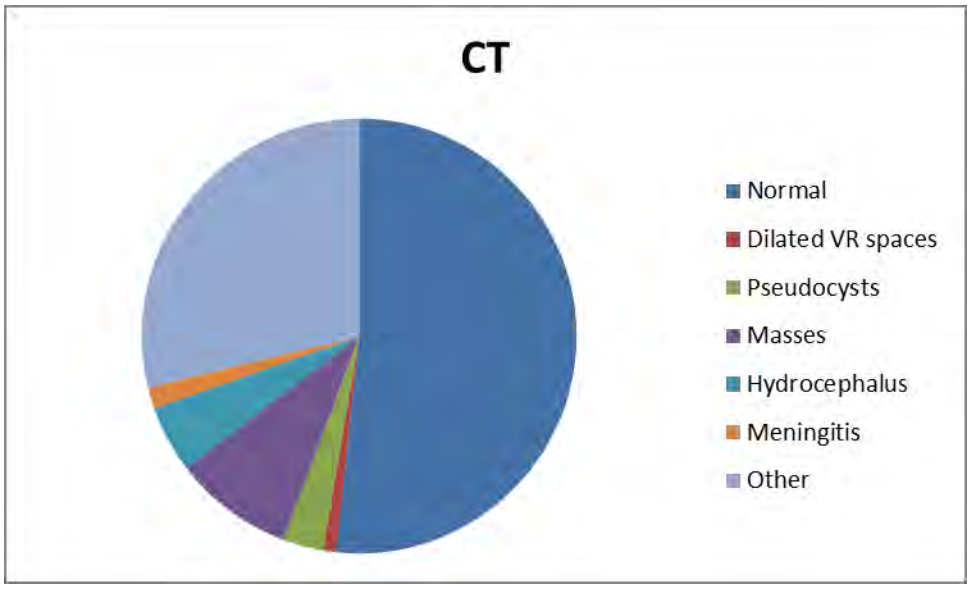

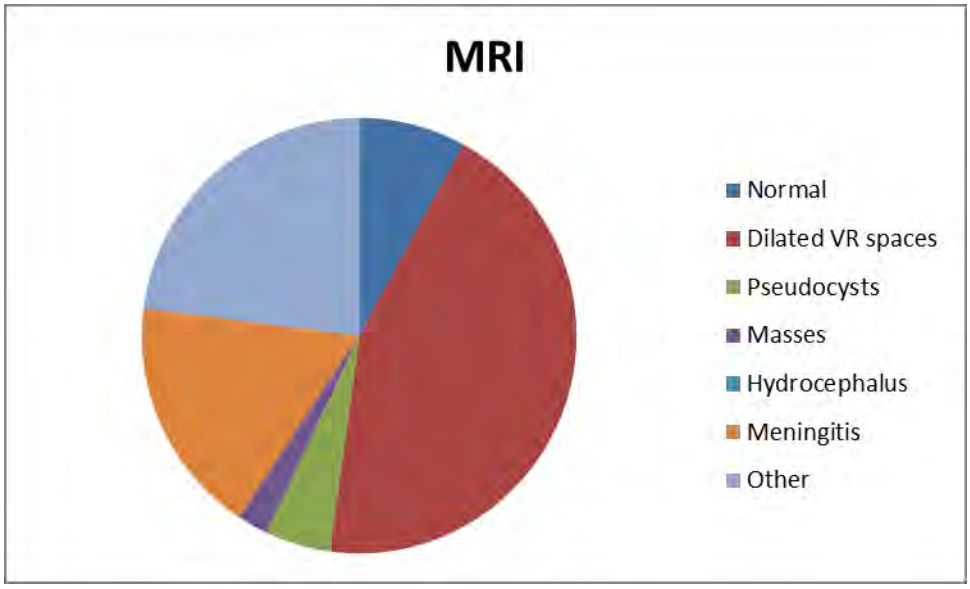

2.4 Visual loss in Cryptococcal meningitis

Complications of CM include visual loss, deafness, cranial nerve palsies, dissemination to other organs and death from raised intracranial pressure [38]. Visual loss is common and reported to occur in 30-45% of cases. Rex et al first classified visual loss as occurring either early or late in the illness [10]. Early visual loss was reported as due to optic nerve infiltration/inflammation and occurred within 6 days of the onset of meningitis symptoms, whereas late visual loss occurred a few weeks into the infection and was due to optic disc oedema from raised intracranial pressure (papilloedema). The rapid visual loss group had elevated CSF pressure in over 90 % of patients, thickened optic nerves on CT scan in 22% and symmetrical visual loss in 93%. The visual loss occurred before or soon after initiation of antifungal therapy and was severe and permanent. The slow visual loss group did not differ much, having elevated CSF pressure in 83%, thickened optic nerves in 22% and symmetrical visual loss in 93%. As to whether there was dilatation of the peri-optic CSF space or thickening of the optic nerve itself was not defined on CT scan for both groups. Therefore, apart from the tempo of presentation, a clear distinction between these groups does seem artificial. We too have previously shown that raised intracranial pressure is common in CM induced visual loss (69%) but that papilloedema was present in only 25% [49].

Various reports have supported or refuted these claims with evidence for and against the optic neuritis and papilloedema model [11-18]. Recovery however has always been documented as poor. Medical treatment alone is insufficient as demonstrated by Graybill et al were steroids alone were ineffective but serial LP's and reduction of CSF pressure were more successful [5]. In Torres's meta-analysis of rapid and slow visual loss cases the outcome was generally poor when only the underlying CM was treated and not the visual loss [50].

Attention to the pathogenesis of visual loss in CM is paramount in survivors due to the profound disability that follows.

By comparing the diffusion imaging findings in CM to those in patients with established and unrelated causes of papilloedema and optic neuritis, we will attempt to establish the pathogenesis of cryptcoccal induced visual loss.

2.4.1 The Papilloedema Model

Raised intracranial pressure in CM is well documented. CSF outflow obstruction by plugging of the arachnoid granulations with the organism or polysaccharide capsule is postulated to result in the elevated intracranial pressure [51]. Good support for obstruction at the arachnoid villi has come from Loyse et al who have shown histopathologically that fungal loading does occur at the arachnoid villi and is positively correlated with elevated intracranial pressure [19]. Bicanic et al have shown that higher fungal burden and higher cryptococcal antigen titre is associated with higher intracranial pressure and have therefore recommended early and aggressive fungicidal treatment with lowering of intracranial pressure by either serial lumbar puncture or lumbar drainage to lower morbidity and mortality in patients with CM [52]. Garrity et al in 1993 performed optic nerve sheath fenestrations in 2 patients with visual loss and papilloedema [53]. Both patients had improved vision following the procedure in conjunction with lowering of intracranial pressure. Cryptococcal organisms were present in the dural sheaths of both patients. At autopsy of one of the patients, patency of the sheath fenestration was still present.

The evidence for visual loss resulting from raised intracranial pressure and papilloedema and the benefit from CSF pressure lowering either by serial lumbar punctures [5, 14, 16, 51, 54],

acetazolamide [54, 55], lumbo-peritoneal (LP) shunt, lumbar drain [15, 17, 56], ventriculo-peritoneal (VP) shunt [51, 57] and optic nerve sheath fenestration [18, 53] are many, but mostly anecdotal. Medical approaches to control of raised intracranial pressure in CM have not been shown to be effective. The risks of lumbar drains, VP and LP shunts are over drainage, shunt infection, distal catheter migration and need for shunt revision [58]. VP shunts are associated with lower risk of shunt obstruction and revision than LP shunts.

CT or MRI scans show normal ventricular size in most cases of CM despite elevated CSF pressure possibly due to equivalent pressure between the intraventricular fluid and the CSF surrounding the brain [51]. No doubt raised intracranial pressure and fungal loading are common and well described in CM sufferers, but inflammation is minimal if any in HIV infection. The significance of raised intracranial pressure cannot be underestimated in visual loss and perhaps optic disc swelling and optic nerve infiltration/inflammation are secondary or co-occurrences. Reports of raised intracranial pressure related visual loss are many in the literature and the benefit of early lowering of intracranial pressure in reversing blindness in cryptococcal induced visual loss is well documented [14, 15, 57, 59].

The effect of papilloedema on DWI and DTI parameters of the optic nerve is unknown. We will endeavor to establish such parameters and compare them to those of normal healthy volunteers.

2.4.2 The Optic Neuritis Model

Evidence for optic nerve infiltration by *Cryptococcus neoformans* has come from case reports only. Lipson et al first described 2 cases of AIDS associated cryptococcal arachnoiditis resulting in bilateral visual loss secondary to an optic neuropathy [13]. Ofner ‘s claim of optic nerve infiltration in a patient with visual loss and elevated intracranial pressure was not

strong [60]. Histology obtained from the optic nerve sheath showed fungal infiltration with inflammation, but optic nerve infiltration was only presumed. Histological evidence of cryptococcal infiltration of the intracanalicular segment of the optic nerve with associated necrosis was provided by Cohen et al in 1993 [12] and further supported by a histopathological case reported by Corti et al in 2010 [61]. Corti's case also showed a perineuritis, but in addition showed optic nerve infiltration by the fungus. By inference, Hoepelman [62] and Seaton [11] have suggested that corticosteroids could only play a beneficial role in cryptococcal induced visual loss by reducing the optic nerve inflammation so induced by the organism. Further support for an optic neuritis model has come from De Schacht's report of a 26 yr. old CM patient who developed an immune reconstitution illness with bilateral blindness after starting antiretroviral therapy [63]. Supposedly, the exaggerated optic nerve inflammation secondary to fungal infiltration caused the bilateral blindness. Unfortunately, such case reports in the literature are scanty and the evidence for optic nerve infiltration is largely speculative [8].

2.5 In vivo examination of Optic Nerve structure and function

In establishing the pathogenesis of CM induced visual loss one is faced with many challenges. Firstly, obtaining autopsies in black patients in South Africa is extremely difficult as it violates the African culture to perform incisions on the human body post mortem [64]. It is believed that the spirit continues to reside in the human body post mortem and provides a protective role to future generations. It is thus avoided unless required for legal purposes. Secondly, the effects of raised intracranial pressure on the optic nerve are lost post mortem and difficult to interpret. In vivo investigations are therefore preferred to investigate the effect of raised pressure on the optic nerve.

In vivo examination of optic nerve structure and function includes visual acuity testing, visual field testing (Humphreys Visual Field (HVF)), Visual evoked potentials (VEP), MRI, DWI and DTI of the optic nerve.

2.5.1 Anatomy of the optic nerve and the peri-optic space

The optic nerve is formed from the ganglion cell axons of the retina and comprises 4 segments (Figure 2). The 1st segment, the optic disc is 1mm long and unmyelinated. The 2nd segment begins at the sieve-like lamina cribrosa where myelination of the nerve begins and extends to the optic canal. This segment is 25 mm long and somewhat S shaped to allow for unrestrained movement of the globe within the orbit. The 3rd segment lies within the optic canal with the ophthalmic artery and is 4 mm long. The 4th segment, which is 16mm long lies intracranially and merges with the opposite nerve at the optic chiasm where crossover of the nasal fibres occur. Both temporal and crossed nasal fibres continue within the optic tract. Myelination of the optic nerve, unlike the other cranial nerves is by oligodendrocytes and is therefore considered to be a white matter tract by some rather than a cranial nerve. The nerve consists of approximately 1.2 million axons of which 10% are responsible for the light reflex. The remainder of the nerve fibres is responsible for colour vision and motion perception with some centripetal fibres of unknown function.

Surrounding the optic nerve from the globe to the optic canal is the optic nerve sheath which consists of the dura, arachnoid and pia. CSF occupies the subarachnoid space and is continuous with the intracranial subarachnoid space. CSF that is produced from the choroid plexus and ependyma of the ventricles flows into the subarachnoid space of the basal cisterns and eventually into the peri-optic subarachnoid space. So presumably, the intracranial

pressure is transmitted via this route to the peri-optic space and ultimately to the lamina cribrosa. In raised intracranial pressure, the raised pressure applied at the lamina cribrosa is responsible for axoplasmic stasis and axonal swelling at the optic nerve head which is visualized as optic disc oedema (papilloedema) [7]. CSF flow within the peri-optic space conceivably is bidirectional towards the globe where it reaches a dead end and then back towards the brain [65, 66]. This process is slower than the flow intracranially due largely to the smaller size of the optic nerve sheath and the presence of septae, trabeculae and pillars within the peri-optic subarachnoid space SAS [67].

Figure 2: Optic nerve anatomy and CSF pathways. Adapted from Killer H.E [66].

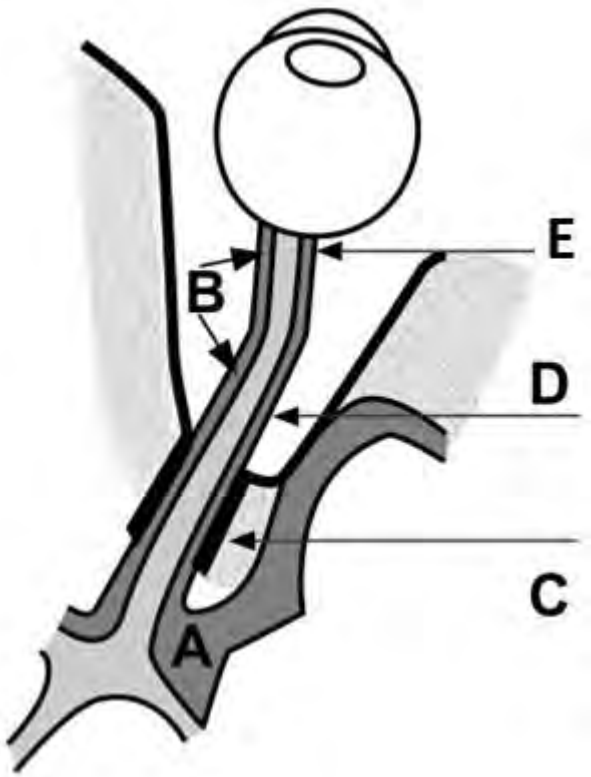

A – Intracranial SAS

B – Peri-optic SAS

C – Optic Canal Segment of the Optic nerve

D – Orbital Segment of the Optic nerve

E – Optic Nerve Sheath

Killer et al have demonstrated by electron microscopy the presence of a meshwork of trabeculae of 5 to 7 µm diameter in the bulbar segment of the nerve closest to the globe. The trabeculae are sometimes linked by a veil-like pattern. In the mid-orbital portion of the nerve, the peri-optic subarachnoid space contains "broad septae and stout pillars" of 10 -30 µm. The pillars have larger bases and attachments to the dura. The subarachnoid space of the canalicular segment is extremely narrow and has large pillars of 0.5mm diameter and smaller ones of 25 µm (Figures 3-6) and few trabeculae but no septae. These trabeculae, septae and pillars are formed by leptomeningeal cells, fibroblasts, collagenous fibrils and blood vessels. Killer describes the peri-optic SAS as therefore 'not a homogeneous space filled with CSF, but a multichambered and subdivided tubular system with a blind end (cul de sac) behind the ocular globe' [67]. Observation of unilateral and asymmetrical papilloedema as occurs in idiopathic intracranial hypertension further support the theory of differential pressure between the peri-optic SAS and intracranial SAS. CSF drainage into the surrounding optic nerve sheath lymphatics is minimal. For technical reasons, the pressure in the peri-optic SAS has not been measured. Cadaveric studies were based on hypotheses and not true measurement[68]. The two CSF systems are not freely connected, due to the presence of this meshwork of trabeculae, septae and pillars within the peri-optic SAS. Presumably, laminar flow of CSF within this space occurs which is necessary to allow for CSF exchange between the intracranial SAS and peri-optic SAS, albeit a slow and compartmentalized process [66]. Seemingly, flow of CSF from the site of production to the peri-optic space is by a combination of bulk flow of newly produced CSF, postural effects, ventricular pulsations and pulse pressure of the choroid plexus.

The role played by the peri-optic CSF space trabeculae, septae and pillars in CM is unknown. Histology from optic nerve sheath fenestration has shown infiltration of the optic nerve

sheath by the cryptococcal organism [18]. We postulate that there is plugging of the optic nerve SAS by the organism which is facilitated by the trabeculae, septae and pillars. The brunt of the blockage must occur at the optic canal level where the SAS has the smallest opening. The maximum intracranial pressure is therefore most likely applied at the optic canal level. Compression at this site is consistent with the compartment syndrome described by Killer et al in optic neuritis and idiopathic intracranial hypertension (IIH) [66, 69].

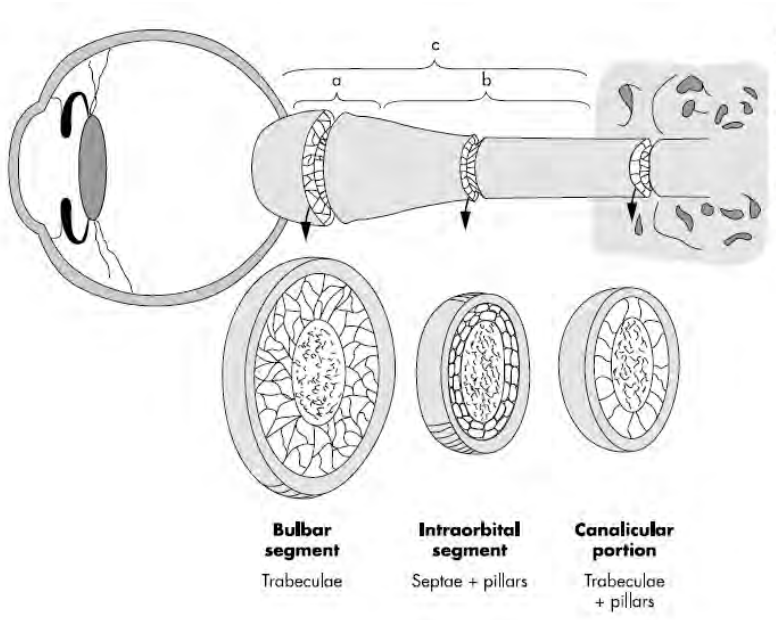

a – bulbar segment, b – mid orbital segment, c – intra-orbital optic nerve

Figure 3: Schematic drawing of the optic nerve demonstrating the bulbar, mid-orbital and canalicular segments of the optic nerve. (From Killer HE et al *Architecture of arachnoid trabeculae, pillars, and septae in the subarachnoid space of the human optic nerve: anatomy and clinical considerations* [67]

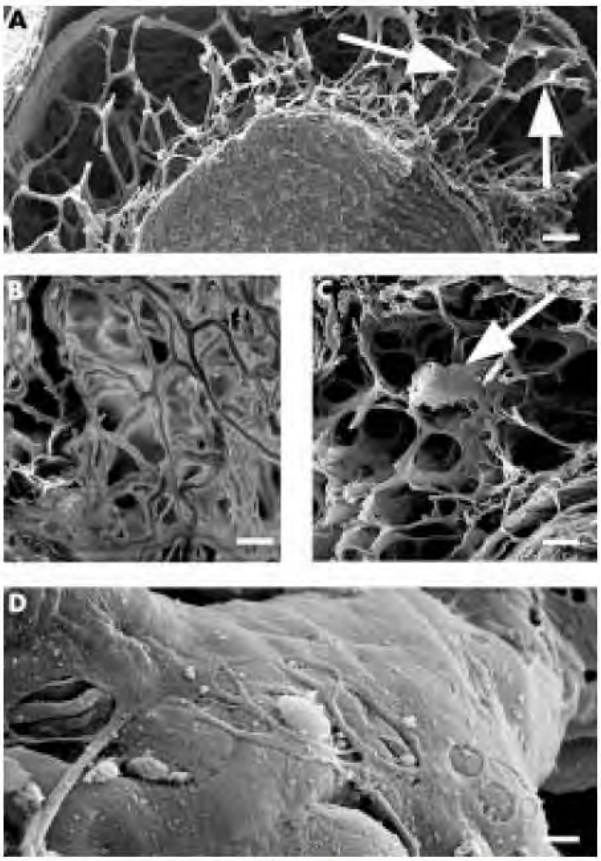

Electron Microscopy appearance of the subarachnoid space in the bulbar segment.

(A) Overview of the subarachnoid space showing the complex network of trabeculae. The arrows point to veil-like cytoplasmic extensions between adjacent trabeculae (bar = 150 µm).

(B, C) Delicate subarachnoid space network formed by branching trabeculae (bar = 50 µm). The arrow points to a trabeculum with a blood vessel. Note again the veil-like cytoplasmic extensions connecting adjacent trabeculae (bar = 2 µm).

(D) Surface of trabeculae covered by flattened cells with distinct intercellular clefts and fenestrations (bar = 0.2 µm).

Figure 4: Electron microscopy appearance of the subarachnoid space of the bulbar segment showing trabeculae and a veil-like cytoplasmic extension between trabeculae. Arrows point to the veil-like cytoplasmic extensions. From Killer HE et al [67]

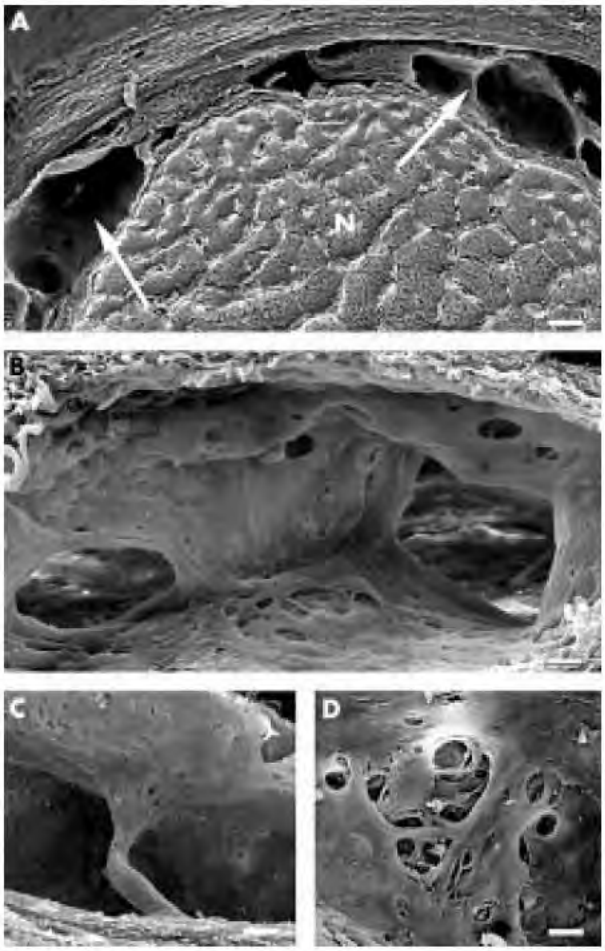

Electron Microscopy morphology of the subarachnoid space in the mid-orbital segment.

(A) Overview of the subarachnoid spacesubdivided by well defined septa (arrows), N = optic nerve (bar = 150 µm).

(B) Arachnoid septum within the subarachnoid space; note the septal perforations connecting adjacent subarachnoid space chambers (bar = 25 µm).

(C) Pillar bridging the subarachnoid space and extending into the dura layer of the arachnoid (bar = 30 µm).

(D) Detail of a septum with typical intercellular clefts (bar = 0.5 µm).

Figure 5: (A,B,C,D) Electron microscopy appearance of the subarachnoid space of the mid-orbital segment showing septae and trabeculae. N = optic nerve. Arrows point to the septae. *From Killer HE et al* [67]

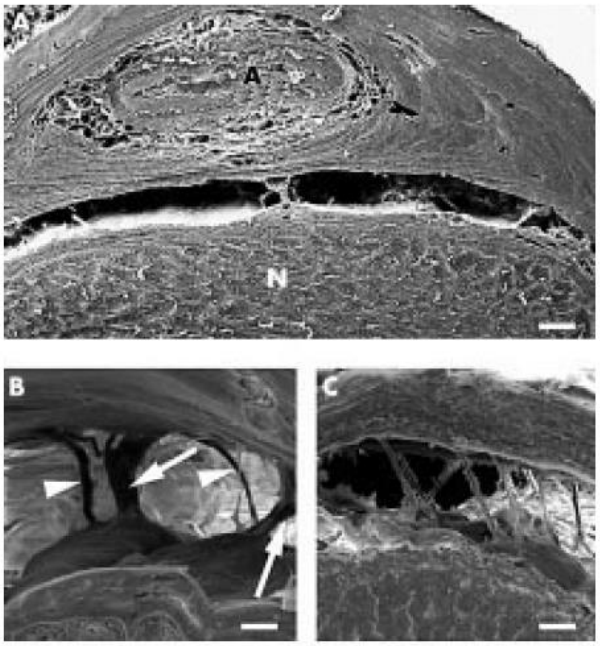

Morphology of the subarachnoid space in the intracanalicular segment.

(A) Overview of the subarachnoid space;

A = ophthalmic artery, N = optic nerve (bar = 15 µm) (the optic nerve is turned 180°).

(B) Pillars (arrows) and trabeculae (arrowheads) transversing the subarachnoid space (bar = 30 µm).

(C) Trabeculae within the subarachnoid space found at the orbital opening of the optic canal (bar 30 µm).

Figure 6: (A,B,C) Electron microscopy appearance of the subarachnoid space of the canalicular segment showing pillars and trabeculae. N = optic nerve. Arrows point to the pillars. *From Killer HE et al* [67]

2.5.2 Clinical evaluation of Optic nerve functioning [70]

There are 5 tests of optic nerve function. The 1st is visual acuity which is tested by using Snellen Charts that range from 6/60 (20/200) to 6/5 (20/15) vision. If vision is worse than 6/60 then either the patient is brought closer to the chart and graded accordingly or vision is evaluated at 1m for counting fingers (CF), hand movements (HM), light perception (LP) or no light perception (NLP). Best corrected visual acuity is obtained with refractive lenses or a pinhole and documented as such. Best corrected visual acuity using Snellen charts are subjective and are especially difficult in encephalopathic patients. LogMar charts are equally difficult to perform on such patients.

The 2nd test is the light reflex which is tested with a bright and focused light source. The direct light reflex is a 4 neuron pathway starting from the optic nerve to the pretectal nucleus,

2nd neuron to the Edinger-Westphal nucleus, 3rd neuron along the 3rd cranial nerve to the ciliary ganglion and finally the 4th neuron from the ciliary ganglion to the iris as the short ciliary nerve. Crossover at the optic chiasm and bilateral innervation of the Edinger-Westphal nuclei from each pretectal nucleus allows for the consensual reflex. The direct light reflex tests the afferent and efferent pathways of the same eye whereas the consensual light reflex tests the afferent pathway of the ipsilateral eye and the efferent pathway of the contralateral eye. Optic nerve disease results in an absolute or relative afferent pupillary defect whereas 3rd nerve palsy causes an efferent pupillary defect.

The 3rd test of optic nerve function is the testing of colour vision which is done using Ishihara pseudo-isochromatic plates. Colour vision is scored according to the number the patient reports correctly. Colour desaturation is tested by asking the patient to comment on the colour of the red top of the Mydriacyl bottle and comparing between eyes for patients with unilateral disease. Colour desaturation is an early and common abnormality in optic neuritis.

The 4th test is visual field testing which at the bedside is done by confrontation. Each eye is tested separately. The central field is tested by asking the patient to comment on the examiners face while the patient fixates on his nose. This detects central scotomas of optic nerve and macular dysfunction. The patient is then asked to count the examiners fingers in the different quadrants. And finally hand comparison is done between the hemispheres to detect subtle field loss.

The 5th test of optic nerve testing is funduscopy. The optic disc is viewed by direct or indirect ophthalmoscopy. Its colour, shape, size, optic cup size, neuro-retinal rim, disc margins, and spontaneous venous pulsations are described.

Contrast sensitivity is becoming the gold standard for assessing optic neuritis in multiple sclerosis but is less often used for other optic neuropathies [71].

For complete assessment of optic nerve structure and function, such tests are required.

2.5.3 Electrophysiological testing of optic nerve function

2.5.3.1 Visual Evoked Potential (VEP) [72]

VEP testing has the advantage of objectivity. Pattern reversal VEP uses a checker board pattern and is used in co-operative subjects who can fixate on a target. The subject is seated 1 metre away from the monitor that flashes the checker board pattern. In pattern reversal, the black squares become white and vice versa after every second. Each eye is tested separately. Active and reference electrodes placed over the occiput detect the evoked potential difference obtained from the occipital lobe. One hundred averages of the evoked response is obtained which produces a triphasic wave of initial negativity after approximately 80 milliseconds (ms) (N80), secondly a following positive wave after 100 ms (P100) and thirdly a negative wave after 145 ms (N145). Flash VEP requires less co-operation and can be done with goggles especially in patients with poor visual acuity. Comparisons are made with reference laboratory ranges. The most reproducible waveform is the P100 wave which is preceded by the N80 wave and followed by the N145 wave. The amplitude and latency of the P100 waveform provides information about the number of functioning axons and the amount of demyelination of the optic nerve respectively. Optic nerve inflammation as occurs in optic neuritis is well documented on VEP. The latency prolongation is an early abnormality of optic nerve inflammation and demyelination. Amplitude reduction of the P100 waveform is secondary to axonal loss and is usually an event that follows an acute or subacute insult. Reduced amplitude occurs less frequently from conduction block. The P100 latency is

measured from the stimulus onset of pattern reversal to the onset of the P100 waveform. Amplitude is measured from the negative peak of the N80 waveform to the positive peak of the P100 waveform. Our laboratory references for these parameters are 104 (±10) ms for VEP P100 latency and 15 (±5) μV for the N80 – P100 amplitude. The effect of raised intracranial pressure on VEP has been studied in Idiopathic Intracranial Hypertension, but not in neuro-infectious disorders.

The advantage of Flash light-emitting diode (LED) goggles is that minimal co-operation is necessary and can be performed on patients with poor visual acuity. However, there is suboptimal reproducibility and marked variability. The P100 waveform latency obtained with Flash LED goggles ranges from 76.1 – 162.5 ms in our laboratory and the normal N80-P100 amplitude ranges from 9.3 – 22.5μV. Quantitative analysis of Flash LED VEP is therefore unreliable. The presence of a waveform is indicative of optic nerve functioning, but the degree of functioning cannot be reliably quantified.

2.5.3.2 Humphrey Visual Field

The automated Humphrey visual field (HVF) provides reliable and early field defects in asymptomatic patients and is therefore a useful tool in detecting subtle visual disturbances in asymptomatic subjects. Automated HVF are usually performed using the 30–2 Swedish interactive threshold algorithm (SITA) standard protocol. HVF 30-2 are more readily available and produce a larger field than the 24-2. Pattern deviation fields that fulfill acceptable reliability indices are included for analysis. Acceptable reliability indices of HVF are fixation losses of 33%, false negatives of 33% and false positives of 33%. Good co-operation is required for HVF testing so encephalopathic patients are poor candidates. The HVF has not been used to evaluate visual loss in CM, but has been studied in HIV infection. Non-specific superior and inferior field defects have been reported by Sample et al, at all

stages of HIV infection unrelated to infectious retinopathy and they have postulated optic nerve pathology [73]. From 151 eyes of 81 HIV positive patients, 88 had normal visual fields, 11 had field loss by mean defect only, 32 had early field loss and 20 had moderate field loss.

Visual field defects are useful in localizing visual pathway pathology. Optic nerve pathology is associated with central scotoma, centrocecal scotoma, arcuate defects, altitudinal defects, hemi-anopic defects and junctional scotoma [74]. In the optic neuritis treatment trial (ONTT) visual field defects in the affected eye at presentation included diffuse visual field loss (48%), altitudinal defects (15%), central or centrocecal scotoma (8.3%), arcuate or double arcuate (4.5%), hemianopic defects (4.2%), and others [75, 76]. Papilloedema is associated with large blind spots, constricted peripheral field and early inferonasal deficits [74]. Other less common field defects described include inferior altitudinal loss, superonasal and superotemporal loss, arcuate defects, and scotomas (central, centrocecal, and paracentral). Goldmann kinetic fields are more sensitive in detecting peripheral visual field loss but are not universally available.

2.6 Imaging of the optic nerve

MRI of the optic nerve is technically challenging due to its small size, the effect of surrounding CSF and orbital fat and the presence of nearby bone structures (Figure 7) [33, 77, 78]. In DWI, the image is sensitized to the microscopic motion of water molecules within the nerve, so the macroscopic motion of the nerve within the orbit poses extra problems [22, 79].

Most advances in optic nerve imaging have come from work done in optic neuritis [80]. Conventional imaging of the optic nerve on MRI includes T1 axial, coronal and sagittal, T2

axial and coronal and T2 fluid attenuated inversion recovery (FLAIR) followed by post contrast images with gadolinium on T1 images. Orbital fat suppression has been an important addition in the last 10 years for better identification of the optic nerve on T1 and T2 imaging. Initially short *tau* inversion recovery (STIR) was used for fat suppression, but was followed by selective partial inversion recovery (SPIR) which has become the more favoured technique. SPIR when combined with FLAIR provides the added advantage of CSF suppression. CSF suppression also allows for better identification of the nerve on axial and coronal imaging but most importantly prevents volume averaging of the surrounding CSF during optic nerve diffusion analysis. Currently, modification of the standard spin echo imaging of the optic nerve within the orbit includes T1 3D fat saturated (SPIR) axial, T2 3D turbo spin echo (TSE) coronal, T2 3D high resolution axial TSE, T1 3D SPIR axial post contrast. Various combinations of fat saturation and fluid attenuation are employed to minimize artifact.

Further developments in optic nerve imaging have included Magnetic Transfer Ratio (MTR) of the entire nerve giving an indication of the degree of demyelination and re-myelination over the entire lesion in optic neuritis. With DTI and DT tractography, it is now possible to trace the entire visual pathway from the optic nerve to the striate cortex [81]. Most significantly, improved DWI and DTI quantitative measurements have provided considerable information on the axonal integrity of the optic nerve.

Figure 7. MR related features of the optic nerve (From *Barker GJ et al, DWI of the spinal cord and optic nerve* [78])

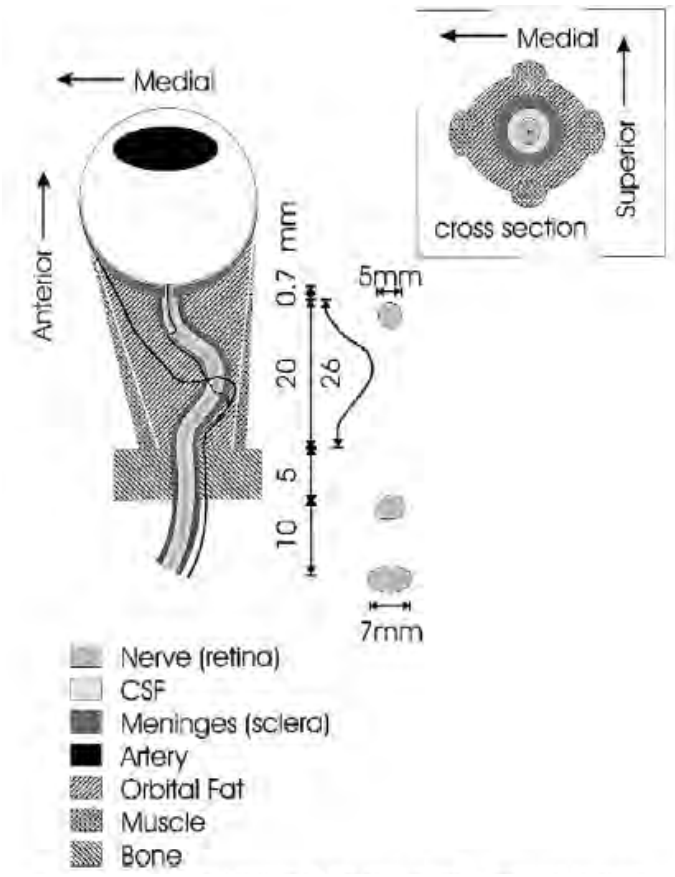

2.6.1 Diffusion

Molecular diffusion, or Brownian diffusion was first described mathematically by Einstein in 1905 [82]. Diffusion of water molecules in a glass of water is unrestricted and occurs randomly and in a defined period of time, the net diffusion is 0 due to its Gaussian distribution. Such diffusion is described as isotropic and is equal in all directions. The volume of diffusion is represented by a sphere. Diffusion of water molecules in neuronal tissue however is restricted due to the tightly packed axons and glial cells that are organized in bundles. Greater diffusion of water molecules occur in the direction of the axons as opposed

to perpendicular to it. Such diffusion is referred to as anisotropic and is represented by an ellipsoid [83].

2.6.2 Diffusion Weighted Imaging

The Brownian motion of water molecules has been imaged on MRI scans since the 1980's and is referred to as DWI. The technique can characterize the water diffusion properties of each pixel of an image. Both qualitative and quantitative data are obtainable from DWI.

The technique is based on detecting signal loss after placing pulsed dephasing and rephasing gradients within the magnetic field during image acquisition.

When there is no gradient, protons (hydrogen atoms within the water molecule) precess at a similar rate and are in phase within the main magnet (Figure 8). When the 1st gradient is applied, depending on their location, protons precess at different speeds and dephasing occurs. After application of the 2nd gradient of opposite magnitude, rephasing of the protons occurs and the original signal is recovered if the same number of protons return the signal. If however there has been movement of the protons during application of these 2 pulse gradients, the signal recovered will be less and signal loss will occur. The greater the signal loss, the greater the amount of water diffusion had occurred during the gradient application [27].

Figure 8. Gradient diagram and signal phases under application of a gradient. From Mori S et al *Diffusion magnetic resonance imaging: its principles and applications* [27].

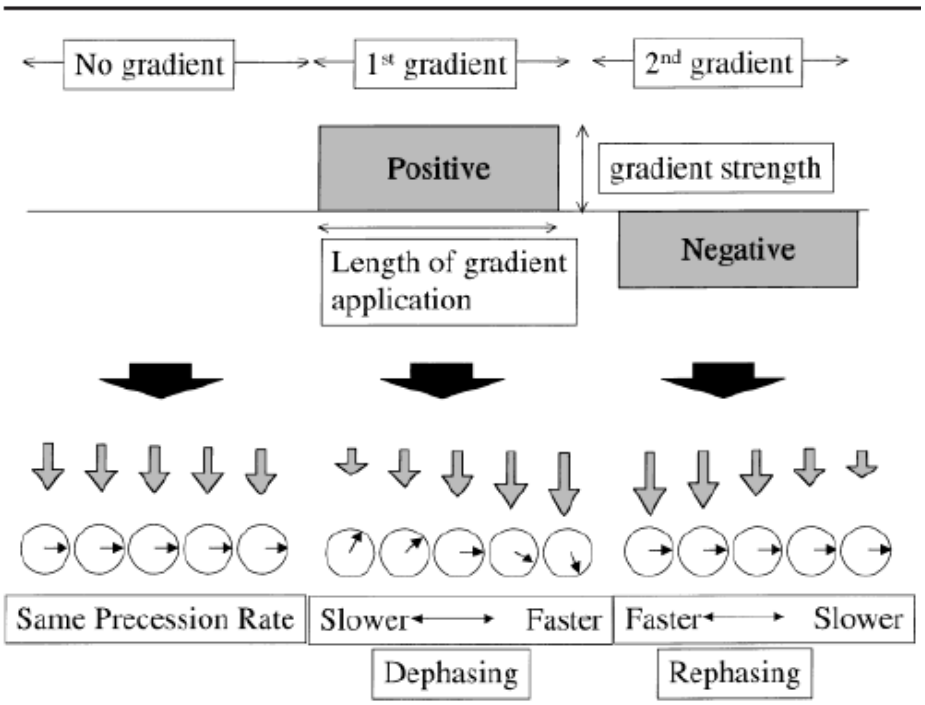

The length of grey arrows indicate schematically the relative strength of the magnetic field

2.6.2.1 Signal strength, ADC and b value

The amount of **signal loss** is described by the Stejskal Tanner equation;

$$\frac{S}{S_0} = e^{-\gamma^2 G^2 \delta^2 \left(\Delta - \frac{\delta}{3}\right) D} = e^{-bD} \qquad [1]$$

Where: S – Signal intensity with gradient application, S_0 – Signal intensity without gradient application, γ – Gyromagnetic ratio (nuclear constant), G – Strength of gradient pulse, δ - Duration of gradient pulse, Δ - Time between the 2 gradient impulses, D – Diffusion coefficient or constant

From the Stejskal Tanner equation **1** it is evident that the higher the diffusion constant *D*, the greater the strength of the gradient (*G*) and the longer it is applied (δ) and the greater the interval between the gradients (Δ), the greater the signal loss.

The **'*b*'** value of a gradient is a useful indication of the strength and duration of the pulse gradient applied and is defined as follows;

$$b = \gamma^2 \; G^2 \delta^2 \left(\Delta - \frac{\delta}{3}\right) \qquad \textbf{[2]}$$

γ – Gyromagnetic ratio (nuclear constant), *G* – Strength of gradient pulse, δ- Duration of gradient pulse, Δ - Time between the 2 gradient impulses

From equation 2 it is evident that the larger the 'b' value, the greater the diffusion weighting. When the value of 'b' is 0, the image is equivalent to a T2 weighted image. With higher values, there is greater strength of the gradient and more time for water diffusion. Table 2 shows the 'b' values used in the different methods of optic nerve diffusion.

Table 2. The 'b' values used in DWI by the listed investigators

Study	**b value s/mm^2**
Iwasawa et al [32]	262.05
Wheeler-Kingshott et al [33]	600
Chabert et al [34]	500
Moodley et al [49]	1000

The amount of signal loss from b0 to a higher 'b' value is expressed as a slope. The gradient of this slope is the Diffusion Coefficient and can be obtained for each pixel in the image (Figure 7). A map of these calculated Diffusion Coefficients creates the ADC image.

Figure 9. Relationship between gradient applied and Signal decay

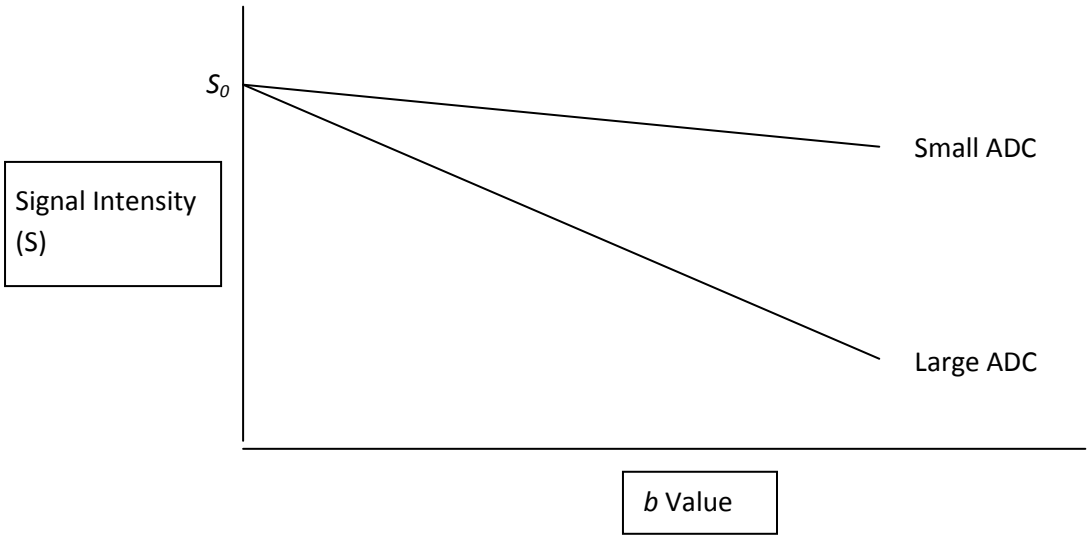

Figure 9 shows the relationship between signal loss and the gradient applied. When the diffusion is greater, the signal loss is more and the slope is steeper resulting in a larger ADC. Therefore a large ADC is indicative of greater diffusion [27].

2.6.3 Diffusion Tensor Imaging

MRI can measure diffusion in any direction using the 3 main axes of X,Y and Z. In the case of an isotropic medium, the ADC measured does not depend on the direction of measurement. There is unrestricted diffusion in the shape of a sphere (Figure 10a). In neuronal tissue however diffusion is ellipsoidal due to the restriction offered by the axons and glial tissue, where greater diffusion occurs along the axons than perpendicular to them. The Diffusion constants in the X,Y and Z direction are no longer equal. Now λ_1 is greater than λ_2

and λ_3 (where λ_1, λ_2 and λ_3 are the principal axes in an ellipsoid) (Figure 10b). When calculated in the direction of imaging this is easy to compute, however if the ellipsoid is oblique to the direction of imaging, then a 3 x 3 Diffusion Tensor is required to calculate the Diffusion constants where each entry is not a zero value (Figure 10c). While DWI is used to assess diffusion in 3 orthogonal axes, DTI can solve the complete diffusion tensor, but requires diffusion to be applied in a minimum of 6 directions.

The mathematical properties of the Diffusion Tensor make it possible to extract a number of useful parameters in assessing diffusion. DTI provides the MD which is a scalar average of the sum of the 3 eigenvectors λ_1, λ_2 and λ_3.

$$MD = 1/3(\lambda_1 + \lambda_2 + \lambda_3). \quad \textbf{[3]}$$

FA is a scalar value that describes the shape of diffusion. It ranges from 0 to 1 where 0 represents isotropic diffusion as occurs resulting in the shape of a sphere and 1 (never happens in life) represents anisotropic diffusion as occurs in the limit of an ellipsoid which is a straight line. FA is computed by comparing each eigenvalue (λ_1, λ_2 and λ_3) to the mean of all eigenvalues and is calculated by using equation 4.

$$FA = \sqrt{\frac{1}{\sqrt{2}}} \frac{\sqrt{(\lambda_1 - \lambda_2)^2 + (\lambda_1 - \lambda_3)^2 + (\lambda_2 - \lambda_3)^2}}{\sqrt{(\lambda_1^2 + \lambda_2^2 + \lambda_3^2)}} \quad \textbf{[4]}$$

Figure 10. Relationship between anisotropic diffusion (upper row), diffusion ellipsoids (middle row), and diffusion tensor (bottom row). (*From Mori S et al* [27])

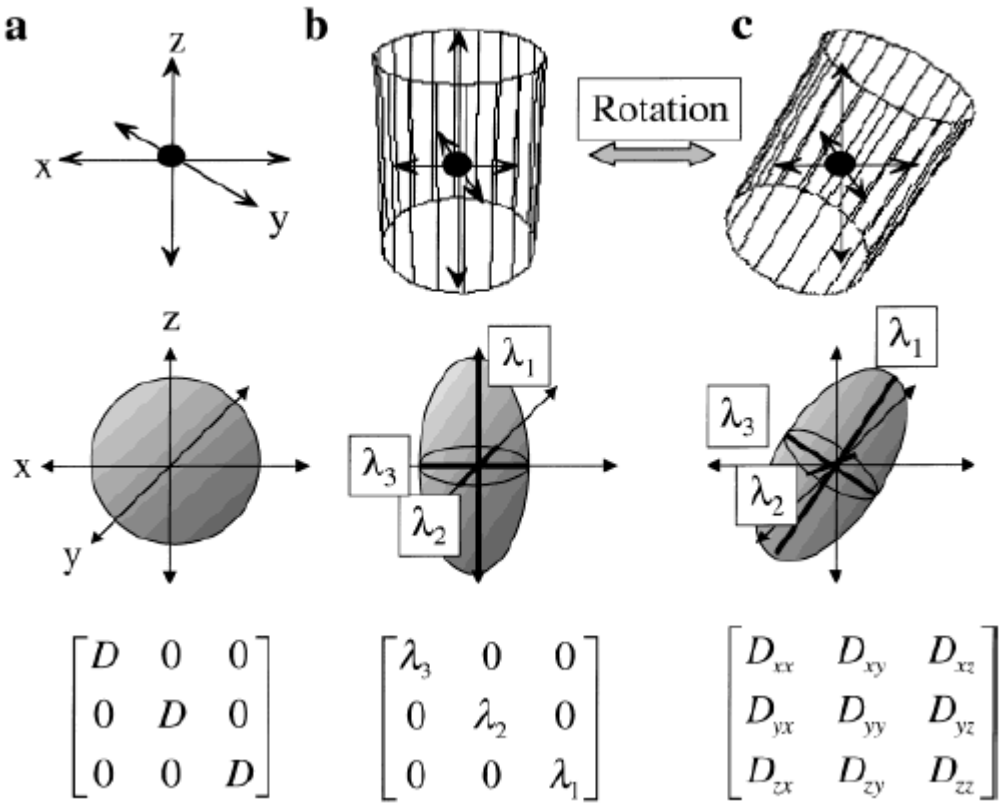

2.6.4 Anisotropic Parameters

Diffusion in an anisotropic medium is described as occurring in an ellipsoidal shape as occurs in the white matter of the brain and in the optic nerve. The ellipsoid has a long axis that describes its length and 2 smaller axes that describe its depth and width. These 3 axes are perpendicular to each other and cross at the midpoint of the ellipsoid. The diffusion vector components along the axes are referred to as eigenvectors and their lengths as eigenvalues. Diffusion is fast along the length of an axon and slow perpendicular to (or across) it. The diffusivity that occurs along the axon (λ_1) is referred to as the longitudinal, axial or parallel

diffusivity and the other 2 minor axes (λ_2, λ_3,) are referred to as the radial diffusivity or perpendicular diffusivity.

2.6.4.1 Axis ratio

The simplest index of anisotropy is the axis ratio i.e. the ratio between the long axis to the short axis of the ellipsoid (λ_1/ λ_2) on DTI or ADC_Z/ADC_Y on DWI. However this is susceptible to measurement noise so other measures have been adopted.

2.6.4.2 Anisotropic Index (AI)

The AI [33] refers to the ratio of the axial diffusivity to the radial diffusivity.

On DWI: $AI = ADC_Z/ADC_{XY}$ **[5]**

Where ADC_Z represents the axial diffusivity and ADC_{XY} is the average of the radial diffusion axes i.e.

$ADC_{XY} = (ADC_X + ADC_Y)/2$

On DTI: $AI = \lambda_{//}/\lambda_{\perp} = 2\lambda_1/(\lambda_2 + \lambda_3)$ **[6]**

The radial diffusivities are often averaged as $\lambda_{\perp} = (\lambda_2 + \lambda_3)/2$, where $\lambda_{\perp}$ represents the radial diffusivity. $\lambda_{//}$ represents the axial diffusivity.

An AI of 1 represents isotropic diffusion, whereas any value larger than 1 indicates a degree of anisotropy.

2.6.4.3 Fractional Anisotropy (FA)

To minimize measurement noise, the FA was introduced (Equation 4). An FA map is determined by solving the diffusion tensor. FA is computed from the eigenvalues of the tensor. FA values are obtained from the signal intensity on the FA maps. FA is therefore an objective and reproducible measure of anisotropy.

2.6.4.4 Relative Anisotropy (RA)

RA represents the ratio of the anisotropic part of diffusion to its isotropic part [84]. RA varies between 0 (isotropic diffusion) and √2 (infinite anisotropy), but is used less often than FA.

$$RA = \sqrt{(\lambda_1 - \langle\lambda\rangle)^2 + (\lambda_2 - \langle\lambda\rangle)^2 + (\lambda_3 - \langle\lambda\rangle)^2} / \sqrt{3\langle\lambda\rangle} \quad \textbf{[7]}$$

2.6.4.5 Volume Ratio (VR)

The VR represents the ratio of the ellipsoid volume to the volume of a sphere of radius (λ). Its range is from 1 (isotropic diffusion) to 0 (anisotropic diffusion), therefore some authors prefer to represent it as (1-VR) [84].

$$VR = \lambda_1\lambda_2\lambda_3 / \langle\lambda\rangle^3 \quad \textbf{[8]}$$

2.6.4.6 Other Scalar Anisotropic Indices

There are other scalar anisotropic indices that are infrequently used. They are less preferred as they are not really quantitative and are dependent on the choice of directions made for their measurements [84]. They include;

1. max[ADC_x, ADC_y, ADC_z]/ min[ADC_x, ADC_y, ADC_z]
2. σ[ADC_x]/ meanADC_x or σ[ADC_y]/ meanADC_y or σ[ADC_y]/ meanADC_y

2.6.5 Optic nerve diffusion imaging

Optic nerve diffusion imaging on DWI and DTI can be used to demonstrate the anisotropic diffusion of water molecules within the optic nerve. Disruption of this process occurs in optic nerve pathology.

Optic nerve diffusion has gained prominence as a useful investigational tool of optic nerve microstructure and pathology [22, 81, 85]. While initially employed to reveal the chronic effects of optic neuritis on optic nerve structure, its usage in recent studies has also shown early changes in acute optic neuritis [79]. The benefit of detecting these early changes would be to offer better understanding of the pathophysiology of processes impacting the optic nerve and hopefully provide direction to devise better strategies to prevent and reverse such damage. Optic nerve diffusion has been determined for other optic nerve disorders viz. ischaemic optic neuropathy, glaucoma and cryptococcal induced visual loss [24, 49, 86]. The diversity of disorders investigated has resulted in a variety of different pulse sequences and imaging protocols being used when performing diffusion studies on the optic nerve and good consistency of diffusion parameters has been shown for all these methods. Such diffusion techniques include Iwasawa's Intravoxel incoherent motion (IVIM) [32], Wheeler-Kingshott's zonal oblique multislice echo planar imaging (ZOOM EPI) [33], Chabert's non-Carr-Purcell-Meiboom-Gill fast spin echo (non CPMG FSE) [34] and our coronal oblique method [49]. All methods unfortunately have their own limitations. The optic nerve is surrounded first by CSF within the optic nerve sheath, then by fat within a bony orbit which is bordered by paranasal sinuses containing air. In most of the optic nerve diffusion techniques, FLAIR and fat saturation are utilized to overcome the CSF and fat artifact surrounding the nerve. In addition to fat saturation to overcome the fat signal, we have used a high diffusion gradient of B1000 instead of FLAIR to overcome CSF artifact [49]. The

benefit of this was the improved identification of the hypo-intense optic nerve on B0 images surrounded by the hyper -intense CSF in the peri-optic space. Susceptibility artifact from the bone and air are overcome by using sensitivity encoding (SENSE), averaging and Rayleigh noise reduction [33]. Optic nerve motion however cannot be eradicated, but merely reduced by asking the subject to relax listen to relaxing music, and focus on a target placed in their central field of view. We have asked subjects to focus on an orange sticker placed overhead on the MRI machine. Despite this, eye movement (voluntary or involuntary) continues and it is not uncommon with single shot echo planar imaging (EPI) to image an apparent 'double nerve' due to movement. The impact of this movement on optic nerve diffusion parameters and the impact of movement on diffusion of the surrounding CSF have not been previously investigated.

2.6.5.1 CSF suppressed ZOOM-EPI technique of Wheeler-Kingshott [33]

The ZOOM –EPI technique is done on both optic nerves coronally and simultaneously using a 1.5T General Electric MR scanner. Oblique imaging at 73° avoids wraparound artifact where a double image is obtained due to a small field of view (Figure 11). Single shot EPI was used for rapid imaging to reduce motion artifact however EPI is still prone to susceptibility artifacts. CSF and fat were also suppressed to reduce the artifact induced by the overlying CSF and orbital fat. Diffusion sensitizing gradients were applied in 3 directions using a 'b' gradient value of 600s/mm^2 with a repetition time of 3.6s and averaging of 40 acquisitions. Twelve 4mm slices were collected in 28min 12s. Matrix and field of view (FOV) were 64 x 32 and 8 x 4 respectively. Repetition time (TR) was 3400ms and echo time (TE) was 100ms. The mean ADC was calculated from the 3 orthogonal planes as (ADC_x + ADC_y + ADC_z)/3 and over the whole nerve was 1.058mm^2/s ± 0.101 x 10^{-3} (range 0.83 – 1.18 x 10^{-3}mm^2/s) (Table 3). The ADC_z obtained in the orthogonal plane was greater than the

ADC obtained in plane to the imaging plane suggesting anisotropic diffusion. The anisotropic index was thus derived from ADC_z/ADC_{xy} where ADC_{xy} was $(ADC_x + ADC_y)/2$. The average of this index was 1.57 with standard deviation (SD) of 0.34 and range (1.16 – 2.4) (Table 3).

The head was positioned in a quadrature birdcage head coil and was used as both transmitter and receiver. The head was positioned with foam padding on either side and the subject was asked to close their eyes and relax during the scan, to minimize motion artifact.

Figure 11. The ZOOM scheme of Wheeler Kingshott avoids wraparound artifact [33, 87]

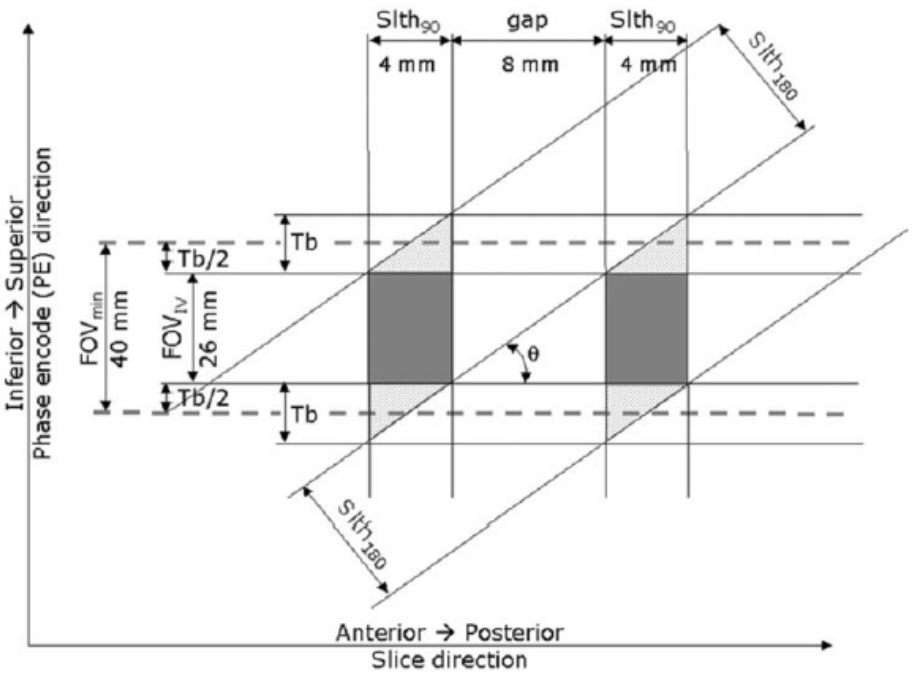

FIG. 1. The ZOOM scheme (not to scale). Abbreviations: $SITh_{90}$ = 90° excitation pulse slice thickness; $SITh_{180}$ = 180° refocusing pulse slice thickness; gap = gap between acquired slices; Tb = transition band; IV = inner volume; FOV_{min} = minimum FOV along the phase-encoding direction. For our protocol, parameters are: IV = 26 mm; $SITh_{90}$ = 4 mm; $SITh_{180}$ = 11 mm; gap = 8 mm; Tb = 13 mm; θ = 73°.

2.6.5.2 Intravoxel Incoherent Motion (IVIM) technique of Iwasawa [32]

Iwasawa et al first studied DWI of the optic nerve and presented imaging parameters they termed the IVIM technique. In their study, DWI was obtained in normal volunteers and compared to that of patients with acute and chronic optic neuritis using a 1.5T GE MR scanner [32].

The IVIM method used cardiac gating and both nerves were imaged simultaneously. The coronal image of the optic nerves was set at 3mm anterior to the Annulus of Zinn (Figure 12). T2 coronal weighted imaging was used before and after application of the diffusion gradient to identify the nerve location. Imaging parameters used were TR of 794 – 1072 ms, TE of 100ms, FOV of 16cm and slice thickness of 3mm with 128 encoding steps and 2 acquisitions. The gradient 'b' factor used was 262.05 s/mm^2 and was calculated using the Stejskal-Tanner equation [88]. Diffusion was obtained in the X, Y and Z directions. Motion artifact marred most of their results. Mean ADC values were therefore obtained in the Y and Z directions only for their control group. The mean ADC in the Y direction was $0.982 \pm 0.741 \times 10^{-3} mm^2/s$ and in the Z direction was $1.559 mm^2/s \pm 0.675 \times 10^{-3}$ (Table 3).

The subject's head was placed in a quadrature head coil with adhesive tape and sponge packing. The eyelids were also taped to attempt to limit eye movements and improve signal to noise ratio. Limitations of their method include the lack of fat suppression and the use of a low 'b' gradient.

Figure 12. Iwasawa's method of Optic nerve diffusion (a) T1 weighted axial image of the orbit. The white line shows the coronal plane used to obtain DWI. (b) The relationship between the optic nerve and the directions of the 3 diffusion sensitizing gradients. The static magnetic field is in the X direction.[32]

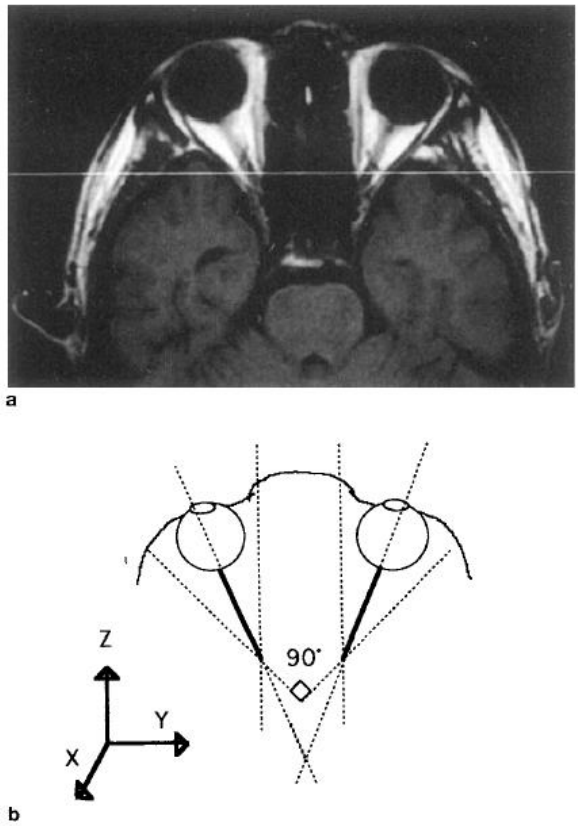

2.6.5.3 The Non-CPMG FSE technique of Chabert [34]

To overcome the susceptibility artifacts of EPI Chabert used the non-CPMG FSE sequence to acquire MR images. Iwasawa and Wheeler-Kingshott acquired diffusion images in 3 planes only to minimize acquisition time; however a minimum of 6 diffusion directions is required to define the diffusion tensor. So Chabert opted for DTI instead.

Images were acquired on a 1.5T General Electric MR scanner. A standard 7.6cm coil was positioned over the subject's left eye to receive the signal. Diffusion gradients were applied along 6 directions using a gradient with 'b' factor of 500s/mm^2. 6 repetitions were used and imaging time was 5 minutes for 5 slices. The FOV was 24 x 12 cm giving an in plane resolution of 0.94 x 0.94 mm. The FSE sequence used was single shot and 256 echoes read with an acquisition bandwidth of 125kHz. TE was 81ms and slice thickness was 3mm.

Care was taken in the positioning of the subject's head to ensure that the entire nerve was in the axial plane during imaging. No additional measures were taken to limit head or eye movement during scanning.

MD and FA were obtained for the optic nerve on axial rather than coronal imaging (Figure 13). Despite the lack of CSF and fat suppression in this technique of Chabert et al, the results are comparable to those of Iwasawa and Wheeler-Kingshott. The mean MD of the optic nerve was 1.1 ± 0.2 x 10^{-3}mm^2/s and FA of the nerve was 0.49 ± 0.06 (Table 3).

Figure 13. Axial images of (a) T2, (b) Diffusion, (c) MD map, (d) FA map [34]

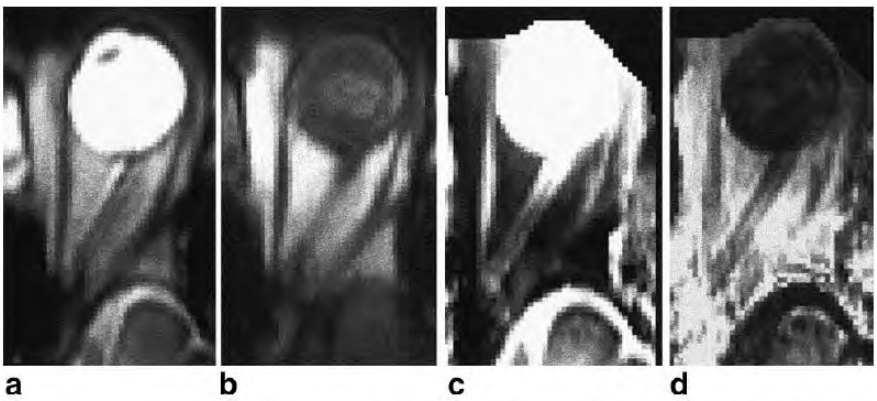

Figure 1. (**a**) T2-weighted image, (**b**) diffusion-weighted image along the R/L–S/I direction, (**c**) MD map, and (**d**) FA map of the human optic nerve. The nerve is clearly seen surrounded on both sides by CSF on images a, c, and d.

Table 3: Summary of Diffusion Parameters using different diffusion sequences

	Wheeler-Kingshott DWI study[33]	Iwasawa DWI study * [32]	Wheeler-Kingshott DTI study [87]	Trip DTI study [22]	Chabert DTI study [34]	Xu DTI study [85]	Kolbe DTI study [23]
Volunteers recruited	3	7	10	15	9	12	20
Diffusion Sequence	ZOOM-EPI	IVIM	ZOOM_EPI	ZOOM-EPI	Non-CPMG FSE	IVI-EPI	Coronal oblique
FAT Suppression	Yes	No	Yes	Yes	No	Yes	Yes
CSF Suppression	Yes	No	Yes	Yes	No	No	Yes
ADC optic nerve : Mean (SD) x 10^{-3} mm^2/s	1.058 ± (0.1)	0.98 ± (0.74)Y 1.56 ± (0.68)Z					
MD optic nerve : Mean (SD) x 10^{-3} mm^2/s			1.22 ± (0.2)	1.08 ± (0.17)	1.1 ± (0.2)	1.09 ± (0.2)	1.25 ± (0.14)
FA optic nerve: Mean (SD)			0.61 ± (0.1)	0.67 ± (0.09)	0.49 ± (0.06)	0.46 ± (0.15)	0.38 ± (0.05)
AI optic nerve : Median (IQR)	1.57 (1.16-2.4)						

SD – Standard Deviation, % - percentage, ADC – Apparent Diffusion Coefficient measured using Diffusion Weighted Imaging, MD – Mean Diffusivity measured using Diffusion Tensor Imaging, FA – Fractional Anisotropy, AI – Anisotropic Index calculated as $2\lambda_1/(\lambda_2 + \lambda_3)$, where λ_1 = axial diffusion and λ_2, λ_3 = radial diffusion. IQR – interquartile range. * Iwasawa et al obtained ADC in the Y and Z axes. ZOOM EPI – Zonal oblique multislice echo-planar imaging, IVIM – Intravoxel incoherent motion, Non-CPMG FSE – Non Carr-Purcell-Meiboom-Gill Fast spin echo, IVI-EPI – inner volume imaging, echo-planar imaging

2.7 Optic Neuritis

2.7.1 Pathophysiology of Optic Neuritis

Typical optic neuritis as described in multiple sclerosis presents with acute unilateral visual loss, pain on eye movements, decreased contrast sensitivity and colour desaturation. Visual loss is usually not complete and on pupillary testing, a relative afferent pupillary defect is detected. Infrequently, patients have Uhthoff's phenomenon, where deterioration of vision occurs when body temperature is elevated and the Pulfrich phenomenon where the asymmetrical slowing of electrical impulses between the eyes cause motion distortion. The inflammation is mostly retrobulbar (65%) and papillitis with optic disc swelling is uncommon [89]. MRI shows nerve enhancement in 94% of cases [90]. Histopathologically, there is perivascular mononuclear inflammation (cuffing), oedema in the myelinated nerve sheaths, and myelin breakdown. Early during inflammation, myelin loss exceeds axonal loss. Inflammation is immune mediated, but the specific target antigen is unknown. T-cell activation results in release of cytokines and other inflammatory agents. B-cell activation is against myelin basic protein and detection of oligoclonal bands in the CSF is evidence of this. The chronic sequela of optic neuritis is further loss of axons and optic atrophy. Visual recovery however is good with significant visual return within 2 to 3 months.

Acute disseminated encephalomyelitis (ADEM) presents as a post viral or post vaccination immune mediated inflammation of the central nervous system [91]. Optic neuritis is usually bilateral and recovery is variable depending on the severity of inflammation. The hallmark of inflammation in ADEM is the perivenular inflammation by lymphocytes and macrophages. The margins of inflammation are indistinct and when aggressive inflammation occurs, haemorrhagic necrosis is an accompaniment.

Optic neuritis in neuromyelitis optica tends to be bilateral, recurrent and visual loss tends to be more severe and less reversible [92, 93]. It is an antibody mediated disease to the aquaporin- 4 water channel. Pathology includes immunoglobulin and complement deposition on the astrocytic processes of the perivascular and superficial glia limitans. There is in addition granulocytic, T-cells and activated macrophage/microglial cell infiltrates with aquaporin -4 and astrocyte loss.

VEP in optic neuritis shows prolonged P-100 latency due to the demyelination and slowing of electrical impulses. P-100 amplitude reduction is minimal in acute optic neuritis and is due to conduction block. In chronic optic neuritis, axonal loss is prominent so the N-80/P100 amplitude is decreased.

2.7.2 Optic nerve diffusion imaging in Optic Neuritis

The application of optic nerve diffusion in optic neuritis constitutes the majority of early work done in optic nerve diffusion.

Iwasawa et al (1997) were the first to apply DWI of the optic nerves in optic neuritis in 9 patients [32]. They utilized the IVIM technique and obtained baseline quantitative parameters. In acute optic neuritis, the mean ADC of the optic nerve was $0.843 \pm 0.742 \times 10^{-3} mm^2/s$ in the Y direction (n = 3) and $0.941 \pm 0.431 \times 10^{-3} mm^2/s$ in the Z direction. There was no significant difference between the acute optic neuritis group and the normal volunteers. However there were significant differences between the optic nerve ADC in the chronic optic neuritis group and the normal volunteers ($p < 0.001$) as well as the acute optic neuritis group ($p < 0.001$) in the Z direction only. The mean ADC of the nerves with chronic optic neuritis was $1.56 \pm 0.69 \times 10^{-3}$ mm^2/s in the Y direction (n = 5) and $4.18 \pm 1.13 \times 10^{-3}$ mm^2/s in the Z

direction (n = 10). The authors postulate that the loss of the myelin sheath after axonal loss in chronic optic neuritis and the increase of extra-axonal spaces increases the ADC; presumably due to the higher water content. Acute plaques are different from chronic plaques. They are hypercellular due to the macrophage/astrocytic response and a variable degree of lymphocytic infiltration. One can postulate that such inflammation would decrease the ADC.

Hickman et al (2005) using the ZOOM-EPI technique have shown similar results to Iwasawa in the imaging of optic neuritis 12 months after the event in 18 patients [21]. 'The mean ADC from diseased optic nerves was 1.324 (standard deviation (SD) 0.379) x 10^{-3} mm^2/s, compared with 0.990 (SD 0.159) x 10^{-3} mm^2/s from healthy contralateral optic nerves (P = .005 versus diseased optic nerves) and 0.928 (SD 0.196) 10^{-3} mm^2/s from control optic nerves (P = .006 versus diseased optic nerves and P = 0 .40 versus healthy contralateral optic nerves'. They too have postulated axonal disruption as cause for the elevated ADC in diseased optic nerves in the chronic setting.

Trip et al using DTI and the ZOOM EPI technique of Wheeler-Kingshott obtained MD and FA values of the optic nerve in 25 patients with optic neuritis acquired in the previous 12 months [22]. The mean MD from affected nerves by optic neuritis was elevated at 1.611 (SD 290) x 10^{-3} mm^2/s compared with 1.191 (SD 198) x 10^{-3} mm^2/s from unaffected contralateral nerves ($p < 0.001$) and 1.083 (SD 168) x 10^{-3} mm^2/s from control nerves ($p < 0.001$). 'Mean FA from affected nerves was lower at 0.435 (SD 0.100), compared with 0.602 (SD 0.100) from clinically unaffected contralateral nerves ($P < 0.001$) and 0.669 (SD 0.093) from control nerves ($P < 0.001$).' They reaffirmed the theory of axonal disruption as resulting in raised MD and decreased FA, but did not discount the contribution by demyelination and gliosis. Furthermore, they were able to show that the mean orthogonal eigenvalue perpendicular to

the nerve was raised compared to clinically unaffected and control nerves. Perhaps increase in the spaces between the axons from axonal loss permitted more orthogonal diffusion.

Naismith et al corroborated Trips's findings in 60 patients with a remote history of optic neuritis using DTI [20]. They were also able to demonstrate that radial diffusivity (orthogonal diffusion to the optic nerve) by Spearman coefficients, were negatively correlated to visual acuity (-0.61), Pelli-Robson contrast sensitivity (-0.60), VEP amplitude (-0.46) and positively correlated to VEP latency (0.61).

Fatima et al were able to show a significant difference in ADC between acute (15 nerves) and chronic (7 nerves) optic neuritis [79]. The ADC value in acute optic neuritis was $0.9 \pm 0.2 \times 10^{-3}$ mm^2/s vs. $1.62 \pm 0.35 \times 10^{-3}$ mm^2/s in chronic optic neuritis ($p = 0.0002$). The normal healthy controls had an ADC of $1.07 \pm 0.1 \times 10^{-3}$ mm^2/s ($p = 0.0088$). FA was not measured. They postulate a similar axonal loss and Wallerian degeneration in chronic optic neuritis that increases ADC. In acute optic neuritis, there is accumulation of macrophages and lymphocytes but the myelin is intact, therefore ADC decreases.

In summary, acute optic neuritis is associated with decreased ADC and chronic optic neuritis with increased ADC and MD, and decreased FA.

2.7.3 Other applications of optic nerve diffusion

Diffusion abnormalities have been described in other disorders.

In a post-operative case of bilateral ischaemic optic neuropathy, Park et al showed restricted diffusion in both optic nerves with reduced ADC values of 0.425×10^{-3} mm^2/s and 0.420×10^{-3} mm^2/s on the right and left respectively. They suggest using DWI in cases of post-

surgical visual loss to detect posterior ischaemic optic neuropathy which is missed on funduscopy [94].

Verma et al have shown restricted diffusion in an optic nerve affected by posterior ischaemic optic neuropathy from aspergillus infection. They too demonstrate reduced ADC of 0.635 x 10^{-3} mm^2/s, but the adjacent nerve had elevated ADC of 1.7 x 10^{-3} mm^2/s presumably due to vasogenic oedema [95]. Similar findings of restricted diffusion have been reported by Chen JS et al, Caquil C et al and Al-Shafai LS et al [24, 96, 97].

Glaucoma is a common cause of optic neuropathy. Recent studies using DWI and DTI have demonstrated degeneration of the optic pathway from the optic nerve to the visual cortex. In an animal model of glaucoma, Hui et al have shown increasing radial diffusivity and decreasing FA of the optic nerve as the disease progresses [98]. The implication is that as axonal degeneration develops from long standing glaucoma, anisotropic diffusion decreases. Axial diffusion was not affected because the 10% of axonal loss did not impact on it.

Zhang et al using DTI have shown decreased FA (0.39 vs. 0.54, $p<0.001$), increased radial diffusivity (1.5 vs. 0.99, $p < 0.001$), increased axial diffusivity (2.83 vs. 2.48, $p = 0.009$) and increased MD (1.94 vs. 1.48, $p<0.001$) when compared to normal controls [81]. The benefit is examination of the status of the optic nerve in glaucoma patients with opaque optic media.

As an indicator of glaucoma severity, Dai et al imaged the brains of 25 glaucoma sufferers using 3T MR DTI and 'b' value of 800 s/mm^2 along 30 directions and compared that to 25 healthy age-matched controls [25]. The chiasm and bilateral optic radiations of glaucoma patients showed significantly reduced FA (chiasm 0.16±0.02 versus 0.20±0.02 $p < 0.05$) (left optic radiation 0.40±0.03 versus 0.46±0.03, right optic radiation 0.38±0.04 versus 0.44±0.04, $p<10^{-3}$) when compared to the healthy controls. Optic radiation radial diffusivity was

decreased compared to controls ($p < 0.05$). No significant differences were noted in the axial diffusivity and the mean diffusivity between the glaucoma patients and healthy controls. Optic chiasm FA was negatively correlated and optic radiation radial diffusivity was positively correlated with glaucoma stage. The authors conclude that these parameters could serve as non-invasive markers of disease severity.

In optic neuritis, there is perivascular lymphocytic infiltration, multifocal demyelination, and reactive astrocytosis [30]. Iwasawa et al (1997) have demonstrated decreased diffusion in acutely inflamed optic nerves with reduced ADC values, but no comparisons were made between perpendicular and parallel diffusion. One may hypothesize a similar diffusion abnormality of the optic nerves in cryptococcal induced visual loss if the predominant disorder is optic nerve infiltration. In the acute optic neuritis model, the ADC values along the parallel axis will be decreased and FA values will also be reduced due to the presence of inflammatory cells and fungi. One may also expect a decrease in the parallel to perpendicular diffusion ratios with AI and FA reduced due to greater isotropic diffusion. The chronic optic neuritis model from myelin and axonal loss will not apply in the acute setting of CM. In chronic optic neuritis there is elevated ADC and reduced FA.

2.8 Papilloedema

2.8.1 Pathophysiology of Papilloedema

In papilloedema from any cause of elevated intracranial pressure, disc swelling results from axoplasmic flow stasis. There is entrapment of the optic nerve axons at the lamina cribrosa due to elevated intracranial pressure transmitted along the subarachnoid space to the junction of the globe and retrobulbar optic nerve. Axoplasm and metabolic products accumulate at the

optic disc resulting in hyperaemia and elevation of the disc. The retrobulbar optic nerve is structurally normal in papilloedema, but little is known about its functional status.

The leakage of axoplasm into the subretinal layer is partially responsible for Paton's lines. The central location of the central retinal vein within the optic nerve makes it susceptible to compression. Loss of spontaneous venous pulsations is due to pressure changes between the peri-optic CSF and the intra-ocular pressure and central retinal vein compression. Longstanding venous compression causes nerve fibre layer oedema, exudates and retinal haemorrhage. Compression of the central retinal artery is responsible for hypoxia, gliosis and finally optic atrophy. The choroidal folds are a mechanical outcome from stretching that occurs following optic nerve sheath distension [7] (Figure 14).

Figure 14: Pathogenesis of Papilloedema. Adapted from Schirmer et al [7]

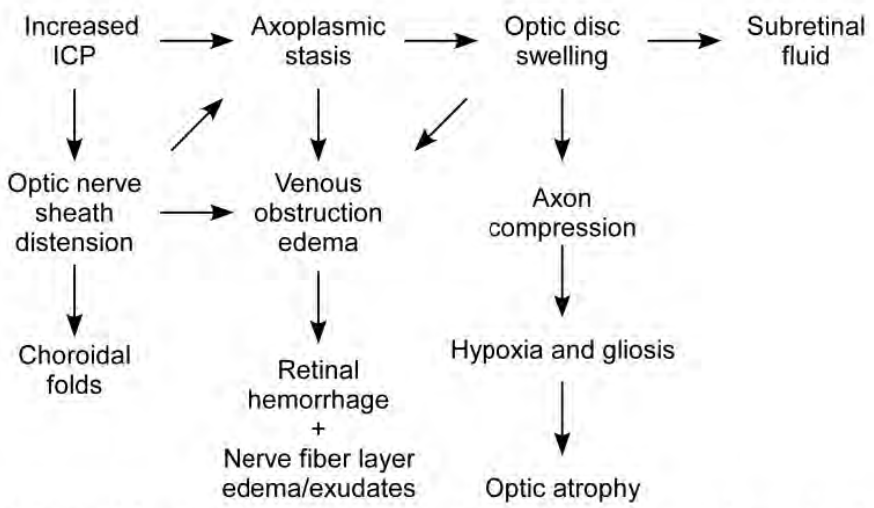

2.8.2 Predicted diffusion parameters of Papilloedema

One can speculate that the effect of elevated pressure on the optic nerve as occurs in papilloedema, will be increased displacement of water molecules along the nerve and therefore increased axial diffusion - as in circumferentially squeezing toothpaste. Higher ADC values will occur in the parallel direction such that AI will increase. One may also speculate that the FA of diffusion along the optic nerve should be unchanged or increase since myelin sheath and axons are preserved in the acute situation. However if secondary axonal degeneration occurs then diffusion parameters will be similar to chronic optic neuritis with high ADC values and low FA.

2.9 The Optic nerve Compartment Syndrome

2.9.1 Pathophysiology of the Optic nerve Compartment Syndrome

The compartmentalisation of the peri-optic SAS has become of interest due to the persistence of papilloedema and visual loss in patients with idiopathic intracranial hypertension (IIH) who have a functioning lumbo-peritoneal shunt [99, 100]. Furthermore, the presence of asymmetrical papilloedema in IIH and IIH without papilloedema has both required explanation [101]. Killer et al have demonstrated the compartmentalization of the peri-optic SAS in patients with IIH [66]. They performed CT-cisternography in 3 patients with asymmetrical papilloedema and were able to demonstrate impaired influx of contrast loaded CSF (CLCSF) into the orbital segment of the nerve. In 2 patients, CLCSF entered the SAS of the optic nerve only within the optic canal, but not within the intra-orbital segment of the nerve. Impaired flow occurred at the intracanalicular portion in these patients. In the 3rd patient with IIH, CLCSF entered the orbital portion of the SAS of the nerve, up to 10 mm on the right and 5 mm on the left. The site of ‘blockage’ depends on the structure and amount of

septae and trabeculae within the peri-optic SAS. Biological evidence for the compartmentalisation of the peri-optic SAS has come from concentration gradient measurement of brain-derived lipocalin-like prostaglandin D synthase (L-PGDS) in the spinal CSF and peri-optic SAS, where much greater concentrations are found [102]. Either flow within the peri-optic space is much slower or additional production of L-PGDS occurs there.

The compartment syndrome results from increased pressure within a confined compartment due to swelling of its constituents. There is subsequent compression of vital structures within the compartment with subsequent vascular compromise (arterial and venous) and nerve compression.

The optic nerve compartment syndrome is dependent on a number of pathophysiological mechanisms [66, 103]. The smallest diameter of the peri-optic SAS is within the optic canal (Figure 15). It is however not the only site of compression. The fact that blockage has also been demonstrated in the orbital portion suggests the importance of the dura and the subarachnoid structures viz. the trabeculae and septae [65]. The compartment syndrome in the setting of anterior ischaemic optic neuropathy AION and anterior optic neuritis and glaucoma suggests that inflammation (arachnoiditis) also plays a role [69, 104, 105]. The presence of inflammatory cells also contributes to the closing of the arachnoid apertures (spaces between trabeculae and septae) and blockage of meningeal lymphatics [65]. Furthermore, there is the toxic effect of reduced clearance of the CSF. L-PGDS is neuroprotective to astrocytes, but modulates inflammatory processes and enhances apoptosis. Damage to the mitochondria especially in the bulbar portion of the nerve is associated with demyelination and visual loss. [99]

Orgul's use of the term compartment syndrome relates to Glaucoma [106]. Remodelling of the lamina cibrosa pores that become more slit like cause compression of the optic nerve

axons as they pass through the lamina cribrosa. He postulates this as the obstruction that causes optic nerve dysfunction even in the presence of normal intra-ocular pressure.
Burde and Kerr use the term to describe the compression of the optic nerve axons that are hypoxic and swollen within a disc at risk [107, 108]. The crowding of swollen axons through this small disc results in compression and further hypoxia from compressed vasculature in the setting of AION.

Free bidirectional flow of CSF between the peri-optic SAS and intracranial SAS has been taken for granted. CSF is produced in the ventricles and by bulk flow reaches the peri-optic SAS. However no hydrodynamic theory explains the reversal of flow in the peri-optic SAS back towards the brain against the volume gradient. The cul-de-sac structure of the optic nerve sheath suggests that other mechanisms must operate to allow drainage of CSF from the peri-optic space. One theory is drainage into the orbit and has been demonstrated in animal studies by leakage of contrast agents and radio-isotopes into the orbit [109]. The more popular theory is by drainage into the optic nerve sheath lymphatics [110, 111].

Figure 15: CSF spaces surrounding the Optic chiasm and the Optic nerve. [66]

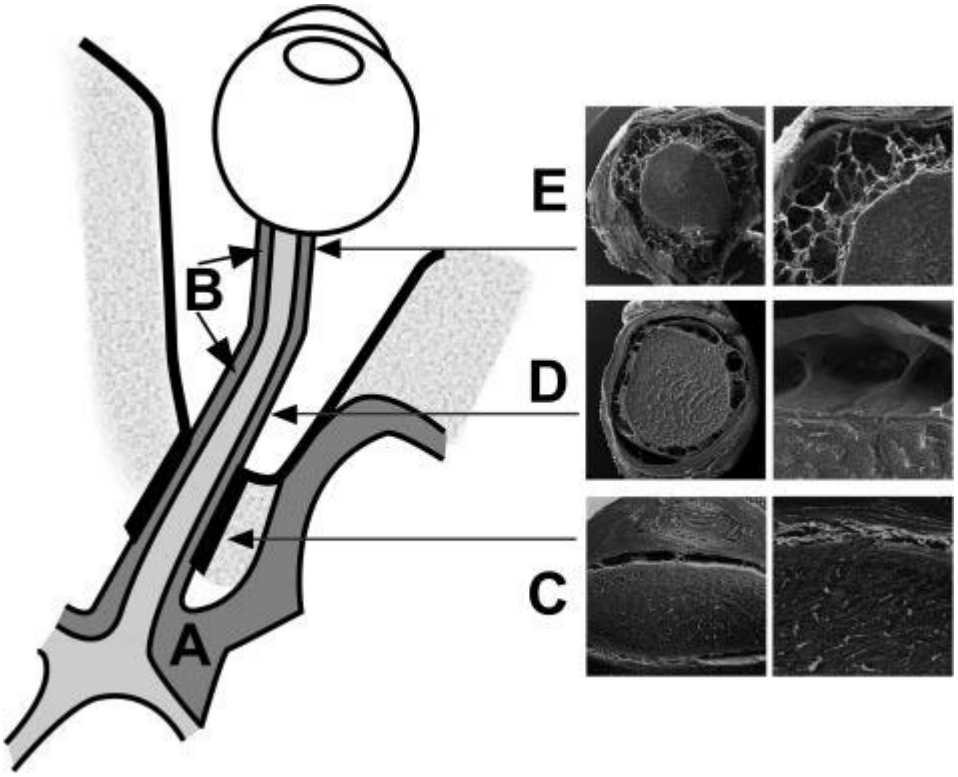

Figure 15 shows the schematic representation of the CSF spaces surrounding the optic chiasm (intracranial CSF space) **(A)** and the CSF surrounding the optic nerve (orbital CSF space) **(B).**

CSF flows from intracranial (**A**) into the SAS of the optic nerve **(B)**. The SAS of the optic nerve is most narrow in the canalicular region (**C**). The intraorbital segment of the SAS is characterized by broad septae **(D)**, whereas the retrobulbar segment is characterized by small trabeculae **(E).** Due to the CSF volume gradient the direction of flow is directed from the intracranial SAS to the orbital SAS.

2.9.2 The Optic nerve Compartment Syndrome and Cryptococcal Meningitis

IIH and CM share key characteristics. Both conditions present with raised intracranial pressure, swollen optic discs, raised intracranial pressure headaches, impaired CSF re-absorption and lack of hydrocephalus. Killer et al explain the asymmetrical papilloedema in IIH to the anatomy of the subarachnoid trabeculae, septae and pillars that limit the transfer of the intracranial pressure to the laminar cribrosa asymmetrically [66]. One may speculate that a similar mechanism operates in CM. However, in CM in addition to the markedly elevated intracranial pressure there is also plugging of the peri-optic CSF space by cryptococcal fungal elements (fungal yeasts and fragments of the polysaccharide capsule). The result would be immense compression of the optic nerve at sites of blockage. We speculate that the resultant axoplasmic stasis would cause optic nerve dysfunction and when axoplasmic stasis is severe and reaches the optic nerve head, papilloedema will result.

The literature abounds with anecdotal evidence for and against the papilloedema and optic neuritis models of visual loss in CM. Unfortunately, clarity is lacking and therefore appropriate preventative strategies and management protocols for visual loss are vague.

Furthermore, the optic nerve compartment syndrome in CM has not hitherto been investigated. Epidemiological data, immunological data, neuro-imaging, VEP and HVF of CM induced visual loss need clear and precise documentation. The use of objective and reproducible investigational tools to study visual loss in vivo and determine the pathogenesis by comparison with established causes of papilloedema and optic neuritis need addressing. The advances made by DWI and DTI of the optic nerve in multiple sclerosis must be exploited in CM and has been the motivation for their use in this study. Antiretroviral therapy and antifungal therapy has made huge strides in the survival of CM patients. Consequently, prevention and treatment of the devastating disability of blindness in survivors is of paramount importance!

CHAPTER 3 AIMS

3.1 To clinically, electrophysiologically and biochemically describe optic nerve dysfunction in cryptococcal-induced visual loss according to

3.1.1 Frequency of visual disturbance

3.1.2 Severity of visual disturbance

3.1.3 Mode of onset of vision loss

3.1.4 Relationship to degree of immunosuppression and treatment

3.1.5 CSF findings

3.2 To optimise DWI and DTI imaging of the optic nerve and thereby obtain standard and reproducible imaging protocols.

3.3 To devise a mathematical model that separates optic nerve diffusion from surrounding CSF diffusion within the optic nerve sheath.

3.4 To propose a probable pathogenesis of Cryptococcal induced visual loss by investigating and comparing the following

3.4.1 Quantitative DWI and DTI of the optic nerves in patients with cryptococcal induced visual loss, using protocols obtained in Aims 2 and 3 above and comparing to normal controls.

3.4.2 Comparison of routine FSE, DWI and DTI of the optic nerves in patients with cryptococcal meningitis stratified into 2 groups with normal and abnormal visual acuity.

.

3.4.3 Comparison of FSE, DWI and DTI of the optic nerves in patients with cryptococcal induced visual loss, to patients with papilloedema (IIH, malignant HPT and RICP) and optic neuritis i.e. optic nerve disorders secondary to elevated CSF pressure and infiltration respectively.

CHAPTER 4 PAPER 1

New insights into the pathogenesis of Cryptococcal-induced visual loss using Diffusion-Weighted Imaging of the optic nerve:

- The paper addresses aims 3.1 (3.1.1, 3.1.2), 3.2 and 3.4 (3.4.1, 3.4.2)
- A Moodley is the main author
- It was published in the journal, *Neuro-ophthalmology* in October 2012.

This paper describes in detail the optic nerve diffusion technique used in the study. The results from 29 asymptomatic controls (9 HIV positive and 20 HIV negative) were compared to that of 52 HIV infected patients with culture confirmed cryptococcal meningitis.

A 1.5T Philips Gyroscan was used for magnetic resonance (MR) diffusion-weighted imaging (DWI) and diffusion-tensor imaging (DTI) of the brain and optic nerves using the coronal oblique technique for each nerve as previously reported [49]. Diffusion gradient of b = 1000 s/mm^2 was selected and fat saturated (SPIR) single shot EPI using SENSE without cardiac gating was used. EPI was acquired using echo time (TE) = 93 ms, relaxation time (TR) = 3000 ms, 180 mm field of view (FOV), matrix = 112 x 128 and 4 mm slice thickness. DTI was obtained in 15 directions and longitudinal, axial and mean diffusivity values were selected for analysis. FA maps were computer generated using the Interanova Release 11.2.1 version software.

Visual loss (best corrected visual acuity < 6/9) was detected in 34.6% of patients with cryptococcal meningitis and in 9.6%, visual loss was profound (<6/60). Elevated CSF pressure (> 20cmCSF) was found in 69% of patients whereas swollen optic discs was present in only 25%. Patients with swollen discs and decreased vision accounted for 17.3%. Patients were more likely to have impaired vision with elevated CSF pressure than with swollen discs.

The optic nerve and optic nerve sheath diameters were similar in the healthy control group and in the CM group regardless of CSF pressure.

Diffusion studies suggested a tendency towards elevated ADC and lowered FA but this needs further investigation. The implication is disruption of the longitudinally arranged axons and myelin sheath early in CM.

The possibility of compression of the optic nerves due to elevated CSF pressure somewhere between the lamina cribrosa and optic canal is discussed. A discussion of the different models of visual loss in CM is presented and the role played by a possible optic nerve compartment syndrome is entertained.

The frequency and severity of visual loss in CM are described. The optic nerve diffusion method is described in detail. Quantitative DWI and DTI optic nerve diffusion parameters are obtained for patients with CM. Comparisons are made between patients with normal and abnormal vision and between patients with normal and elevated CSF pressure.

Neuro-ophthalmology, 36(5), 186–192, 2012
© 2012 Informa Healthcare USA, Inc.
ISSN: 0165-8107 print/1744-506X online
DOI: 10.3109/01658107.2012.715716

informa
healthcare

ORIGINAL ARTICLE

New Insights into the Pathogenesis of Cryptococcal Induced Visual Loss Using Diffusion-Weighted Imaging of the Optic Nerve

Anand Moodley[1,3], William Rae[2], Ahmed Bhigjee[3], Noleen Loubser[1], and Andrew Michowicz[4]

[1]*Department of Neurology, Greys Hospital, Pietermaritzburg, South Africa,* [2]*Department of Medical Physics, University of The Free State, Bloemfontein, South Africa,* [3]*Department of Neurology, University of KwaZulu Natal, Durban, South Africa, and* [4]*Department of Medicine, Edendale Hospital, Pietermaritzburg, South Africa*

ABSTRACT

Despite a successful antiretroviral drug rollout in South Africa, cryptococcal induced visual loss continues to be a major complication of cryptococcal meningitis. Preventive measures are lacking due to poor understanding of its pathogenesis. Optic nerve diffusion has shown some promise in investigating inflammatory and axonal changes of the optic nerve *in vivo*. The lack of post-contrast enhancement on T1 magnetic resonance imaging (MRI) and signal changes on T2 MRI with slightly increased apparent diffusion coefficient and reduced fractional anisotropy on diffusion imaging suggest that pressure-related effects are the dominant mechanism over inflammation and that there is early untested evidence of a compartment syndrome rather than papilloedema as the main contributor.

KEYWORDS: Apparent diffusion coefficient, Compartment syndrome, Cryptococcal meningitis, Fractional anisotropy, Optic nerve diffusion

Copyright © 2012 Informa Healthcare
Not for Sale or Commercial Distribution
Unauthorised use prohibited. Authorised users can download, display, view and print a single copy for personal use

INTRODUCTION

In South Africa, cryptococcal meningitis (CM) is a common opportunistic infection in severely immunocompromised human immunodeficiency virus (HIV)-infected patients. Despite the efficient national antiretroviral rollout program, the incidence of CM has not declined.[1] CM was the initial defining illness in the acquired immune deficiency syndrome (AIDS) in 84% of patients, and in 50% of HIV-infected patients neurological abnormalities were detected.[2] Visual loss is common and is reported in 35–52.6% of patients with CM. Visual loss continues to deteriorate in 17.3% despite antifungal therapy and in 3.7% of patients follows commencement of antifungal therapy, which alone is insufficient in reversing vision loss.[3] Visual recovery is unpredictable and requires early and effective adjunctive therapy to prevent or reverse the frequent and sometimes catastrophic loss of vision.

Appropriate interventional therapy can only be identified and implemented once the pathophysiology of vision loss in CM is well understood. Unfortunately, there are conflicting reports concerning its pathophysiology and standard treatment protocols are disappointingly lacking.

Rex et al.[4] in 1993 postulated a dual mechanism of vision loss. The first mechanism was that of rapid visual loss early in the disease or soon after commencing treatment, usually within 6 days. Optic neuritis was the postulated pathogenic mechanism due to fungal infiltration of the nerve and ensuing inflammation. Catastrophic visual loss in such patients was described as developing within 12 hours. The second mechanism was slow visual loss, due to papilloedema from chronically elevated cerebrospinal fluid (CSF) pressure that developed over several weeks.

These mechanisms may not be mutually exclusive and one that incorporates both theories is also conceivable. We performed an in vivo study that investigates the pathogenesis of visual loss by using optic nerve diffusion on magnetic resonance imaging (MRI). Diffusion of water molecules within

Received 07 June 2012; accepted 15 June 2012

Correspondence: Anand Moodley, Department of Neurology, Greys Hospital, Private Bag X9001, Pietermaritzburg, 3200 South Africa. E-mail: anand.moodley@kznhealth.gov.za

RIGHTSLINK

the optic nerve is anisotropic due to the longitudinal orientation of axons and intact myelin.[5,6] Water diffuses preferentially along the longitudinal/axial plane rather than the perpendicular/radial plane of the optic nerve. The quantitative entities that describe optic nerve diffusion are apparent diffusion coefficient (ADC), which can be measured in the orthogonal planes and obtained on diffusion-weighted imaging (DWI), mean diffusivity (MD), a scalar quantity obtained on diffusion tensor imaging, and fractional anisotropy (FA). FA describes the directional diffusion of water molecules within the nerve occurring preferentially in a longitudinal direction. FA ranges from 0 to 1 where 0 represents isotropic diffusion, which is equal in all directions and 1 represents anisotropic diffusion, which is preferential diffusion in one direction. The normal value obtained for the optic nerve is 0.4–0.5, suggesting preferential diffusion of water molecules in the axial rather than the radial plane in optic nerves.[7]

Optic nerve diffusion measurement has been shown to be of benefit in acute and chronic optic neuritis in multiple sclerosis.[7,8] For example, Naismith et al.[7] in their cohort of acute optic neuritis demonstrated decreased ADC values in the axial plane due to the presence of inflammatory cells that supposedly restrict axial diffusion. FA values were also decreased due to greater isotropic diffusion from disruption of the axons and myelin. Hickman et al.,[8] on the other hand, demonstrated increased mean diffusion for similar reasons of disruption of cellular integrity; however, no differentiation was made between axial and radial diffusion. Their cohort comprised patients with a remote history of optic neuritis (12 months) and resultant optic atrophy. In optic neuropathy from glaucoma, Engelhorn et al.[9] have shown increased radial diffusion and decreased FA of the optic nerve consistent with axonal disruption. Furthermore, Wang et al.[10] demonstrated increased radial diffusion, unaffected axial diffusion, and reduced FA in subacute ischaemic optic neuropathy. The benefits of optic nerve diffusion as an experimental tool are increasing. The effect of papilloedema on optic nerve diffusion, however, is not described.

In this study, we aimed to firstly compare optic nerve diffusion in patients with CM to that of a healthy control population and secondly, to correlate clinical parameters (vision loss, elevated CSF pressure, and disc swelling) with imaging parameters (ADC on DWI, and MD on diffusion tensor imaging [DTI], FA, and anisotropic index). We postulated that an increase in ADC and/or MD and a reduction in FA might suggest axonal disruption. Preferential reduction in axial diffusion might suggest optic nerve infiltration. Where axial and radial diffusion are equally affected, the anisotropy index should be similar to the control group, a scenario one would expect in papilloedema or a compartment syndrome. For analysis of the axial and radial diffusion, the anisotropic index was calculated as a ratio of the axial diffusion to the mean radial diffusion.

MATERIALS AND METHODS

The study was approved by the Greys Hospital and the University of KwaZulu Natal ethics committees. Informed consent was obtained from 52 culture positive CM patients within 4 weeks of disease onset. Patients were consecutively recruited between February 2008 and January 2011 and excluded if they were co-infected with tuberculosis, toxoplasmosis, progressive multifocal leucoencephalopathy, bacterial meningitis, or suffered any other central nervous system space–occupying disease such as lymphoma. Patients underwent full neuro-ophthalmological evaluation and examination of immune status and were subjected to MRI, DWI, and DTI of the brain, orbits, and optic nerves, using standard and modified imaging protocols on a Phillips 1.5-Tesla Gyroscan magnetic resonance scanner. ADC using DWI, MD and FA using DTI, and an anisotropic index of axial diffusion to radial diffusion were compared between groups and to a sample of 29 healthy volunteers with normal visual acuity. The optic nerve diffusion results are presented.

Unlike the zonal oblique multislice echo planar imaging (ZOOM-EPI) method used by Wheeler-Kingshott et al.,[6] we opted for separate imaging of each optic nerve in the coronal plane (Figure 1). The axial and radial axes of each nerve were first obtained, followed by 5 coronal oblique slices perpendicular to the long axis of the nerve within the orbit. The intracanalicular portion of the nerve was avoided to minimize susceptibility artifacts. Fat-saturated single shot echo planar imaging (EPI) using sensitivity encoding (SENSE) without cardiac gating was used. To allow for localization of the nerve on the B0 image, fluid attenuation inversion recovery

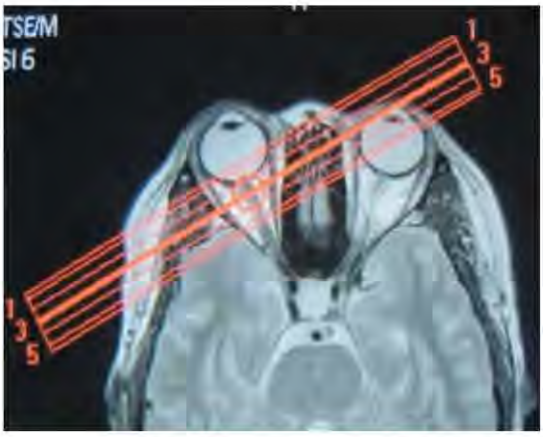

FIGURE 1 MRI T2 axial view of the optic nerve with selection of coronal slices shown. Slices are selected in a coronal oblique plane perpendicular to the orientation of the optic nerve, which is selected on a T2-weighted axial image. The coronal slice with best visualisation of the optic nerve is selected on DWI and DTI for further analysis. DWI = diffusion-weighted image; DTI = diffusion tensor image.

© 2012 Informa Healthcare USA, Inc.

RIGHTSLINK

(FLAIR) was not used. A higher B1000 gradient was used to overcome the influence of the surrounding CSF within the optic nerve sheath on the optic nerve diffusion. To minimise movement artefact, the patient was asked to lie comfortably and focus on an orange sticker placed directly in line of their central field of view during DWI and DTI.

During analysis, a region of interest (ROI) of 2 × 2 pixels was placed centrally on the optic nerve on the slice with best optic nerve visualization (Figure 2)—usually slice 2 or 3. ADC was obtained in the axial and radial planes. The mean diffusivity was a scalar average of the 3 ADC values obtained in the x, y, and z planes. The DTI was obtained in 15 directions; however, only axial, radial, and mean diffusivity values were selected for analysis. In addition to the fractional anisotropy obtained from DTI (Figure 3), an anisotropic index was calculated from both the DWI and DTI using the formula: anisotropic index = $2\lambda_1/(\lambda_2 + \lambda_3)$, where λ_1 = axial diffusion and λ_2, λ_3 = radial diffusion in the other two orthogonal axes.

Statistical analyses were performed using OpenStat 2008. All measures for the left and right eyes were submitted to a two-way analysis of variance (ANOVA). As no significant differences were noted between the eyes, the mean values for both eyes are presented.

RESULTS

All 52 cryptococcal meningitis patients were HIV positive and culture positive for *Cryptococcus neoformans*. Of the 29 healthy controls, 9 were HIV positive and 20 were HIV negative. The values of ADC, MD, FA, and anisotropic index for HIV-positive versus HIV-negative controls showed no significant difference and will be presented as a mean for the groups combined.

None of the 52 CM scanned showed any optic nerve signal change on T1, T2, T2 FLAIR, and T1 post-contrast images.

Table 1 shows the demographic data and clinical parameters of the 52 CM patients. Of these, 34.6% of patients had decreased best corrected visual acuity (BCVA) of ≤6/9 on the Snellen chart. Only 5 patients had profound vision loss of ≤6/60, but none of these developed catastrophically within 12 hours. Sixty-nine percent of all CM patients had elevated CSF pressure and 25% had swollen discs. Decreased vision was associated with elevated CSF pressure in 26.9% and 15.4% of patients had all of impaired vision, elevated CSF pressure and swollen discs. All 13 patients with swollen discs had bilateral swelling.

There was no significant difference in optic nerve sheath diameters among the healthy control group, and the CM patients with normal and with elevated CSF pressure. Similar optic nerve diameters between those groups were also documented and suggest no optic nerve infiltration or oedema (Table 2).

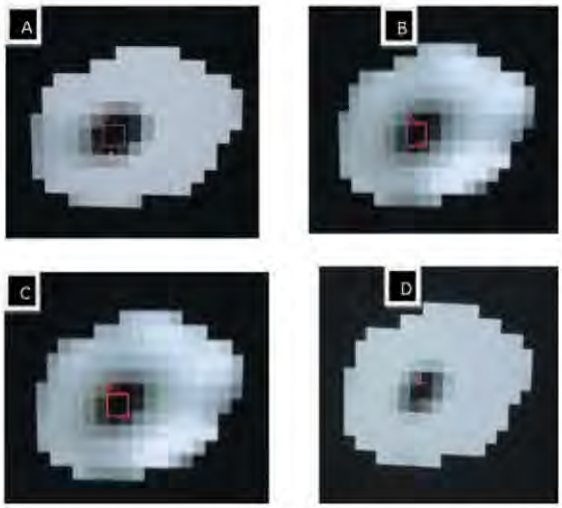

FIGURE 2 ADC images of B1000 images showing ROI of 2 × 2 pixels on optic nerve. (A) axial diffusion; (B, C) radial diffusion; (D) mean diffusion. ADC = apparent diffusion coefficient; ROI = region of interest.

FIGURE 3 Coronal slice of fractional anisotropy on DTI, showing ROI on the optic nerve. DTI = diffusion tensor imaging; ROI = region of interest.

In 6 patients, the optic nerves were poorly visualised due to susceptibility and movement artefact. Optic nerve diffusion was therefore only analysed in 46 patients. Thirty-five patients had elevated CSF pressure and 11 patients had normal CSF pressure. The average CSF pressure was 34 cm H_2O (range 21–50 cm H_2O) in the elevated CSF pressure group and 14 cm H_2O (range 7–20 cm H_2O) in the normal pressure group. The Analysis of variance of ADC, FA, and the anisotropy index showed no significant differences between the normal and elevated CSF pressure groups or the normal healthy volunteers (Table 3). Graphs 1 and 2, however, show a tendency towards a high ADC and low FA in the CM patients with elevated pressure.

Only 5 patients presented with severe vision loss of 6/60 or worse, 2 with symmetrical loss of vision, 2 with asymmetrical loss of vision, and 1 with unilateral loss of vision. None had the catastrophic vision loss described by Rex et al.[4] and none developed after the commencement of antifungal therapy. The analysis of variance of

RIGHTSL

TABLE 1 Demographics and incidence of vision loss, elevated CSF pressure, and swollen discs.

	Average	Range
Age of 29 controls	31	21–47
Age of 52 CM patients	34	22–49
	Number	Percentage
Healthy controls, Males	11	37.9
Healthy controls, Females	18	62.1
CM patients Males	25	48.1
CM patients Females	27	51.9
	Number	Percentage
CM patients with swollen discs	13	25
CM patients with decreased vision	18	34.6
CM patients with VA ≤ 6/60	5	9.6
CM patients with elevated pressure	36	69
CM patients with swollen discs and decreased vision	9	17.3
CM patients with swollen discs and elevated pressure	12	23
CM patients with decreased vision and elevated pressure	14	26.9
CM patients with decreased vision, swollen discs, and elevated pressure	8	15.4
CM patients with normal vision, discs, and pressures	12	23.1

Note. CM = cryptococcal meningitis; VA = visual acuity.

TABLE 2 Comparison of optic nerve and optic nerve sheath diameters.

	Mean optic nerve sheath diameter in mm (range)	Mean optic nervediameter in mm (range)
Control	6.03 (5.4–7)	2.3 (1.6–3)
CM with normal CSF pressure	6.37 (5–8.1)	2.2 (1.3–3.4)
CM with elevated CSF Pressure	6.5 (5.2–8.5)	2.3 (1.6–3.5)
p-value	0.152	0.451

Note. CM = cryptococcal meningitis; CSF = cerebrospinal fluid.

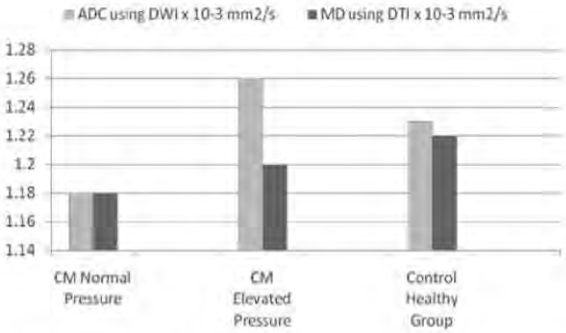

GRAPH 1 ADC and MD in CM normal and elevated pressure and controls. CM = cryptococcal meningitis; ADC = apparent diffusion coefficient; MD = mean diffusivity; DWI = diffusion-weighted imaging; DTI = diffusion tensor imaging.

ADC, FA, and the anisotropy index showed no significant differences between any of the four groups viz. the normal vision with CM, decreased vision of ≤6/9 with CM, decreased vision of ≤6/60, and the normal healthy control with normal vision (Table 4).

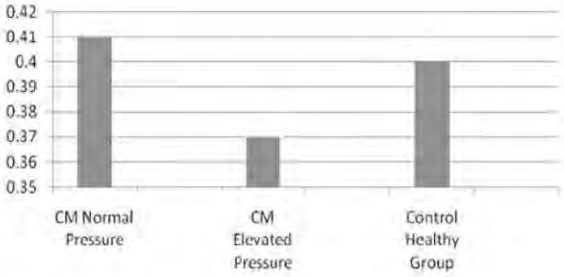

GRAPH 2 FA in CM normal pressure, CM-elevated pressure, and controls. CM = cryptococcal meningitis; FA = fractional anisotropy.

DISCUSSION

Cryptococcal meningitis continues to be a common opportunistic infection amongst severely immunocompromised HIV-infected patients in South Africa despite the availability of antiretroviral therapy. Poor compliance of antiviral drug therapy and the failure of voluntary testing are major setbacks.[1] The ongoing pandemic of HIV infection and opportunistic infections, notably CM, means appropriate and early measures need to be taken to prevent impending blindness. By using diffusion-weighted imaging of the optic nerve we have attempted to elucidate the pathogenesis of cryptococcal induced visual loss with the aim of preventing blindness by goal-directed intervention.

Studies supporting and opposing the mechanisms of optic neuritis and papilloedema have been many but mostly anecdotal. The inflammatory (optic neuritis) model of visual loss was made popular by many authors in the past by showing visual improvement with corticosteroid therapy and demonstrating active inflammation and necrosis of the optic nerve and optic chiasm on histology.[3,11,12] Strong evidence for optic nerve infiltration also came from a case report of a patient with centrocaecal scotomata on visual field testing.[13] The importance of identifying an optic neuritis model ensures that anti-inflammatory therapy features early in the intervention of CM to prevent blindness. Alternatively, the raised intracranial pressure (papilloedema) model was suggested by the accompanying constricted visual fields and enlarged blind spot in these patients and the beneficial response to serial lumbar punctures, ventriculoperitoneal shunts, and lumbar peritoneal shunt.[14–16] Such evidence together with benefit from optic nerve sheath fenestration favours strategies that lower intracranial pressure to prevent and treat blindness due to the infection.[17] The likelihood of a combination of both models with or without a compartment syndrome is also conceivable.

None of the 52 cryptococcal meningitis patients scanned showed any optic nerve signal change on T1, T2, T2 FLAIR, or T1 post-contrast image. The absence of signal change reflects a paucity of inflammatory reaction had there been any optic nerve infiltration by

© 2012 Informa Healthcare USA, Inc.

RIGHTSL

TABLE 3 Quantitative parameters of imaging and CSF pressure.

	ADC using DWI × 10^{-3} mm²/s (± SD)	MD using DTI × 10^{-3} mm²/s (± SD)	FA (± SD)	Anisotropy index using DWI	Anisotropy index using DTI
CM normal pressure	1.18 (± 0.34)	1.18 (± 0.37)	0.41 (± 0.1)	1.92	1.68
CM elevated pressure	1.26 (± 0.43)	1.2 (± 48)	0.37 (± 0.13)	1.80	1.72
Control healthy group	1.23 (± 0.41)	1.22 (± 0.34)	0.40 (± 0.12)	1.81	1.88
p-value	0.841	0.972	0.517	0.859	0.524

Note. CM = cryptococcal meningitis; ADC = apparent diffusion coefficient; DWI = diffusion-weighted imaging; DTI = diffusion tensor imaging; MD = mean diffusivity; FA = fractional anisotropy given as an index from 0 to 1. Anisotropic index = $2\lambda_1/(\lambda_2 + \lambda_3)$, where λ_1 = axial diffusion and λ_2, λ_3 = radial diffusion.

TABLE 4 Quantitative parameters of imaging and visual acuity.

	ADC using DWI × 10^{-3} mm²/s (± SD)	MD using DTI × 10^{-3} mm²/s (± SD)	FA (± SD)	Anisotropy index using DWI	Anisotropy index using DTI
CM normal vision	1.24 (± 0.29)	1.13 (± 0.32)	0.38 (± 0.09)	1.86	1.67
CM decreased vision 6/9 and below	1.21 (± 0.39)	1.28 (± 0.33)	0.36 (± 0.1)	1.65	1.78
CM severely decreased vision 6/60 and below	1.24 (± 0.34)	1.38 (± 0.34)	0.44 (± 0.11)	1.20	1.88
Healthy control group	1.23 (± 0.41)	1.22 (± 0.34)	0.40 (± 0.12)	1.81	1.88
p-value	0.995	0.566	0.697	0.755	0.664

Note. CM = cryptococcal meningitis; ADC = apparent diffusion coefficient; DWI = diffusion-weighted imaging; DTI = diffusion tensor imaging; MD = mean diffusivity; FA = fractional anisotropy given as an index from 0 to 1. Anisotropic index = $2\lambda_1/(\lambda_2 + \lambda_3)$, where λ_1 = axial diffusion and λ_2, λ_3 = radial diffusion.

the organism, a situation that is reflected by minimal CSF changes in CM.[2] Conversely, the absence of signal change suggests that no infiltration of the optic nerve occurs by the organism or inflammatory cells and that an optic neuritis model does not occur in early CM to explain visual loss.

Testing of visual acuity is difficult in patients presenting acutely with CM for various reasons. Patients are confused, poorly attentive, systemically unwell, have raised intracranial pressure, and frequently have 6th nerve palsies as false localising signs. Despite these setbacks, we were able to demonstrate visual loss as a complication in 34.6% of our patients, similar to the incidence previously reported by Moosa et al.[2] All cases occurred within 4 weeks of disease onset and none after commencement of treatment. Severe visual loss occurred in 5 patients (9.6%), but none developed catastrophically within 12 hours as described by Rex et al.[4] in their series. Conceivably, none of our patients complicated with optic nerve infiltration. Based on the mode of onset of vision loss, the optic neuritis model seems unlikely.

Raised intracranial pressure was common, occurring in 69% (36/52) at an average of 34 cm H_2O, whereas disc swelling was noted in 25% of patients. Extremely high CSF pressures were noted in 7 patients at levels greater than 50 cm H_2O. Patients with decreased vision were more likely to have elevated CSF pressure and swollen discs; however, only 44% had both, suggesting that elevated CSF pressure impairs optic nerve functioning not predominantly at the optic nerve head but somewhere between the lamina cribrosa and the optic canal. Despite elevated CSF pressure being common in cryptococcal meningitis, swollen optic discs is not as common (Figure 4). Only 23% of all patients had both elevated pressure and swollen discs. The possibility of pressure-related effects on the optic nerve exists but not at the optic nerve head. Whilst not entirely supporting the papilloedema model for vision loss, this lends support for the compartment syndrome occurring somewhere along the nerve, either at the optic canal or the intra-orbital segment of the nerve.

The lack of any significant difference between the optic nerve sheath diameter in the cryptococcal meningitis patients with and without elevated CSF pressure also supports the likelihood of a compartment syndrome (Table 2). The lack of appreciable swelling of the optic nerve sheath in the presence of elevated CSF pressure as confirmed on lumbar puncture is possibly due to a blockage proximally at the rigid optic canal or somewhere along the intra-orbital optic nerve where septae in the subarachnoid space have created a blockage to CSF flow.

Optic nerve diffusion has been found to be a useful tool in examining the optic nerve following acute optic neuritis and in the chronic setting in establishing axonal loss in multiple sclerosis.[5,7,18,19] It is gaining momentum as an investigational tool into the pathogenesis of other optic nerve disorders too, such as ischaemic optic neuropathy and glaucoma.[9,10] This is the first study that looks at the pathogenesis of cryptococcal induced visual loss using DWI and DTI of the optic nerve.

The technique used to scan the optic nerve was different to that of Wheeler- Kingshott's zonal oblique multislice echo planar imaging (ZOOM-EPI), Iwasawa's intravoxel incoherent motion sequence (IVIM), and

RIGHTSL

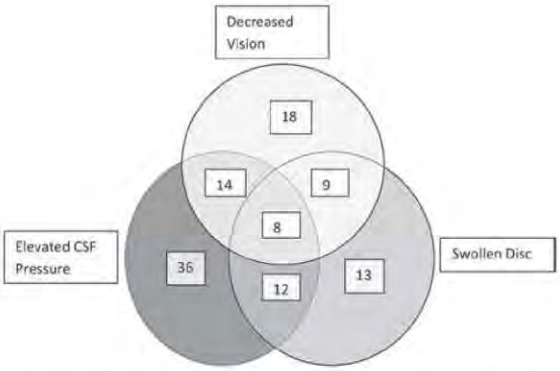

FIGURE 4 Relationships between CSF pressure, decreased vision, and swollen disc. CSF = cerebrospinal fluid.

Chabert's non-Carr-Purcell-Meiboom-Gill fast spin echo sequence (non-CPMG FSE).[5,6,19] We used a higher B1000 gradient to eliminate CSF artefact rather than FLAIR, single-shot fast spin echo to limit the effect of motion and a coronal oblique slice to image the optic nerves separately. By not using FLAIR, identification of the optic nerve on B0 images was made much simpler. The MD values reported for healthy optic nerves in the studies of Wheeler-Kingshott et al.,[6] Iwasawa et al.,[5] and Chabert et al.[20] range between 1.0 and 1.3×10^{-3} mm^2/s and FA range between 0.4 and 0.6. The method we used revealed comparable values of $1.2 \pm 0.34 \times 10^{-3}$ mm^2/s for MD and 0.4 ± 0.12 for FA of healthy optic nerves.

Axonal disruption within the optic nerve following optic neuritis is associated with an increase in ADC and a decrease in FA.[19] Whilst no significant difference in MD or FA was found between the elevated and normal CSF pressure groups in cryptococcal meningitis (Graphs 1 and 2 and Table 3), the tendency towards an elevated ADC and reduced FA suggests axonal disruption in the elevated CSF pressure group, implying that elevated CSF pressure and papilloedema do play an early role in vision loss in patients with cryptococcal meningitis.

The similar anisotropy index in all pressure groups (Table 3) and all vision groups (Table 4) suggests that axial diffusion along the nerve is not preferentially affected in cryptococcal meningitis. Optic nerve infiltration therefore seems unlikely as a plausible explanation for visual loss in early cryptococcal meningitis, contrary to the widely accepted theory of Rex et al.[4] This tendency towards increased ADC and reduced FA needs to be confirmed in future studies by recruiting larger number of patients, using 3-Tesla MRI and by comparison to other causes of papilloedema.

The lack of convincing evidence for either an optic neuritis or papilloedema model using optic nerve diffusion suggests either that this is an unhelpful investigative tool for infective disorders affecting the optic nerve such as cryptococcal meningitis or that an optic nerve sheath compartment syndrome is the main mechanism by which visual loss occurs. The usefulness of optic nerve diffusion as an investigative tool in optic neuritis and ischaemic optic neuropathy has been well established.[7,8,19] Killer et al.[21] have adequately shown with computed tomography (CT) cisternography that the optic nerve sheath subarachnoid space is interrupted by septae and trabeculae and that in raised intracranial pressure as in idiopathic intracranial hypertension there is compartmentalisation between the intracranial and optic nerve sheath subarachnoid spaces. This theory sufficiently explains idiopathic intracranial hypertension with unilateral and asymmetrical papilloedema and cases without papilloedema. It is very likely that in patients with cryptococcal meningitis, entrapment of cryptococci by these septae and trabeculae that occur naturally causes obstruction to the free flow of CSF around the optic nerve and perhaps when subjected to the raised intracranial pressure transmitted along the subarachnoid space results in a compartment syndrome. Such entrapment of cryptococci within the optic nerve sheath has been demonstrated in a patient who showed resolution of papilloedema and improved vision following optic nerve sheath fenestration.[17] The raised pressure on the nerve results in optic nerve dysfunction and morphological changes depending on the site of obstruction. Obstruction at the lamina cribrosa results in papilloedema, whereas that at the optic canal or along the intra-orbital nerve results in axoplasm stasis or venous congestion and resultant optic nerve dysfunction. The absence of signal changes in the optic nerve on MRI in patients with elevated CSF pressure and decreased vision makes axoplasm stasis the more plausible.

Pressure-related effects with a compartment syndrome seem to be the most attractive theory currently that explains the early loss of vision in cryptococcal induced visual loss and deserves further investigation.

ACKNOWLEDGEMENTS

We are most grateful to Mrs. Shireen Mathews and Mrs. Garcia Rudolph for all the radiographic work, including the many hours spent on post-processing of the diffusion data. This study was supported in part by a grant from the Medical Research Council, South Africa.

***Declaration of interest*:** The authors report no conflicts of interest. The authors alone are responsible for the content and writing of the paper.

REFERENCES

[1] Lightowler JV, Cooke GS, Mutevedzi P, Lessells RJ, Newell ML, Dedicoat M. Treatment of cryptococcal meningitis in Kwazulu Natal, South Africa. *PLoS ONE* 2010;5:e8630.

[2] Moosa MY, Coovadia YM. Cryptococcal meningitis in Durban, South Africa: a comparison of clinical features, laboratory findings, and outcome for human immunodeficiency

© 2012 Informa Healthcare USA, Inc.

virus (HIV)-positive and HIV-negative patients. *Clin Infect Dis* 1997;24:131–134.

[3] Seaton RA, Verma N, Naraqi S, Wembri JP, Warrell DA. Visual loss in immunocompetent patients with Cryptococcus neoformans var. gatti meningitis. *Trans R Soc Trop Med Hyg* 1997;91:727–728.

[4] Rex JH, Larsen RA, Dismukes WE, Cloud GA, Bennett JE. Catastrophic visual loss due to Cryptococcus neoformans meningitis. *Medicine (Baltimore)* 1993;72:207–224.

[5] Iwasawa T, Matoba H, Ogi A, Kurihara H, Saito K, Yoshida T, Matsubara S, Nozaki A. Diffusion-weighted imaging of the human optic nerve: a new approach to evaluate optic neuritis in multiple sclerosis. *Magn Reson Med* 1997;38:484–491.

[6] Wheeler-Kingshott CAM, Parker GJM, Symms MR, Hickman SJ, Tofts PS, Miller DH, Barker GJ. ADC Mapping of the human optic nerve: increased resolution, coverage, and reliability with CSF-suppressed ZOOM-EPI. *Magn Reson Med* 2002;47:24–31.

[7] Naismith RT, Xu J, Tutlam NT, Trinkaus K, Cross AH, Song SK. Disability in optic neuritis correlates with diffusion tensor-derived directional diffusivities. *Neurology* 2009;72:589–594.

[8] Hickman SJ, Wheeler-Kingshott CA, Jones SJ, Miszkiel KA, Barker GJ, Plant GT, Miller DH. Optic nerve diffusion measurement from diffusion-weighted imaging in optic neuritis. *AJNR Am J Neuroradiol* 2005;26:951–956.

[9] Engelhorn T, Michelson G, Waerntges S, Otto M, El-Rafei A, Struffert T, Doerfler A. Changes of radial diffusivity and fractional anisotopy in the optic nerve and optic radiation of glaucoma patients. *Sci World J* 2012;2012:849632.

[10] Wang MY, Qi PH, Shi DP. Diffusion Tensor Imaging of the Optic Nerve in subacute anterior ischemic optic neuropathy at 3T. *AJNR Am J Neuroradiol* 2011;32:1188–1194.

[11] Cohen DB, Glasgow BJ. Bilateral optic nerve cryptococcosis in sudden blindness in patients with acquired immune deficiency syndrome. *Ophthalmology* 1993;100:1689–1694.

[12] Corti M, Solari R, Cangelosi D, Domínguez C, Yampolsky C, Negroni R, Arechavala A, Schtirbu R. Sudden blindness due to bilateral optic neuropathy associated with cryptococcal meningitis in an AIDS patient. *Rev Iberoam Micol* 2010;27:207–209.

[13] Lipson BK, Freeman WR, Beniz J, Goldbaum MH, Hesselink JR, Weinreb RN, Sadun AA. Optic Neuropathy associated with cryptococcal arachnoiditis in AIDS patients. *Am J Ophthalmol* 1989;107:523–527.

[14] Ferreira RC, Phan G, Bateman JB. Favorable visual outcome in cryptococcal meningitis. *Am J Ophthalmol* 1997;124:558–560.

[15] Clauss JJ, Portegies P. Reversible blindness in AIDS-related cryptococcal meningitis. *Clin Neurol Neurosurg* 1998;100:51–52.

[16] Ng CW, Lam MS, Paton NI. Cryptococcal meningitis resulting in irreversible visual impairment in AIDS patients—a report of two cases. *Singapore Med J* 2000;41:80–82.

[17] Milman T, Mirani N, Turbin RE. Optic nerve sheath fenestration in cryptococcal meningitis. *Clin Ophthalmol* 2008;2:637–639.

[18] Kolbe S, Chapman C, Nguyen T, Bajraszewski C, Johnston L, Kean M, Mitchell P, Paine M, Butzkueven H, Kilpatrick T, Egan G. Optic Nerve diffusion changes and atrophy jointly predict visual dysfunction after optic neuritis. *Neuroimage* 2009;45:679–686.

[19] Trip SA, Wheeler-Kingshott C, Jones SJ, Li WY, Barker GJ, Thompson AJ, Plant GT, Miller DH. Optic nerve diffusion tensor imaging in optic neuritis. *Neuroimage* 2006;30:498–505.

[20] Chabert S, Molko N, Cointepas Y, Le Roux P, Le Bihan D. Diffusion tensor imaging of the human optic nerve using a non-CPMG fast spin echo sequence. *J Magn Reson Imaging* 2005;22:307–310.

[21] Killer HE, Jaggi GP, Flammer J, Miller NR, Huber AR, Mironov A. Cerebrospinal fluid dynamics between the intracranial and the subarachnoid space of the optic nerve. Is it always bidirectional? *Brain* 2007;130(Pt 2):514–520.

RIGHTSL

CHAPTER 5 PAPER 2

The impact of optic nerve movement on optic nerve and peri-optic CSF diffusion:

- This paper addresses the aims 3.2 and 3.3 above.
- A Moodley is the main author
- It has been submitted to the journal, *Magnetic Resonance in Medicine* and awaiting review.

The paper addresses the technique of optic nerve diffusion used in this study and compares the technique to that used by other investigators. We have used a 1.5 Tesla MRI scanner and a gradient of b1000. Fat saturation was included in the Diffusion sequence, but fluid attenuation was not. We have found that to be a useful way of identifying the optic nerve on the b0 images of the diffusion scanner. Furthermore, by not suppressing the CSF signal, we have been able to measure the diffusion parameters from the surrounding (peri-optic) CSF which differs from the optic nerve. Both DWI and DTI of the optic nerve were done using this technique. Findings are equivalent to those of other studies that use and do not use fat saturation and fluid attenuation. The peri-optic CSF shows higher ADC and MD values as expected but the anisotropic index indicates that the flow in the peri-optic CSF space is not isotropic.

The study also measures the amount of optic nerve movement during a standard Diffusion study, both in the distance and area covered. Optic nerve tracking was done using single shot EPI and 20 snapshots of the nerve were taken in the 3 minute period of recording.

The optic nerve movement parameters were then correlated with optic nerve and peri-optic CSF diffusion parameters. No significant correlations were noted, indicating that macroscopic movement of the nerve has no significant impact on the microscopic movement of water molecules (diffusion) within the nerve and peri-optic CSF space.

The impact of the non-suppressed CSF signal on optic nerve diffusion and peri-optic CSF diffusion was then analysed. Linear regression analysis of optic nerve and CSF diffusion parameters showed low R^2 values with minimal statistical but no clinical or practical significance.

We have been able to obtain standard and reproducible DWI and DTI imaging protocols of the optic nerve. No mathematical model was required to correct for the surrounding CSF signal as demonstrated by the low R^2 values on linear regression.

The impact of optic nerve movement on optic nerve and peri-optic CSF diffusion parameters

Anand A Moodley[1, 3], William ID Rae[2] , Yarish Brijmohan[4], Ahmed I Bhigjee[3], Cathy Connolly[5], Andrew Michowicz[6]

[1] *Department of Neurology, Greys Hospital, Pietermaritzburg, South Africa*

[2] *Department of Medical Physics, University of the Free State, South Africa*

[3] *Department of Neurology, University of KwaZulu Natal, South Africa*

[4] *Department of Electrical, Electronic and Computer Engineering, University of KwaZulu Natal, South Africa*

[5] *Biostatistics Unit, Medical Research Council of South Africa, Durban, South Africa*

[6] *Department of Medicine, Edendale Hospital, Pietermaritzburg, South Africa*

Corresponding author: AA Moodley, Department of Neurology, Greys Hospital, Pietermaritzburg, South Africa.

Postal Address: PO Box 13833, Cascades, 3202, South Africa.
Email: anand.moodley@kznhealth.gov.za Tel: +2733 897 3298 Fax: +2733 8973409
Mobile: +2784 5955077

Word Count (excluding abstract, tables, figures and references): 2188

Number of References: 16

Keywords: Optic nerve diffusion, Apparent Diffusion Coefficient, Mean Diffusivity, Fractional anisotropy, Anisotropic Index, peri-optic CSF

Abstract

Introduction: Optic nerve diffusion imaging is a useful investigational tool of optic nerve microstructure, but is limited by eye-movement and artifact from surrounding cerebrospinal fluid (CSF), fat, bone and air. Attempts at getting patient cooperation thus voluntarily limiting eye movement during a standard diffusion imaging sequence are usually futile and suppression of the surrounding CSF makes identification of the nerve difficult. The aim of this study was to establish the impact of eye movement and the CSF signal on diffusion parameters of the optic nerve and the peri-optic CSF space.

Method: Twenty nine healthy volunteers with intact vision and intact conjugate gaze were recruited and subjected to magnetic resonance (MR) diffusion-weighted imaging (DWI) and diffusion-tensor imaging (DTI) of the optic nerves. Twenty right eyes had nerve tracking done using single shot EPI at twenty time points over 3 minutes. Eye movement measures were correlated with diffusion parameters of apparent diffusion coefficient (ADC), mean diffusivity (MD), fractional anisotropy (FA) and anisotropy index (AI) using Spearman's rank correlation. Linear regression analyses were also done between optic nerve and CSF diffusion parameters to determine any association.

Results: No significant correlations were noted between eye movement parameters and ADC and MD of the optic nerve and peri-optic CSF space. Low to moderate correlations were noted between eye movement parameters and AI and FA of the optic nerve and peri-optic CSF space, but none were statistically significant. Regression analysis of optic nerve and CSF diffusion parameters showed low R^2 values with no significant relationship demonstrated.

Conclusion: Minimal optic nerve movement during standard diffusion sequences (DWI and DTI) does not impact significantly on diffusion parameters of the optic nerve and peri-optic CSF space. Not suppressing the surrounding CSF has minimal impact on optic nerve diffusion parameters and when compared to other studies, does not have any clinical significance.

Introduction

Optic nerve (ON) diffusion imaging has gained prominence as a useful investigational tool of optic nerve microstructure and pathology [1-3]. While initially employed to demonstrate the chronic effects of optic neuritis on optic nerve structure, its use in recent studies has also revealed early changes in acute optic neuritis[4]. The anticipated benefit of detecting these early changes would be to offer better understanding of the pathophysiology of processes impacting the optic nerve and hopefully provide direction to devise better strategies to prevent and reverse such damage. Optic nerve diffusion has been determined for other optic nerve disorders viz. ischaemic optic neuropathy, glaucoma and cryptococcal induced visual loss [5-7]. The diversity of imaging parameters available for use by the various investigating institutions for the entire range of disorders investigated has resulted in a variety of different pulse sequences and imaging protocols being used when performing diffusion studies on the optic nerve. This lack of standardization of imaging parameters has had apparently little effect on the quantitative assessment of the ON diffusion parameters. This is shown by the good consistency for the diffusion parameters determined using all these methods. Such diffusion techniques include Iwasawa's Intravoxel incoherent motion (IVIM) [8], Wheeler-Kingshott's ZOOM EPI [9], Chabert's non CPMG FSE [10] and our coronal oblique method [7] that scans the optic nerves separately. All methods unfortunately have their own limitations. The optic nerve is surrounded first by CSF within the optic nerve sheath, then by fat within a bony orbit which is bordered by paranasal sinuses containing air. In most of the optic nerve diffusion techniques, FLAIR and fat saturation are utilized to overcome the CSF and fat artifact surrounding the nerve. We have used fat saturation to overcome the fat signal and a high diffusion gradient (b1000) instead of FLAIR, to overcome the CSF artifact [7]. The benefit of this was the improved identification of the hypo-intense optic nerve on b0 images surrounded by the hyper-intense CSF in the peri-optic space. Susceptibility artifact from the bone and air are overcome by using SENSE, averaging and Rayleigh noise reduction [9]. Optic nerve motion however cannot be eradicated, but merely reduced by asking the subject to relax listen to relaxing music, and focus on a target placed in their central field of view. We asked subjects to focus on an orange sticker placed overhead on the MRI machine. Despite this,

eye movement (voluntary and/or involuntary) continues and it is not uncommon with single shot echo planar imaging (EPI) to image an apparent 'double nerve' due to movement. Neither the impact of this movement on optic nerve diffusion parameters nor the impact of movement on diffusion of the surrounding CSF has been previously investigated.

The principal aims of this study were to determine the amount of movement of the optic nerve that occurs during the timespan of a standard diffusion imaging study and determine the impact of this movement on the diffusion parameters viz. apparent diffusion coefficient (ADC), mean diffusivity (MD), fractional anisotropy (FA) and anisotropic index (AI) of the optic nerve and the peri-optic CSF space. The secondary aim was to determine if there is an association between the peri-optic CSF and optic nerve diffusion parameters when the CSF signal is not suppressed.

Method

Informed consent was obtained from healthy volunteers with intact visual acuity and oculomotor function demonstrating preserved conjugate eye movements in the horizontal and vertical axes. Full ethical approval for the study was obtained from the Greys Hospital Ethics Committee and the University of Kwazulu-Natal Ethics Department. Each volunteer underwent full neuro-ophthalmological examination to ensure normality of visual function, and an MRI scan of the orbits and brain. A Philips Gyroscan 1.5T was used for MR DWI and DTI of the brain and optic nerves using the coronal oblique technique for each nerve as previously reported [7]. Twenty-nine volunteers were recruited who demonstrated bilateral visual acuity of 6/6 or better, full range of extra-ocular movement and preserved conjugate eye movements. Twenty images using single shot EPI of the optic nerve were acquired in a plane perpendicular to the long axis of the nerve and positioned to include the orbital segment of the nerve midway between the optic canal and the globe where minimal artifact from surrounding bone and paranasal sinus air were present. Optic nerve and peri-optic CSF diffusion parameters were acquired viz. ADC, MD, FA and AI. The single shot EPI was acquired using TE = 93 ms, TR = 3000 ms, 180 mm FOV, matrix = 112 x 128 and 4 mm slice thickness. Eye

tracking using single shot EPI followed immediately after DWI and DTI of the optic nerve. Conjugate eye movements were essential as only the movement of the right optic nerve was imaged. The optic nerve movement measurements so obtained could therefore be correlated to diffusion parameters from the right and left eyes. The 20 snapshots of the optic nerve were done in 3 minutes which was the equivalent duration of the standard optic nerve diffusion study. The images were spaced at 9 second intervals from each other. During both studies, the subject was asked to fixate on an orange sticker placed in the field of view of the subject on the inner anterior surface of the MRI scanner, while relaxing and listening to light music.

Optic nerve tracking was done on the image series acquired for 20/29 volunteers using the 20 images obtained for each subject over a 3 minute period. A target of 1 pixel size was placed in the centre of the optic nerve in the coronal oblique image (Figure 1). The position of the optic nerve in image 1 was labeled as the reference point (x_1, y_1) to which all subsequent 19 images were compared. The optic nerve movement parameters viz. total distance moved from the reference point, total area of displacement and displacement in the x and y axes were recorded (Figures 2A,2B and 2C). All simulations were performed in MATLAB R2009b. The total distance from the reference point was calculated using the formula: distance$(x_{20}, y_{20}; x_{19}, y_{19})$ + distance $(x_{19}, y_{19}; x_{18}, y_{18})$ + …distance$(x_2, y_2; x_1, y_1)$, where distance $(a,b;c,d) = ((a-c)^2 + (b-d)^2)^{1/2}$ and is expressed in mm. The displacement in the x and y axes were calculated in reference to the starting points x_1 and y_1 respectively. Area of displacement was calculated as (max x – min x) x (max y – min y) and is expressed in mm^2.

The diffusion parameters viz. ADC, MD, FA and AI were obtained by imaging the optic nerves separately in the coronal oblique plane on DWI and DTI. ADC and AI were obtained on DWI whereas MD and FA were obtained from DTI. The slice approximately midway through the orbital segment of the nerve was used for analysis. A 4 pixel, square region of interest (ROI) was placed on the centre of the nerve and in the peri-optic CSF space superiorly, inferiorly, laterally and medially to the nerve. The average of the 4 quadrants of the CSF signal was used for analysis.

Statistics:

Spearman's rank correlation was used to assess the association between movement and diffusion parameters and the t-test used to test for significance. A linear regression model was fit to the diffusion measurements using data from both eyes and including a robust estimate of the standard error to allow for intra correlation between eyes. The predicted estimates from the model are plotted including the regression equation, its significance and the explained variance, R^2 Statistical Analysis was done in STATA, Version 12

Results

Of the 29 healthy volunteers recruited 26 right and 26 left eyes were analyzed for diffusion parameters due to poor visualization of the nerve in those excluded. Table 1 shows the demographic profile of the volunteers and the diffusion parameters recorded. Comparison is made to other reported diffusion sequences. As expected, the peri-optic CSF had a higher mean ADC and MD and lower mean FA and AI than the optic nerve. Of the 29 volunteers, 20 had right optic nerve tracking recorded by the single shot EPI method. The average total distance moved by the optic nerve during the 3 minutes recording was 11.8 mm (range 5.7 – 23.7) despite asking the patient to fixate on the orange sticker placed above on the MRI scanner (Table 2). Eye movement was perhaps a combination of voluntary and involuntary saccadic movement. Spearman's rank correlation showed low to moderate negative correlations between eye movement parameters and AI and FA of the optic nerve and moderate positive correlation between eye movement parameters and AI of the peri-optic space (Table 2). However none showed any significant correlation. Furthermore, no significant correlations were noted between any of the optic nerve movement parameters and ADC and MD of the optic nerve and peri-optic CSF (Table 2).

Regression analysis of MD CSF and MD optic nerve ($R^2 = 0.15$, $p = 0.02$) and AI CSF and AI optic nerve ($R^2 = 0.11$, $p = 0.02$) shows minimal association but low R^2 values (Figures 3B and D).

However between ADC CSF and ADC optic nerve ($R^2 = 0.08$, $p = 0.13$) and between FA CSF and FA optic nerve ($R^2 = 0.05$, $p = 0.06$), no significant association is found (Figures 3 A and C). Thus suggesting that the CSF signal in the coronal oblique method we used did not impact significantly on the optic nerve ADC and AI from DWI or on the FA and MD from DTI. Furthermore, table 1 shows that regardless of the diffusion sequence used i.e. with or without CSF suppression, fairly similar diffusion parameters have been reported.

Discussion

Optic nerve diffusion as an investigational tool of optic nerve structure in normal and pathological conditions is gaining in popularity [2,5,6,11,12]. Objective, reproducible and verifiable MR sequences for diffusion is paramount in maintaining this impetus. The impact of eye movement however remains a problem. Intuitively one may predict that optic nerve movement would impact on optic nerve diffusion and the diffusion of the CSF in the peri-optic space. After all, it is postulated that eye movement may provide the pumping action that circulates CSF between the intracranial subarachnoid space (SAS) and the peri-optic SAS and thus supplement the pressure gradient between those 2 spaces [13]. The range of movement between the immediate retrobulbar portion of the intra-orbital optic nerve is far more than the pre-canalicular portion which is fixed [9]. Optic nerve diffusion studies usually examine the mid portion of the orbital optic nerve which is relatively free from the susceptibly artifacts of the surrounding bone and air [1,4,14]. The amount of movement by this portion of the nerve therefore is of relevance to the diffusion parameters measured in that region. Obsessive attempts to limit this movement do result in frustrated and less co-operative subjects. Wheeler-Kingshott et al have shown that asking the subject to fixate on a point over a period of 5 minutes or more does not significantly reduce eye movement [15].

Optic nerve movement distorts diffusion imaging of the optic nerve. We lost 6 eyes from analysis due to poor visualization from eye movement. Where analysis was possible, table 1 shows us that the results obtained were reliable. The ADC, MD, FA and AI of the optic nerve obtained in this study are comparable to those of Wheeler-Kingshott et al, Iwasawa et al and Chabert et al (Table 1). The values

for the peri-optic CSF space however are novel. The peri-optic CSF has a higher ADC and MD and lower FA and AI indicative of the higher water content of the space. The greater isotropic diffusion is expected, but the AI > 1.0 reveals laminar rather than turbulent flow of CSF in this space. As to whether there is bidirectional flow of CSF within this space back intracranially [13] or unidirectional flow to the optic sheath cul-de-sac and extravasation into the orbit and optic nerve sheath lymphatics [16], cannot be determined from this data.

Despite attempts at limiting optic nerve movement both voluntary and involuntary saccadic movements are unavoidable during a 3-5 minute DWI or DTI recording. Macroscopically, the optic nerve moves appreciably during a 3 minute recording. We recorded a mean of 11.8 mm (range 5.7 – 23.7) over a mean area of 5.2 mm^2 (range 0.6-22.1). Fortunately, our data shows that optic nerve movement has no significant impact on optic nerve and peri-optic CSF diffusion parameters (Table 2). Even more pleasing is the result that not suppressing the peri-optic CSF has no significant impact on optic nerve diffusion parameters on DWI and DTI. The advantage of not suppressing the CSF signal is better identification of the nerve on b0 images and the benefit of recording peri-optic CSF diffusion parameters which can be applied to disorders such as papilloedema.

Unfortunately, we were unable to track movement of the eyes during the actual performance of DWI and DTI of the optic nerve, but this was done immediately thereafter which is a limitation of this study. Nevertheless, we do feel that the amount of movement is a good reflection of the mental and physical status of the subject as no time was wasted between imaging sequences.

We feel that this study provides convincing evidence not to suppress CSF during DWI of the optic nerve which allows for better identification of the nerve and that optic nerve movement does not impact on diffusion parameters obtained from the mid-portion of the orbital segment of the optic nerve and peri-optic CSF. While there are limitations to this study, notably the inability to track optic nerve movements and perform diffusion imaging simultaneously, and the inability to do both eyes at different angles simultaneously, we feel that the recording of optic nerve movement as obtained with

rapid sequential single shot EPI is valid and a reasonable reflection of the amount of eye movement during standard MR sequences.

Table 1: Summary of demographic data (where available), diffusion sequences and parameters of the optic nerve and peri-optic CSF

	This Study	Wheeler-Kingshott DWI study[9]	Iwasawa DWI study * [8]	Wheeler-Kingshott DTI study [15]	Trip DTI study [2]	Chabert DTI study [10]	Xu DTI study [1]	Kolbe DTI study [12]
Volunteers recruited	29	3	7	10	15	9	12	20
No. of eyes analyzed	52							
Diffusion Sequence	Coronal Oblique	ZOOM-EPI	IVIM	ZOOM_EPI	ZOOM-EPI	Non-CPMG FSE	IVI-EPI	Coronal oblique
FAT Suppression	Yes	Yes	No	Yes	Yes	No	Yes	Yes
CSF Suppression	No	Yes	No	Yes	Yes	No	No	Yes
Mean Age (Range)	30 (21-46)		30.9 (28-34)					
Females No. (%)	14 (54%)							
ADC optic nerve : Mean (SD) x 10^{-3} mm^2/s	1.30 ± (0.4)	1.058 ± (0.1)	0.98 ± (0.74)Y 1.56 ± (0.68)Z					
ADC peri-optic CSF : Mean (SD) x 10^{-3} mm^2/s	2.10 ± (0.4)							
MD optic nerve : Mean (SD) x 10^{-3} mm^2/s	1.35 ± (0.5)			1.22 ± (0.2)	1.08 ± (0.17)	1.1 ± (0.2)	1.09 ± (0.2)	1.25 ± (0.14)
MD peri-optic CSF : Mean (SD) x 10-3 mm^2/s	2.20 ± (0.3)							
FA optic nerve: Mean (SD)	0.44 ± (0.1)			0.61 ± (0.1)	0.67 ± (0.09)	0.49 ± (0.06)	0.46 ± (0.15)	0.38 ± (0.05)
FA peri-optic CSF: Mean (SD)	0.30 ± (0.08)							
AI optic nerve : Median (IQR)	1.8 (1.4-2.7)	1.57 (1.16-2.4)						
AI peri-optic CSF : Median (IQR)	1.2 (1.1-1.4)							

SD – Standard Deviation, % - percentage, ADC – Apparent Diffusion Coefficient measured using Diffusion Weighted Imaging, MD – Mean Diffusivity measured using Diffusion Tensor Imaging, FA – Fractional Anisotropy, AI – Anisotropic Index calculated as $2\lambda_1/(\lambda_2 + \lambda_3)$, where λ_1 = axial diffusion and λ_2, λ_3 = radial diffusion. IQR – interquartile range. * Iwasawa et al obtained ADC in the Y and and Z axes. ZOOM EPI – Zonal oblique multislice echo-planar imaging, IVIM – Intravoxel incoherent motion, Non-CPMG FSE – Non Carr-Purcell-Meiboom-Gill Fast spin echo, IVI-EPI –Inner Volume Imaging- Echo-planar imaging

Table 2: Amount of optic nerve movement and impact on diffusion parameters in 20 patients

	Mean (range)	vs. ADC optic nerve SCC	vs. ADC periotic CSF SCC	vs. MD optic nerve SCC	vs. MD Peri-optic CSF SCC	vs. FA optic nerve SCC	vs. FA peri-optic CSF SCC	vs. AI optic nerve SCC	vs. AI peri-optic CSF SCC
Total distance moved. mm	11.8 (5.7 – 23.7)	0.16	-0.27	0.07	-0.003	-0.32	-0.16	-0.33	0.07
Total area of displacement. mm^2	5.2 (0.6-22.1)	0.24	-0.16	0.08	-0.06	-0.28	0.15	-0.3	0.38
Displacement in the X-axis. mm	2.1 (0.8-5.1)	0.27	-0.10	0.18	0.15	-0.07	-0.03	-0.45	0.14
Displacement in the Y-axis. mm	2.2 (0.7-7.5)	0.09	-0.17	-0.07	-0.23	-0.37	0.09	-0.17	0.30

ADC – Apparent Diffusion Coefficient measured using Diffusion Weighted Imaging, MD – Mean Diffusivity measured using Diffusion Tensor Imaging, FA – Fractional Anisotropy, AI – Anisotropic Index calculated as $2\lambda_1/(\lambda_2 + \lambda_3)$, where λ_1 = axial diffusion and λ_2, λ_3 = radial diffusion. SCC – Spearman's Correlation Coefficient: Low or no correlation $0 \leq r < 0.3$, Moderate correlation $0.3 \leq r < 0.7$, Strong correlation $0.7 \leq r \leq 1$. (- indicates negative correlation)

Figure 1: EPI Snapshot of coronal oblique view of the right optic nerve

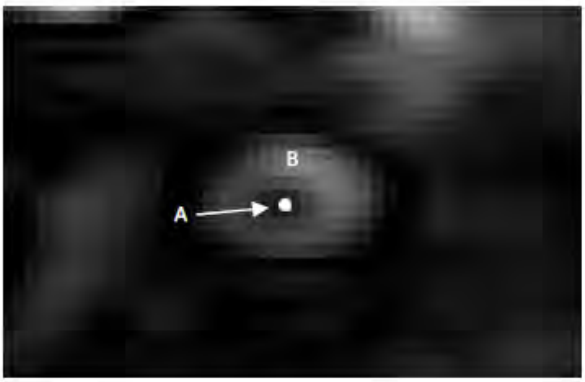

A pixel size target (white dot) was placed on the centre of the optic nerve and movement recorded over 3 minutes with 20 snapshots. A – Optic nerve. B - Peri-optic CSF space.

Figure 2: Movement of the optic nerve in 20 snapshots. A – x-axis, B – y-axis, C – x-y plane

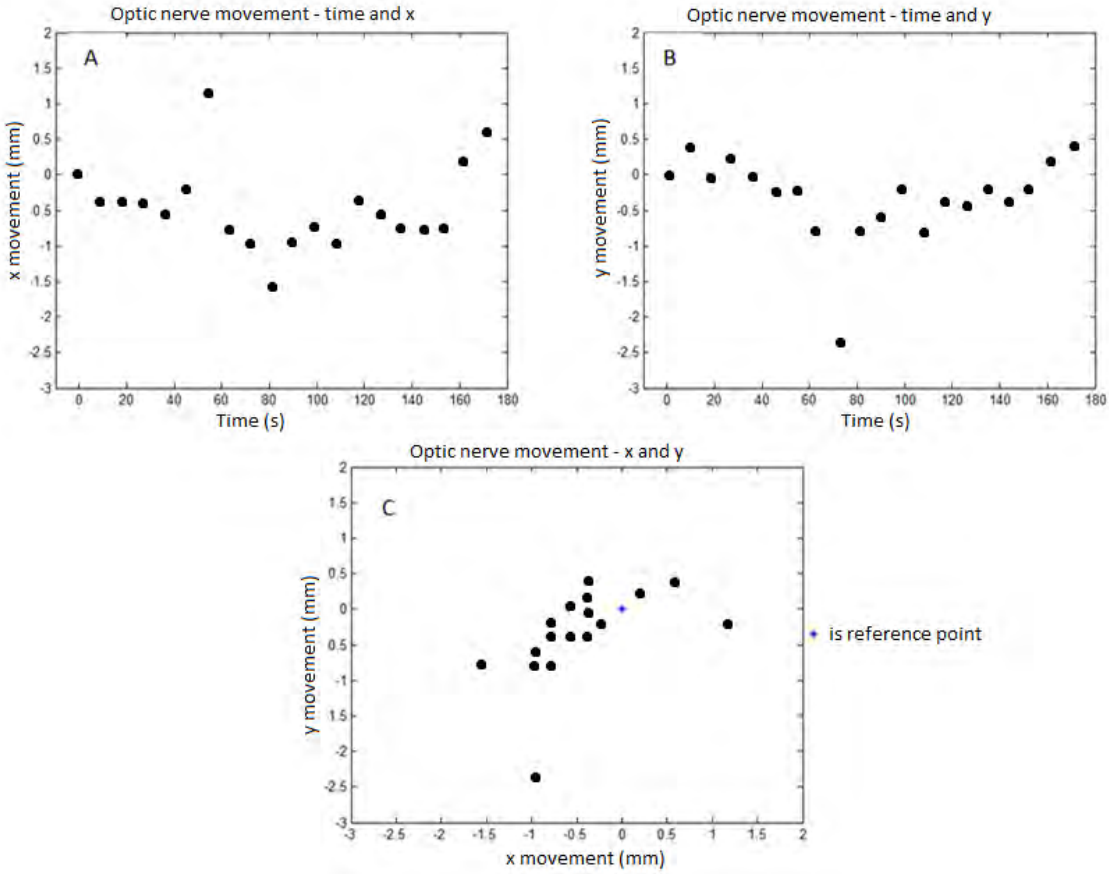

Figure 3: Diffusion parameters of Optic nerve vs. peri-optic CSF. A- ADC, B – MD, C – FA, D – AI

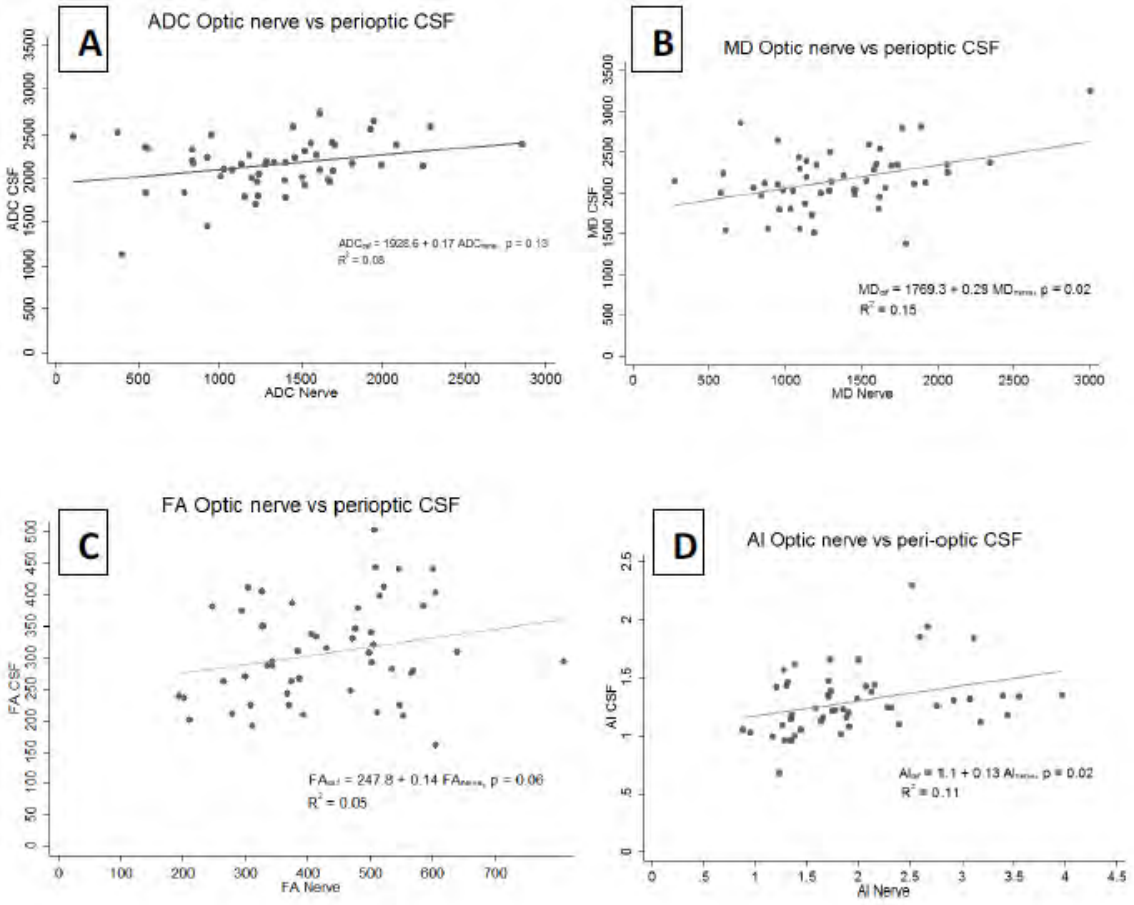

ADC- Apparent Diffusion Coefficient, MD – Mean Diffusivity, FA – Fractional Anisotropy, AI – Anisotropic Index

References

1. Xu J, Sun SW, Naismith RT, Snyder AZ, Cross AH, et al. (2008) Assessing optic nerve pathology with diffusion MRI: from mouse to human. NMR Biomed 21: 928-940.

2. Trip SA, Wheeler-Kingshott C, Jones SJ, Li WY, Barker GJ, et al. (2006) Optic nerve diffusion tensor imaging in optic neuritis. Neuroimage 30: 498-505.

3. Zhang Y, Wan SH, Wu GJ, Zhang XL (2012) Magnetic resonance diffusion tensor imaging and diffusion tensor tractography of human visual pathway. Int J Ophthalmol 5: 452-458.

4. Fatima Z, Motosugi U, Muhi A, Hori M, Ishigame K, et al. (2012) Diffusion-Weighted Imaging in Optic Neuritis. Can Assoc Radiol J.

5. Cauquil C, Souillard-Scemama R, Labetoulle M, Adams D, Ducreux D, et al. (2012) Diffusion MRI and tensor tractography in ischemic optic neuropathy. Acta Neurol Belg 112: 209-211.

6. Chen Z, Lin F, Wang J, Li Z, Dai H, et al. (2012) Diffusion tensor MRI reveals visual pathway damage that correlates with clinical severity in glaucoma. Clin Experiment Ophthalmol.

7. Moodley A, Rae W, Bhigjee A, Loubser N, Michowicz A (2012) New Insights into the Pathogenesis of Cryptococcal Induced Visual Loss Using Diffusion-Weighted Imaging of the Optic Nerve. Neuro-ophthalmology 36: 186-192.

8. Iwasawa T, Matoba H, Ogi A, Kurihara H, Saito K, et al. (1997) Diffusion-weighted imaging of the human optic nerve: a new approach to evaluate optic neuritis in multiple sclerosis. Magn Reson Med 38: 484-491.

9. Wheeler-Kingshott CA, Parker GJ, Symms MR, Hickman SJ, Tofts PS, et al. (2002) ADC mapping of the human optic nerve: increased resolution, coverage, and reliability with CSF-suppressed ZOOM-EPI. Magn Reson Med 47: 24-31.

10. Chabert S, Molko N, Cointepas Y, Le Roux P, Le Bihan D (2005) Diffusion tensor imaging of the human optic nerve using a non-CPMG fast spin echo sequence. J Magn Reson Imaging 22: 307-310.

11. Hickman SJ, Wheeler-Kingshott CA, Jones SJ, Miszkiel KA, Barker GJ, et al. (2005) Optic nerve diffusion measurement from diffusion-weighted imaging in optic neuritis. AJNR Am J Neuroradiol 26: 951-956.

12. Kolbe S, Chapman C, Nguyen T, Bajraszewski C, Johnston L, et al. (2009) Optic nerve diffusion changes and atrophy jointly predict visual dysfunction after optic neuritis. Neuroimage 45: 679-686.

13. Killer HE, Jaggi GP, Flammer J, Miller NR, Huber AR, et al. (2007) Cerebrospinal fluid dynamics between the intracranial and the subarachnoid space of the optic nerve. Is it always bidirectional? Brain 130: 514-520.

14. Naismith RT, Xu J, Tutlam NT, Trinkaus K, Cross AH, et al. (2010) Radial diffusivity in remote optic neuritis discriminates visual outcomes. Neurology 74: 1702-1710.

15. Wheeler-Kingshott CA, Trip SA, Symms MR, Parker GJ, Barker GJ, et al. (2006) In vivo diffusion tensor imaging of the human optic nerve: pilot study in normal controls. Magn Reson Med 56: 446-451.

16. Ludemann W, Berens von Rautenfeld D, Samii M, Brinker T (2005) Ultrastructure of the cerebrospinal fluid outflow along the optic nerve into the lymphatic system. Childs Nerv Syst 21: 96-103.

CHAPTER 6 PAPER 3

Neurological, visual, and MRI brain scan findings in 87 South African patients with HIV-associated cryptococcal meningoencephalitis.

- This paper addresses aims 3.1 (3.1.1, 3.1.2, 3.1.3, 3.1.4)
- A Moodley and A Loyse are equally responsible for writing this paper.
- The paper has been submitted to *Clinical Infectious Disease* and is awaiting review

Eighty seven patients with culture confirmed CM underwent MRI scanning within 2 weeks of presentation. Eleven patients had a repeat scan at 1 month follow up. The neurological, visual and MRI findings of these patients are presented in this paper.

In this cohort of 87 patients, the median CD4 count was 29 (IQR 12-69), 22% were on ARV's at diagnosis and 6% had abnormal mental status. 71% had elevated intracranial pressure and the median opening pressure was 30cmCSF (IQR 18-42). The median fungal burden at MRI scanning of 26 patients was 4.71 log CFU/mL of CSF [3.58-5.64].

33/85 (39%) patients had an abnormal finding on neurological examination. 19 patients complained of diplopia, and 18/85 patients (21%) had cranial nerve (CN) palsies. 14/18 (78%) CN palsies were VIth nerve palsies, of which seven were bilateral. 3/18 (17%) patients had VIIIth nerve palsies. 19/85 (22%) patients had abnormal coordination and, for the 78 patients who were ambulant, 15/78 (19%) patients had an abnormal gait.

In 38/85 (48%) patients, a best corrected visual acuity measurement of <6/6 was found on examination of either eye on the day of MRI scanning. In 31/38 (82%) patients the visual loss was bilateral.

In 2/87 (2.2%) of patients, the MRI scan was reported as normal. There were 55/87 (63%) patients with cryptococcal related radiological lesions viz. enlarged VRS 31/87 (36%), pseudocysts 19/87 (22%), meningeal enhancement 24/87 (28%), enhancing nodules 23/87 (27%), lacunar infarcts 12/87 (14%), cortical infarcts 5/87 (6%), cerebral oedema 14/87 (16%) and hydrocephalus 2/87 (2%). Visual loss correlated with the presence of presumed cryptococcal-related lesions ($p = 0.02$)

Paired scans show that brain swelling is not common early in CM and perhaps does not contribute to raised intracranial pressure.

Neurological, visual, and MRI brain scan findings in 87 South African patients with HIV-associated cryptococcal meningoencephalitis.

Loyse A [1,2,3,4], Moodley A [5], Rich P [6], WID Rae[7], AI Bhigjee[8], ND Loubser[5], AJ Michowicz[3], Leesa Bishop[3], Douglas Wilson[5], Thomas S Harrison[4]

1. Infectious Diseases Unit, GF Jooste Hospital, Cape Town, South Africa
2. Desmond Tutu HIV Centre, Institute of Infectious Disease and Molecular Medicine, University of Cape Town, South Africa
3. Department of Medicine, Edendale Hospital, Pietermaritzburg, South Africa
4. Cryptococcal Meningitis Group, Research Centre for Infection and Immunity, Division of Clinical Sciences, St. George's University of London, UK
5. Department of Neurology, Grey's Hospital, Pietermaritzburg, South Africa
6. Department of Neuroradiology, St George's Hospital, London, UK
7. Department of Medical Physics, University of the Free State, South Africa
8. Department of Neurology, University of KwaZulu Natal, South Africa

*AL and AM contributed equally to this study

Keywords:

Cryptococcal meningitis; HIV; MRI; radiology; clinical correlations; visual loss; cryptococcomas; dilated Virchow Robin spaces; hydrocephalus; radiological meningitis; HIV-encephalopathy (HIVE); lacunar infarct; cortical infarct; brain swelling.

Contact details:

Corresponding author:

Dr Angela Loyse

Cryptococcal Meningitis Group,

Research Centre for Infection and Immunity,

Division of Clinical Sciences,

St. George's University of London,

Blackshaw Rd

London

SW17 0QT

UK

Tel: 00442087250443

Fax: 00442087253487

E-mail: angelaloyse@hotmail.com

Data presented in part at 52nd Interscience Conference on Antimicrobial Agents and Chemotherapy in San Franscisco, California, US.

Word count: 3010

Abstract

Background

HIV-associated cryptococcal meningoencephalitis (CM) is a leading cause of adult meningitis in sub-Saharan Africa. Neuroradiological data is however limited to case reports and small case series from developed countries and/or immunocompetent patients.

Methods

87 patients aged ≥18 hospitalized with a first episode of CM had magnetic resonance imaging (MRI) imaging during the first two weeks of admission. A subset of 11 patients had follow-up scans approximately one month from their initial MRI scan. All had prospectively-recorded, detailed neurological and visual examinations.

Results

33/85 (39%) patients had an abnormal finding on neurological examination. 38/85 (48%) of patients had visual loss, as defined by a visual acuity of <6/6 in either eye. 55/87 (63%) patients had neuroradiological lesions presumed to be cryptococcosis-related, as defined by the presence of: dilated Virchow Robin spaces (36%), pseudocysts or cryptococcomas (22%), enhancing nodules (27%), infarcts (20%), meningitis (28%), focal peri-lesional oedema (16%) and hydrocephalus (2%). 18/87 (21%) had MRI findings suggestive of a second diagnosis. All three patients with motor deficits had cortical infarcts on MRI scan. Visual loss correlated with the presence of presumed cryptococcal-related lesions (p=0.02). Of 11 patients with paired scans, brain swelling was identified on the initial scan in only one patient, whose cerebrospinal fluid (CSF) opening pressure was over 50 cmH_2O.

Conclusion

The majority of patients had MRI brain scan abnormalities presumed secondary to CM. Scanning may also suggest additional treatable diagnoses. Visual loss was associated with the degree of cerebral involvement as reflected by the presence of MRI abnormalities. Initial generalised brain swelling does not appear to be common, but further studies with paired scans are needed.

Background

CM is a leading cause of adult onset meningoencephalitis in sub-Saharan Africa [1-4]. CM-associated mortality remains unacceptably high, with reported ten week mortality rates ranging between 20 and 50% worldwide, and an estimated 500 000 deaths annually in the developing world [1,5,6,7].

Neuroradiological lesions related to CM include: dilated periventricular spaces, masses, pseudocysts, cryptococcomas, basal meningitis and hydrocephalus [8-16]. Magnetic resonance imaging (MRI) is a more sensitive modality for the detection of neuroradiological lesions in cryptococcosis than computed tomography (CT) [11,13,14]. In a recent French cohort of 62 patients with CM, baseline brain imaging was reported as abnormal in 92% of MRI scans performed compared to 53% of CT scans [14]. Furthermore, for the 17 patients who underwent both modes of imaging, MRI imaging detected significantly more cryptococcosis-related lesions than CT imaging (78% versus 24% respectively, p=0.005) [14].

This case series from France represents the largest clinically correlated series of MRI images to date, and included MRI scans from 24 patients. Radiological data from CM patients is otherwise limited to case reports and smaller case series from the USA, South America, Western Europe and, most recently, from immunocompetent patients in China and Taiwan [8-16]. Herein we present a clinically correlated case series of MRI findings from 87 South African patients with HIV-associated CM. Neuroradiological findings were correlated with prospectively-collected clinical features derived from full neurological and visual examinations by a resident consultant neurologist, and clinical outcomes.

Methods

Study population

Between September 2008 and October 2010, 87 patients were recruited at Edendale and Grey's Hospital Hospital in Pietermaritzburg, Kwazulu-Natal, South Africa. The study was approved by the Research Ethics Committees of the University of Kwazulu-Natal, Edendale Hospital, Grey's Hospital, St George's Hospital (London) and the Kwazulu-Natal Department of Health. 26 patients were recruited as part of a previously described phase II randomised controlled trial at Edendale Hospital of amphotericin B deoxycholate (AmBd)-based combination antifungal therapy for the treatment of CM [17].

HIV-infected patients aged ≥18 hospitalized with a first episode of CM diagnosed by CSF India ink were eligible for enrollment. CM was confirmed by positive cerebrospinal fluid (CSF) culture for *C neoformans*. Written informed consent was obtained from each patient, or next of kin for patients with altered mental status (Glasgow Coma Scale (GCS) <15). All patients received AmBd-based antifungal therapy.

Parameters

The following blood tests were performed on all study patients prospectively: CD4 count, Full Blood Count (FBC), Urea & Electrolytes (U&Es), Liver Function tests (LFTs), blood glucose (BG) and HIV testing. The patients' CSF was examined for the following: opening pressure (OP), microscopy, culture and sensitivity (MC&S), total protein (TP), glucose (CSF and serum) and India Ink staining (II). Two and ten week clinical outcome, weight and baseline fungal burden data were available in addition for the 26 patients enrolled as part of the trial of combination antifungal therapy [17].

All recruited patients had a full neuro-ophthalmological examination by a resident consultant neurologist, Dr Anand Moodley, on the day of MRI scanning. Neurological examination included examination of higher functioning, cranial nerve examination, full motor and sensory neurological examination, and an assessment of coordination and gait. Pupillary reflexes, visual fields, best corrected visual acuity and fundoscopy examinations were performed.

Radiological investigations & findings

A neuroradiologist, Dr Philip Rich, blinded to patient clinical data and outcomes, analysed the radiological data retrospectively. MRI scanning was performed during the initial two weeks of induction therapy. A subset of 11 patients, from the 26 patients recruited to the aforementioned trial of combination antifungal therapy, had follow-up scans approximately one month from their initial MRI scan.

All MRI examinations were acquired on the same 1.5 Tesla scanner and included the following sequences: sagittal T1-weighted, axial T1-weighted, T2-weighted, Fluid attenuated inversion recovery (FLAIR) and diffusion weighted imaging (DWI), supplemented by gadolinium contrast enhanced scans in one or more planes. A full neuroradiological review of each scan was undertaken and specific features sought relating to cryptococcal and HIV infection.

Consistent with earlier published work, we defined dilated Virchow-Robin spaces (VRS) as dilated if they measured between 2-3 mm in diameter (on the axial T2 weighted scan) and cystic spaces measuring >3mm diameter were diagnosed as cryptococcoma/pseudocysts [18]. Hydrocephalus was diagnosed if there was ventricular dilatation with ballooning of third ventricular recesses and temporal horns, or periventricular signal abnormality suggestive of increased transependymal CSF flux. Cerebral atrophy was judged and graded subjectively on

the basis of enlarged cerebral sulci and ventricular dilatation in a non-hydrocephalic pattern. An assessment of brain swelling was possible in 11 cases with paired scans in which there was a change in the size of cerebral sulci and ventricles between the two examinations, apart from the two patients who had documented hydrocephalus on their initial MRI scan.

Other CM related MRI findings recorded were meningitis (abnormal brain surface enhancement or meningeal thickening on contrast-enhanced scans), enhancing nodules (small lesions without mass effect) or other areas of abnormal enhancement and any perilesional oedema. Areas of restricted diffusion were documented and, depending on appearance and location, were diagnosed as lacunar infarcts or other conditions. Cortical infarcts were also recorded. Signs of co-existing HIV Encephalopathy (HIVE) or Progressive Multifocal Leukoencephalopathy (PML) and any lesions suggestive of toxoplasmosis or tuberculomas were also sought. Non-specific white matter lesions were categorised as minor (<1 lesion per scan slice; effectively within normal limits), mild (scattered small dots), moderate (irregular patches or mixed dots and patches) and severe (diffuse confluent lesions). The latter three stages approximate to one of the validated rating scales commonly used in assessment of small vessel ischaemic change on MRI [19].

Statistical analysis

Statistical analyses were performed using STATA version 12.0 (STATA Corporation, College Station, Texas, USA). The chi-square or Fischer's exact test was used to assess associations between discrete variables and linear regression used to assess linear relationships between continuous and discrete variables.

Results

Patient characteristics

The median patient age was 34 [IQR 29-37] years. 48/87 (55%) of patients were male. All patients tested HIV positive. The median CD4 count was 29 /mm^3 [IQR 12-69]. 19/87 (22%) patients were receiving antiretroviral treatment. Data for 87 patients with MRI imaging, 85 patients with full neurological examination, and 71 patients who had visual fields done are presented. 5/87 (6%) patients had abnormal mental status. 71% patients had raised intracranial pressure (ICP) at the time of the MRI scan with a median opening pressure (OP) of 30 cm H_20 [IQR 18-42]. The median interval between onset of symptoms and MRI scanning was 21 [IQR 14-28] days. The median interval between start of antifungal treatment and MRI scanning was 7 [IQR 6-12] days.

For the subset of 26 patients with additional clinical data available, the median weight was 60 kg [IQR 50-68] and the median fungal burden at MRI scanning was 4.71 log CFU/mL of CSF [3.58-5.64]. All 26 patients were alive at two weeks but 5/25 (20%) died by ten weeks and one patient was lost to follow-up.

Neurological examination findings

33/85 (39%) patients had an abnormal finding on neurological examination. 19 patients complained of diplopia, and 18/85 patients (21%) had cranial nerve (CN) palsies. 14/18 (78%) CN palsies were VIth nerve palsies, of which seven were bilateral. One patient had concurrent 7th nerve palsy. 3/18 (17%) patients had 8th nerve palsies and one patient had a partial left 3rd nerve palsy. A motor deficit was detected in 3/85 (4%) patients and one patient had a demonstrable sensory deficit. 19/85 (22%) patients had abnormal coordination and, for the 78 patients who were ambulant, 15/78 (19%) patients had an abnormal gait. Abnormal coordination signs were appendicular and included mild, bilateral impaired finger-to-nose, rapid alternating movements and heel-knee-shin testing, ataxic gait and impaired tandem walking. Patients did not exhibit nystagmus, speech abnormalities or titubation.

Additional visual examination findings

52/85 (61%) patients reported a subjective deterioration in their vision prior to MRI scanning and for 5/52 (10%) of patients the onset of the visual loss was acute, occurring over less than a week. The visual loss was pre-chiasmal. In 38/85 (48%) patients, a best corrected visual acuity measurement of <6/6 was found on examination of either eye on the day of MRI scanning. In 31/38 (82%) patients the visual loss was bilateral.

3/71 (4%) patients had large blind spots and constricted visual fields. 26/84 (31 %) patients had a swollen optic disk. 14% and 13% patients had a relative afferent pupillary defect detected in their right and left eyes respectively. 4 patients (5%) had optic atrophy in a single eye.

Radiological findings

Only 2/87 (2%) patients had a MRI scan reported as entirely normal, although in 12/87 (14%) additional patients the only radiological abnormalities detected were non-specific white matter changes. 55/87 (63%) patients had lesions presumed to be cryptococcosis-related, as defined by the presence of: masses/enhancing nodules, dilated Virchow Robin spaces [figure 1], pseudocysts or cryptococcomas [figure 2], enhancing nodules [figure 3], hydrocephalus [figure 4], meningitis [figure 5], focal oedema and infarcts. Focal (i.e. perilesional) cerebral oedema occurred in 14 (16%) patients. There was some degree of hydrocephalus in 2/87 (2%) patients, but both cases were mild with associated meningeal enhancement. Lesions showing restricted diffusion, thought to represent cryptococcosis-related lacunar infarcts, occurred in 12 (14%) patients [figure 6].

18/87 (21%) patients had other significant MRI findings, thought unrelated to cryptococcosis: sinusitis (3/87 (3%) patients), ring enhancing lesions (6/87 (7%) patients, suggestive of the possibility of toxoplasmosis or tuberculosis) and miscellaneous abnormalities (1 each of meningioma, pituitary adenoma, anterior communicating aneurysm, cavernoma, upper cervical prevertebral collection, and an old cavity of uncertain aetiology in the left pre-central gyrus).

Clinical correlations with MRI findings

All three patients with motor deficits had cortical infarcts on MRI scan (p=0.02). Visual loss, as defined by a best corrected visual acuity of <6/6 in either eye, correlated with the presence of presumed cryptococcal-related lesions (p=0.02). When MRI findings were examined individually, associations were identified between visual loss and the presence of dilated Virchow Robin spaces (p=0.05), and cryptococcomas or pseudocysts (p=0.05). No other significant associations were found between, for example, altered mental status, raised CSF pressure, CD4 count, whether on ART or ART-naïve, and, when available, fungal burden at presentation, and survival, and particular MRI findings.

Regarding possible mechanisms of visual loss, patients with swollen optic disks and sixth nerve palsies had high CSF pressure [Median pressure without swollen disk: 25 [C.I 22.27-27.72], median pressure with swollen disk: 44 [C.I 41.9-46.1], p< 0.001; median pressure without 6th nerve palsy: 30 [C.I 27.17-32.83], median pressure with 6th nerve palsy: 47.5 [C.I 44.48-50.52], p=0.02]. Patients with a relative afferent nerve lesion had reduced visual acuity (VA). However, in this small dataset, no significant association was found between raised ICP and visual loss [Median pressure without reduced VA (defined as <6/6 in either eye): 30 [C.I 27.06-32.94], median pressure with reduced VA: 32.5 [C.I 29.41-35.59], p=0.428].

Paired scan data

11 patients had follow-up scans at a median of 41 days from initial MRI scanning for comparison. Of note, when comparing paired scans, initial brain swelling which had improved on follow-up scanning was only identified on one initial MRI scan (patient 4) [figure 7]. CSF OP for patient 4 was over 50 cmH_2O. No change in MRI appearances was noted between initial and follow-up scans for two patients (patients 1,11) [Table 2]. Improved radiological appearances were noted for four patients (patients 2,3,5,6), with, for example, less pronounced dilated VRS, radiological meningitis or resolved hydrocephalus. The appearances of scans for a further two patients had improved overall, but both follow-up MRI scans showed new cerebellar lesions (patients 7,8). Lastly, the radiological appearances for three patients had deteriorated significantly (patients 4,9,10) [Table 2].

Patient 9 (baseline CD4 14) was treated with concurrent antituberculous therapy and also developed subsequent *Klebsiella* sepsis. On the basis of new ring-enhancing nodules on follow-up scanning, patient 9 was empirically treated for toxoplasmosis and the lesions subsequently regressed [figure 8]. Patient 10 (baseline CD4 27) was on concurrent antituberculous therapy for culture proven TB adenitis. Following discharge, prior to starting antiretroviral therapy, the patient developed acute on chronic visual and hearing loss, recurrent headaches and vomiting. Follow-up MRI scanning demonstrated new, significant radiological abnormalities[Table 2]. Repeat lumbar puncture was acellular, India Ink positive with a rising total protein but culture (including prolonged fungal and TB culture) negative. Empirical therapy consisted of AmBd, a broad spectrum cephalosporin, antituberculous therapy and dexamethasone. Fundoscopy demonstrated CMV retinitis and intraocular ganciclovir was commenced. Despite these measures, the patient died two months following readmission, having sustained two cerebrovascular accidents. Tuberculous meningitis was thought the most likely diagnosis.

Discussion

These results form the largest case series of clinically correlated MRI findings from severely immunosuppressed, HIV-infected CM patients from Kwazulu-Natal, South Africa. The detailed neurological and visual assessments performed significantly add to the data available on neurological and visual signs present in CM patients in this setting.

MRI scanning has again been demonstrated here to be an extremely sensitive imaging modality in the setting of central nervous system (CNS) cryptococcosis [14]. The overall percentage of presumptive cryptococcosis-related lesions radiological findings is in line with results from the French case series (63% (55/87) vs 79% (19/24) presumed cryptoccosis-related lesions, respectively) [14]. We detected significant numbers of patients with focal oedema (16% (14/97). No patients with generalised oedema were detected in the French series. 2% (2/87) patients had hydrocephalus versus 0% (0/24) in the French series, and we detected more cases of pseudocysts/cryptococcomas, radiological meningitis and infarcts [14]. These discrepancies might be explained by differences in the radiological definitions used, the relatively small sample sizes, and the disparate patient populations studied. Oedema was defined here as focal and reactive to an underlying lesion. Reported hydrocephalus was mild. Variations in radiological diagnoses of hydrocephalus may vary between radiologists as it is a judgement based on the size and shape of the ventricles rather than a precise measurement.

In this case series, 20/87 (20%) patients had either cortical or lacunar infarcts that were presumed to be CNS cryptococcosis-related. This finding is in keeping with recent Taiwanese data from immunocompetent patients where acute/subacute cerebral infarction (ASCI) occurred in 7/37 (20%) of patients [15]. Cerebral infarction, presumably related to

some vascular, or perivascular inflammation, may not be uncommon in CM even in profoundly immunosuppressed patients with low CD4 cell counts.

In this dataset, visual loss significantly correlated with the presence of presumed cryptococcosis-related lesions. Contrary to our clinical experience, visual loss did not correlate with raised ICP in this small patient sample [20], and few patients (4/85, 5%) had a demonstrable relative afferent defect. The lack of a correlation between visual loss and raised ICP is most likely because the CSF OP measurement was not systematically performed on the same day as the visual assessment. While undoubtedly patients with extremely high CSF pressure are at risk of visual loss, which can recover when pressure is controlled, this data suggests that the mechanisms underlying CNS cryptococcosis-related visual loss may be multifactorial, and in some cases visual loss may be due to the combination of raised ICP and optic neuritis [20]. Elevated CSF pressure no doubt plays a significant role but recent studies indicate that the site of optic nerve compression from raised pressure is not at the lamina cribrosa but at the optic canal segment. Elevated CSF pressure occurs in 69% of CM patients but papilloedema occurs in only 25% suggesting that compression occurs upstream at the optic canal level. With the immense fungal loading, elevated CSF pressure and narrow optic canal, a possible compartment syndrome develops between the intracranial and intra-orbital optic nerve segments resulting in visual loss [21,22]. The finding of early asymptomatic optic nerve dysfunction on electrophysiological testing is also good evidence of pre-chiasmatic optic nerve pathophysiology.

It is difficult to determine the presence of brain swelling on a single brain scan in the context of late stage HIV-disease when significant but variable degrees of cerebral atrophy are very common. We were particularly interested to see if paired initial and follow up scans suggested the presence of initial relative brain swelling in the first few days after presentation when any inflammatory response is likely to be maximal [23]. However, initial brain swelling

was only identified in one patient on this basis. Brain swelling may not be a common or significant factor in explaining the raised CSF pressure or abnormal mental status associated with CM. However, in the study initial MRI scanning was carried out a median of seven days from patients starting antifungal therapy and it is conceivable that this was perhaps too late to detect early brain swelling that may have improved after initial antifungal therapy and appropriate management of CM complications such as raised ICP. Further studies including larger numbers of patients, more patients with abnormal mental status, earlier scans, and specific radiological techniques to identify small differences in brain volume, are required to elucidate the role of brain swelling in CNS cryptococcosis.

The deterioration in the radiological appearances of three patients on follow-up MRI scanning was in keeping with their lack of clinical progress. A significant number of patients (18/87 (21%)) had significant secondary diagnoses identified on scanning requiring additional treatment, or monitoring. Scaling up of brain imaging facilities in resource poor settings is required to not only aid the management of CM, but to identify the significant number of patients who have a secondary diagnosis evident on brain scan.

	n (%)
Total	**87**
Normal Imaging	2 (2)
Presumed Cryptococcal –related lesions	55 (63)
VRS Dilatation	31 (36)
Pseudocysts/Cryptococcomas	19 (22)
Radiological meningitis	24 (28)
Intracerebral mass(es)/nodules	23 (27)
Lacunar Infarcts	12 (14)
Cortical Infarcts	5 (6)
Cerebral Oedema	14 (16)
Hydrocephalus	2 (2)
Other lesions:	
HIV-encephalopathy	9 (10)
Cerebral atrophy	39 (45)
Non-specific white matter changes	74 (85)
Other:	18 (21)
Ring enhancing lesions	6 (7)
Sinusitis	3 (3)
Miscellaneous	9 (10)

Table 1. Radiological findings

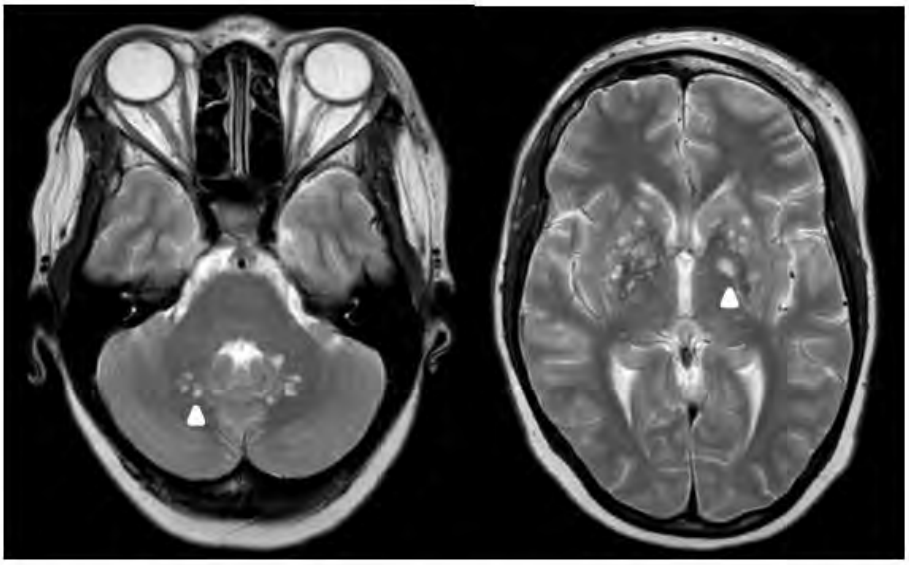

Figure1. Axial T2 -weighted scans through the cerebellum (1st scan) and basal ganglia showing multiple abnormally dilated perivascular spaces – arrow heads.

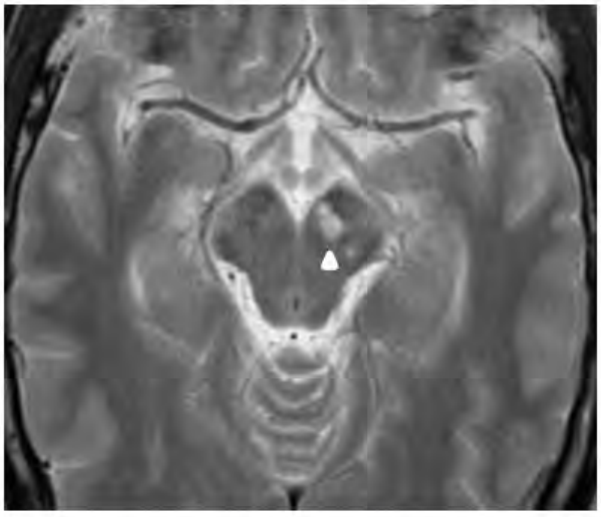

Figure 2. Axial T2-weighted scan showing a cryptococcoma/ pseudocyst in the left side of the midbrain – arrow head. Cavities larger than 3mm in diameter defined as cryptococcoma/pseudocysts.

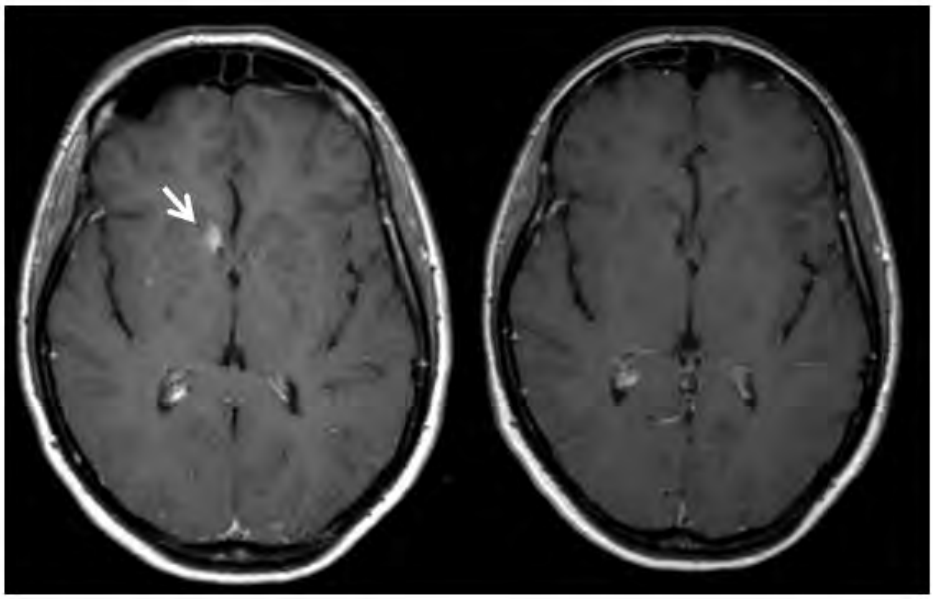

Figure 3. Paired axial T1-weighted scans post gadolinium contrast enhancement. There is an enhancing nodule in the head of the right caudate nucleus (arrow) which has regressed on the second scan.

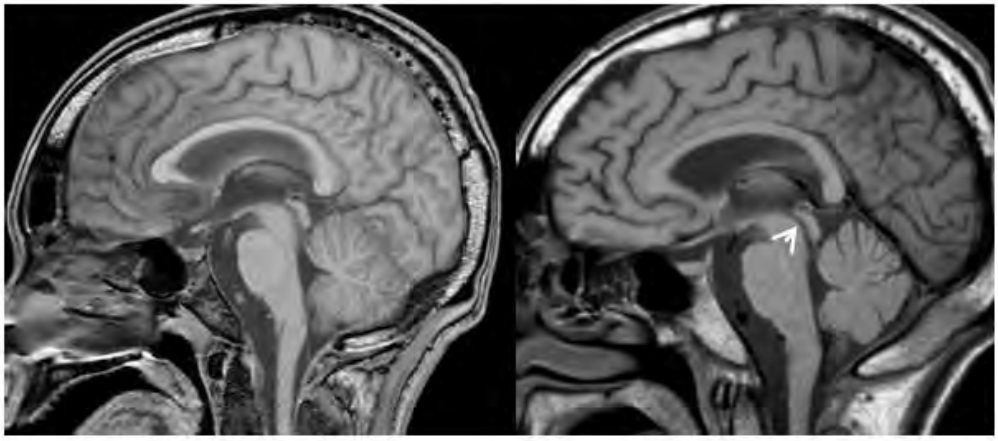

Figure 4. Paired sagittal T1-weighted scans show mild hydrocephalus on the first scan. Note reduction in width of the cerebral aqueduct on second scans - arrow.

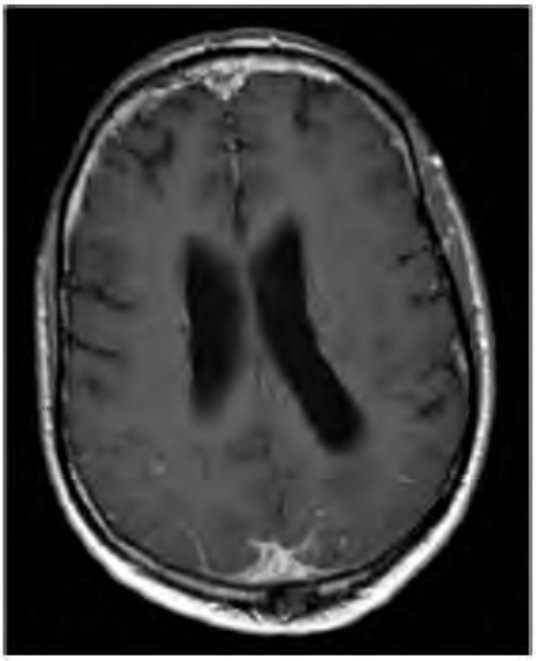

Figure 5. Axial T1-weighted post gadolinium contrast enhancement showing abnormal enhancement in parietal sulci bilaterally due to leptomeningeal inflammation and thickening of the meninges.

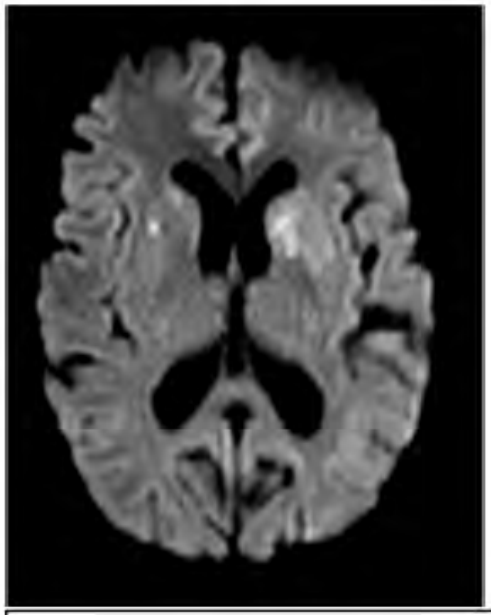

Figure 6.
Axial diffusion weighted imaging shows bilateral basal ganglia acute lacunar infarcts.

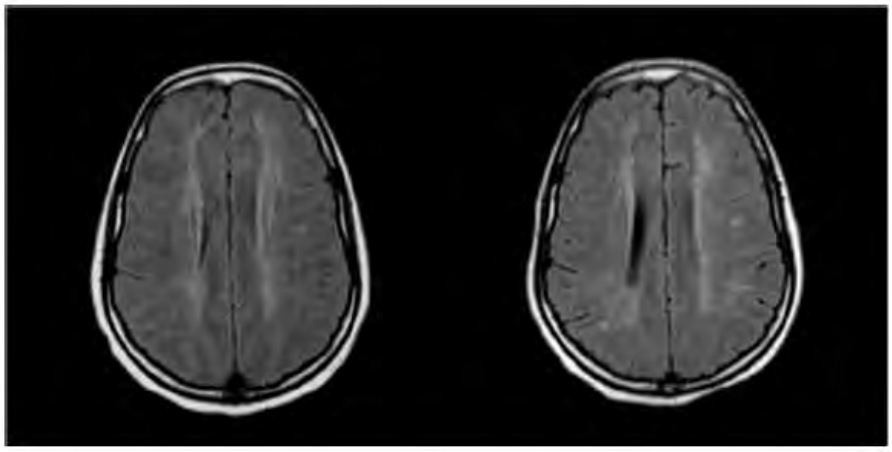

Figure 7. Paired axial FLAIR (Fluid attenuated inversion recovery) scans show brain swelling on first scan with regression subsequently – note increased width of lateral ventricles and cerebral sulci on second scan. Widespread white matter signal changes are also shown on both scans.

Patient	Initial Scan	Follow-up scan	Brain volume comparison*	Concurrent diagnoses
1	Nonspecific white matter changes	No change	No change in brain volume	
2	Mild hydrocephalus, meningitis left insula (mild), HIVE, cerebral atrophy (mild), nonspecific white matter changes	No change except for reduced radiological meningitis & less non-specific white matter changes	Hydrocephalus on initial scan so unable to comment on brain size	
3	Dilated VRS, midbrain cryptococcoma, mild diffuse meningitis, enhancing nodule right caudate	Right caudate scarring, reduced radiological meningitis	No change in brain volume	?TB (pulmonary)
4	Dilated VRS, diffuse brain surface meningitis, enhancing pallidum caudates, oedema surrounding left occiput, restricted diffusion, cortical and lacunar infarcts, non-specific white matter changes, brain swelling	More extensive dilated vrs, mild hydrocephalus, cavitated pallidum caudates, more extensive nonspecific white matter changes	Less brain swelling	Gram negative sepsis, Probable PID, ?TB
5	Mild cerebral atrophy, mild nonspecific white matter changes	No change	No change in brain volume	
6	Mild cerebral atrophy, mild nonspecific white matter changes	No change	No change in brain volume	

* initial versus follow-up scan

Table 2. Paired Scan Findings

Patient	Initial Scan	Follow-up scan	Brain volume comparison *	Concurrent diagnoses
7	Mild meningitis, small enhancing nodule left caudate, mild cerebral atrophy, moderate nonspecific white matter changes	Improved appearances of radiological meningitis, new white matter changes left cerebellum	No change in brain volume	
8	Mild cerebral atrophy, minor white matter changes, paranasal sinus disease	Small acute right cerebellar cortical infarct, new restrictive defect in cerebellum	No change in brain volume	
9	Mild hydrocephalus, diffuse surface enhancement brain, meningeal enhancing nodules, minor non-specific white matter changes	Improved hydrocephalus, new ring enhancing lesions which regressed after treatment for toxoplasmosis	Hydrocephalus on initial scan so unable to comment on brain size	?toxoplasmosis ?Cryptococcal IRIS
10	Dilated VRS, bilateral basal ganglia cryptococcomas, mild meningitis, localised right posterior temporal oedema, mild non-specific white matter changes	Smaller dilated VRS, slightly smaller cryptococcomas, increased radiological meningitis with shallow frontal subdural collections, regressed oedema, more extensive non-specific white matter changes	No change in brain volume	?TB meningitis
11	No radiological abnormality detected	No change	No change in brain volume	

* initial versus follow-up scan

Table 2. Paired Scan Findings (continued)

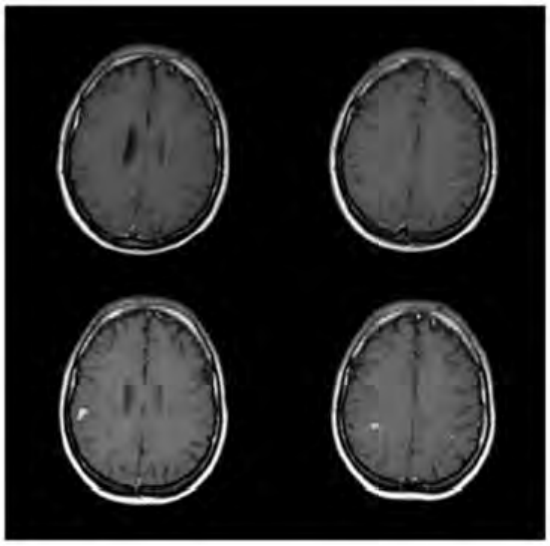

Figure 8. Paired axial T1 post contrast scans show progression of brain surface enhancement and development of enhancing nodules (paired follow-up scans shown below).

References

1. Park B.J, Wannemuehler KA, Marston BJ, *et al.* Estimation of the global burden of cryptococcal meningitis among persons living with HIV/AIDS. *AIDS* 2009, 23: 525-530.

2. Jarvis J.N, Meintjes G, Williams A *et al.* Adult meningitis in a setting of high HIV and TB prevalence: findings from 4691 suspected cases. *BMC Infectious Diseases* 2010, 10: 67.

3. Hakim JG, Gangaidzo IT, Heyderman RS *et al.* Impact of HIV infection on meningitis in Harare, Zimbabwe: a prospective study of 406 predominantly HIV patients. *AIDS* 2000, 14: 1401-1407.

4. French N, Gray K, Watera C *et al.* Cryptococcal infection in a cohort of HIV-1 infected Ugandan adults. *AIDS* 2002, 16: 1031-1038.

5. Kambugu, A, Meya DB, Rhein J *et al.* Outcomes of cryptococcal meningitis in Uganda before and after the availability of highly active antiretroviral therapy. *Clinical Infectious Diseases* 2008.46:1694-701.

6. Schaars CF, Meintjes GA, Morroni C *et al.* Outcome of AIDS-associated cryptococcal meningitis initially treated with 200mg/day or 400mg/day of fluconazole. *BMC Infectious Diseases* 2006; 6: 118-123.

7. Bicanic T, Jarvis J, Loyse A. *et al.* Determinants of Acute Outcome and Long-term Survival in HIV-associated Cryptococcal Meningitis: Results from a Combined Cohort of 523 Patients. Abstract # 892. 18th Conference on Retroviruses and Opportunistic Infections. Boston February 2011.

8. Sahraian MA, Motamedi M, Azimi AR, Paknejad SM. Bilateral pulvinar thalamic calcification in a patient with chronic cryptococcal meningitis. *European Journal of Neurology* 2007; 14: e1-e2.

9. Awasthi M, Patankar T, Shah P & Castillo M. Cerebral cryptococcosis: atypical appearances on CT. *The British Journal of Radiology* 2001; 74: 83-85.

10. Lance A, Castillo M, Heinz RE, Scatliff JH, Enterline D. Unusual pattern of enhancement in cryptococcal meningitis: In vivo findings with post-mortem correlation. *Journal of Computer Assisted Tomography* 1996; 20 (6): 1023-1026.

11. Popovich M.J, Arthur R.H, Helmer E. CT of Intracranial Cryptococcosis. *American Journal of Roentgenology* 1990; 154: 603-606.

12. Andreula C.F, Burdi N, Carella A. CNS cryptococcosis in AIDS: Spectrum of MR findings. *Journal of Computer Assisted Tomography* 1993; 17(3): 438-441.

13. Tien RD, Chu PK, Hesselink JR *et al.* Intracranial cryptococcosis in immunocompromised patients-CT and MRI findings in 29 cases. *American Journal of Neuroradiology* 1991; 12 (2):283-289.

14. Charlier C, Dromer F, Lévêque C *et al.* Cryptococcal neuroradiological lesions correlate with severity during cryptococcal meningoencephalitis in HIV-positive patients in the HAART era. *PlosOne* 2008; 3(4): e1950.

15. Chen S, Cheng-Hsien L, Lui C. *et al.* Acute/subacute cerebral infarction (ASCI) in HIV-negative adults with cryptococcal meningoencephalitis (CM): a MRI-based follow-up study and a clinical comparison to HIV-negative CM adults without ASCI. *BMC Neurology* 2011. 11:12.

16. Chen S, Chen X, Zhang Z. *et al.* MRI findings of cerebral cryptococcosis in immunocompetent patients. *Journal of medical imaging and radiation oncology* 2011; 55(1): 52-57.

17. Loyse A, Wilson D, Meintjes G. *et al.* Comparison of the Early Fungicidal Activity of High-dose 5-FC, Voriconazole, and Flucytosine, as Second Drugs Given in Combination with Amphotericin B, to Treatment of HIV-associated Cryptococcal Meningitis. *Clinical Infectious Diseases* 2012; 54(1):121-8.

18. Misziel KA, Hall-Craggs MA, Miller RF *et al.* The spectrum of MRI findings in CNS cryptococcosis in AIDS. *Radiology* 1996 (51): 842-850.

19. Wahlund LO, Barkhof F, Fazekas F *et al.* A new rating scale for age-related white matter changes Applicable to MRI and CT. *Stroke* 2001; 32:1318-1322.

20. Rex J.H, Larsen RA, Dismukes *et al.* Catastrophic visual loss due to *Cryptococcus neoformans* meningitis. *Medicine* 1993; 72(4): 207-24.

21. Moodley AA, Rae WID, Bhigjee AI *et al.* Early Clinical and Subclinical Visual Evoked Potential and Humphrey's Visual Field Defects in Cryptococcal Meningitis. PLoS ONE 7(12): e52895. doi:10.1371/journal.pone.005.

22. Moodley AA, Rae WID, Bhigjee AI *et al.* New Insights into the Pathogenesis of Cryptococcal Induced Visual Loss Using Diffusion-Weighted Imaging of the Optic Nerve. *Neuro-ophthalmology* 2012; 36(5):186–192.

23. Siddiqui AA, Brouwer AE, Wuthiekanun V *et al.* IFN-g at the Site of Infection Determines Rate of Clearance of Infection in Cryptococcal Meningitis. *Journal of Immunology* 2005; 174: 1746-1750.

CHAPTER 7 PAPER 4

Early Clinical and Subclinical Visual Evoked Potential and Humphrey's Visual Field Defects in Cryptococcal Meningitis:

- This paper addresses aim 3.1 (electrophysiological optic nerve dysfunction)
- A Moodley is the main author
- The paper was published in *PLoS One,* in December 2012

We undertook a prospective study on 90 HIV sero-positive patients with culture confirmed CM. Seventy-four patients underwent visual evoked potential (VEP) testing and 47 patients underwent Humphrey's visual field (HVF) testing.

Decreased best corrected visual acuity (BCVA) was detected in 46.5% of patients. VEP was abnormal in 51/74 (68.9%) right eyes and 50/74 (67.6%) left eyes. VEP P100 latency was the main abnormality with mean latency values of 118.9 (±16.5) ms and 119.8 (±15.7) ms for the right and left eyes respectively, mildly prolonged when compared to our laboratory references of 104 (±10) ms ($p<0.001$). Subclinical VEP abnormality was detected in 56.5% of normal eyes and constituted mostly latency abnormality. VEP amplitude was also significantly reduced in this cohort but minimally so in the visually unimpaired.

HVF was abnormal in 36/47 (76.6%) right eyes and 32/45 (71.1%) left eyes. The predominant field defect was peripheral constriction with an enlarged blind spot suggesting the greater impact by raised intracranial pressure over that of optic neuritis. Subclinical HVF abnormalities were minimal.

Elevated CSF pressure resulting in a compartment syndrome possibly along the nerve within the orbit or at the optic canal seems the best explanation for optic nerve dysfunction

demonstrated on VEP and HVF. Early optic nerve dysfunction can be detected by testing of VEP P100 latency, which may precede the onset of visual loss in CM.

Early Clinical and Subclinical Visual Evoked Potential and Humphrey's Visual Field Defects in Cryptococcal Meningitis

Anand Moodley[1,3]*, William Rae[2], Ahmed Bhigjee[3], Cathy Connolly[4], Natasha Devparsad[1], Andrew Michowicz[5], Thomas Harrison[6], Angela Loyse[6]

1 Department of Neurology, Greys Hospital, Pietermaritzburg, South Africa, **2** Department of Medical Physics, University of The Free State, Bloemfontein, South Africa, **3** Department of Neurology, University of KwaZulu Natal, Durban, South Africa, **4** Biostatistics Unit, Medical Research Council, Durban, South Africa, **5** Department of Medicine, Edendale Hospital, Pietermaritzburg, South Africa, **6** Cryptococcal Meningitis Group, Research Centre for Infection and Immunity, Division of Clinical Sciences, St. George's University of London, London, United Kingdom

Abstract

Cryptococcal induced visual loss is a devastating complication in survivors of cryptococcal meningitis (CM). Early detection is paramount in prevention and treatment. Subclinical optic nerve dysfunction in CM has not hitherto been investigated by electrophysiological means. We undertook a prospective study on 90 HIV sero-positive patients with culture confirmed CM. Seventy-four patients underwent visual evoked potential (VEP) testing and 47 patients underwent Humphrey's visual field (HVF) testing. Decreased best corrected visual acuity (BCVA) was detected in 46.5% of patients. VEP was abnormal in 51/74 (68.9%) right eyes and 50/74 (67.6%) left eyes. VEP P100 latency was the main abnormality with mean latency values of 118.9 ($\pm$16.5) ms and 119.8 ($\pm$15.7) ms for the right and left eyes respectively, mildly prolonged when compared to our laboratory references of 104 ($\pm$10) ms ($p<0.001$). Subclinical VEP abnormality was detected in 56.5% of normal eyes and constituted mostly latency abnormality. VEP amplitude was also significantly reduced in this cohort but minimally so in the visually unimpaired. HVF was abnormal in 36/47 (76.6%) right eyes and 32/45 (71.1%) left eyes. The predominant field defect was peripheral constriction with an enlarged blind spot suggesting the greater impact by raised intracranial pressure over that of optic neuritis. Whether this was due to papilloedema or a compartment syndrome is open to further investigation. Subclinical HVF abnormalities were minimal and therefore a poor screening test for early optic nerve dysfunction. However, early optic nerve dysfunction can be detected by testing of VEP P100 latency, which may precede the onset of visual loss in CM.

Citation: Moodley A, Rae W, Bhigjee A, Connolly C, Devparsad N, et al. (2012) Early Clinical and Subclinical Visual Evoked Potential and Humphrey's Visual Field Defects in Cryptococcal Meningitis. PLoS ONE 7(12): e52895. doi:10.1371/journal.pone.0052895

Editor: Chaoyang Xue, University of Medicine & Dentistry of New Jersey – New Jersey Medical School, United States of America

Received September 2, 2012; **Accepted** November 22, 2012; **Published** December 21, 2012

Copyright: © 2012 Moodley et al. This is an open-access article distributed under the terms of the Creative Commons Attribution License, which permits unrestricted use, distribution, and reproduction in any medium, provided the original author and source are credited.

Funding: This study was partly sponsored by the Medical Research Council, grant number RN 2721. No additional external funding received for this study. Sponsorship was for technical and statistical costs. The funders had no role in study design, data collection and analysis, decision to publish, or preparation of the manuscript.

Competing Interests: The authors have declared that no competing interests exist.

* E-mail: anand.moodley@kznhealth.gov.za

Introduction

Cryptococcal meningitis (CM) and other opportunistic infections in HIV infected patients continue to be a burden in developing countries despite established antiretroviral drug treatment programmes [1]. A major challenge facing satisfactory management of CM is the late presentation of patients with advanced AIDS at initial presentation. Fifty percent of patients with CM present with neurological complications, of which visual loss is the most disabling in patients that recover [2]. Visual loss is severe, occurs early in infection and is recorded in up to 40% of patients [3–6].

Visual loss in CM is well documented, however the pathogenesis remains controversial. Rex et al. have suggested a dual mechanism of early optic neuritis and late papilloedema resulting from optic nerve infiltration and raised intracranial pressure respectively [7]. Nevertheless, conflicting reports of the optic neuritis, papilloedema and the more recent compartment syndrome models abound in the literature [8–11]. A definitive model is still lacking but the compartment syndrome occurring along the nerve or at the optic canal level seems most plausible [12,13]. A better understanding of the pathogenesis of cryptococcal induced visual loss will certainly provide better guidance to management and prevention of blindness in this group. The recommended intervention to prevent visual loss is lowering of CSF pressure, either by serial lumbar punctures, in situ lumbar drain or optic nerve sheath fenestration [8,14–16]. However the likelihood of optic nerve infiltration and the benefit of corticosteroids have not been entirely excluded as treatment option as demonstrated pathologically by Corti et al that fungal infiltration of the optic nerve does occur and by De Schacht et al of the benefit of corticosteroids especially in the setting of immune reconstitution [17,18].

The Visual Evoked Potential (VEP) is reproducible and the P100 waveform is easily identified and analysed. Full field monocular pattern-reversal VEP is a useful test of pre-chiasmic optic nerve function. VEP findings of prolonged latency and reduced amplitude suggest optic nerve dysfunction, which in the setting of early visual loss in CM points to optic nerve infiltration.

Chronic papilloedema may also have similar VEP changes but will not be expected to occur early in the disease. Furthermore, central and centrocecal scotomata early in CM point to optic nerve dysfunction whereas a large blind spot and constricted field will suggest papilloedema related dysfunction. Automated Humphrey's Visual Field (HVF) is not operator dependent and qualitatively offers useful localization of visual pathway dysfunction. Its limitation however is in patients with severe visual loss who cannot be tested. The electrophysiology of optic nerve dysfunction in CM is poorly documented and whether it can contribute towards the discussion of pathogenesis and subclinical disease has not hitherto been explored. Mwanza et al. have demonstrated VEP abnormalities in 57% and 42% of HIV infected patients with and without neurological symptoms, although it is unclear what the burden of CM disease was in these patients [19].

The primary aim of this study was to establish the extent of the electrophysiological disturbance within the optic nerve in patients with CM by examining VEP and comparing with automated HVF. The detection of subclinical disease within the optic nerve by electrophysiological means could potentially identify patients most at risk of developing visual loss. Further correlation with the patients' immune status, visual acuity, optic disc appearance and CSF pressure was made. The secondary aim was to determine if VEP and HVF could contribute to the optic neuritis vs. papilloedema vs. compartment syndrome debate with regard to the pathogenesis of cryptococcal induced visual loss.

Materials and Methods

Ethical approval was obtained from the University of KwaZulu-Natal and Greys Hospital ethics committees. Informed consent was obtained from 90 patients with CM, confirmed on fungal culture, who were consecutively recruited from February 2008 to January 2011. Patients underwent visual evoked potential testing, visual field testing, neuro-ophthalmological assessment and lumbar punctures, which formed part of their routine work-up for chronic meningitis. Recruitment of patients occurred within 2 weeks of commencement of treatment and usually within 4 weeks of symptom onset of meningitis. CNS co-infection with tuberculosis, toxoplasmosis, syphilis or any other opportunistic infection, when identified, was an exclusion criterion. Lack of co-operation by encephalopathic patients precluded VEP and HVF testing. Flash light emitting diode (LED) goggles VEP was done for 6 patients who could not fixate due to severe visual loss or inattention.

VEP recordings were obtained monocularly. Full field pattern-reversal VEPs were elicited by checkerboard stimuli of large 1 degree (i.e. 60 min of arc) checks and detected using silver electrodes placed over the scalp in accordance with ISCEV guidelines [20]. The P100 latency and peak to peak N80 – P100 amplitude were considered for analysis.

Automated Humphreys Visual Fields were performed using the 30–2 SITA standard protocol. Only pattern deviation fields that fulfilled acceptable reliability indices were included for analysis. Acceptable reliability indices of HVF were fixation losses <33%, false negatives <33% and false positives <33%.

Stastistics

Visual acuity, VEP latency and amplitude were dichotomized into abnormal and normal groups using standard normal references. A best corrected visual acuity of <6/6 on the Snellen chart, VEP P100 latency of >114 ms and VEP N80-P100 amplitude of <10 μV were considered abnormal. A CSF opening pressure of ≤20 cmH2O was considered normal. One sample t tests were used to compare mean latency and amplitude to laboratory references. Tests for association between groups were analysed using a Chi Square test or Fisher's exact test as appropriate. Statistical analysis was done in STATA, version 12.

Results

All 90 patients recruited were HIV sero-positive and co-infected with *Cryptococcus neoformans*. All were black African, 50 (55.6%) were males and the mean age of the entire group was 33.5 yrs (range 17–51).

Of the 90 patients recruited, 86 patients had visual acuity testing but 4 were too encephalopathic for testing. Seventy-four patients underwent VEP testing and 47 patients underwent HVF testing. Ten right eyes and 8 left eyes had absent VEP responses therefore 64 right eyes and 66 left eyes were subjected to quantitative VEP analysis for discrete latency and amplitude evaluation. HVF was done on 47 right eyes and 45 left eyes. The disparity was due to an old enucleation of one eye and post traumatic blindness in the other eye (Table 1). Sixteen patients had profound visual loss of <6/60 on whom HVF could not be performed. The results of flash LED-goggles VEP on 6 patients, who were unco-operative, were not reproducible, too unreliable and not included for analysis. Only full field pattern reversal VEPs were included for analysis.

While 40/86 (46.5%) patients had decreased best corrected visual acuity (BCVA), profound visual loss of <6/60 was detected in 16/40 (40%) of those patients (19% in total). VEP was abnormal in 51/74 (68.9%) right eyes and 50/74 (67.6%) left eyes (Table 1). Of the 85 eyes with normal visual acuity, 48 (56.5%) had an abnormal VEP parameter (latency and/or amplitude). The mean VEP P100 latency was prolonged and N80-P100 amplitude reduced in both eyes when compared to our laboratory references. The mean VEP P100 latencies for the right and left eyes were 118.9 (±16.5) ms and 119.8 (±15.7) ms respectively, and for the N80-P100 amplitude were 7.4 (±3.9) μV and 7.0 (±3.7) μV respectively. Our laboratory references for these parameters are 104 (±10) ms for VEP P100 latency and 15 (±5) μV for the N80 – P100 amplitude. Mean latency and amplitude differed significantly from hospital references, $p<0.001$. A further breakdown of these abnormalities show that the P100 latency alone was abnormal in 55/130 (42.3%) eyes, the N80-P100 amplitude alone was reduced in 19/130 (14.6%) eyes and together was abnormal in 9/130 (6.9%) eyes (Table 2).

HVF was abnormal in 36/47 (76.6%) right eyes and 32/45 (71.1%) left eyes (Table 1). Peripheral constriction of the visual field and a large blind spot were the predominant defects, followed by central and paracentral scotomata, suggesting the greater impact by raised intracranial pressure over optic nerve infiltration (Figure 1).

Table 1. Frequencies of Abnormal VA, VEP and HVF.

	Visual acuity	VEP	VEP	HVF	HVF
	<6/6	Right Eye	Left Eye	Right Eye	Left Eye
	N (%)	N (%)	N (%)	N (%)	N (%)
Total Number	86 (100)	74 (100)	74 (100)	47 (100)	45 (100)
Normal	46 (53.5)	23 (31.1)	24 (32.4)	11 (23.4)	13 (28.9)
Abnormal	40 (46.5)	51 (68.9)	50 (67.6)	36 (76.6)	32 (71.1)

N – Number, VEP – Visual Evoked Potential, HVF – Humphrey's Visual Field.
doi:10.1371/journal.pone.0052895.t001

Table 2. VEP latency and amplitude findings in 66 patients.

VEP Latency and Amplitude	VA Right Eye		Total for Right Eye	VA Left Eye		Total for Left eye	VA Combined (%)		Total for both eyes
	Normal	Abnormal	n = 64	Normal	Abnormal	n = 66	Normal n = 85	Abnormal n = 45	n = 130 (100)
Norm lat/Norm amp	18	5	23	19	5	24	37 (78.7)	10 (21.3)	47 (36.2)
Norm lat/Abn amp	9	2	11	7	1	8	16 (84.2)	3 (15.8)	19 (14.6)
Abn lat/Norm amp	12	14	26	16	13	29	28 (50.9)	27 (49.1)	55 (42.3)
Abn lat/Abn amp	1	3	4	3	2	5	4 (44.4)	5 (55.6)	9 (6.9)
Total Abn Latency	13	17	30	19	15	34	32 (50)	32 (50)	64
Total Abn Amplitude	10	5	15	10	3	13	20 (71.4)	8 (28.6)	28

VEP – Visual Evoked Potential, VA – Visual Acuity, Norm – normal, lat – latency, amp – amplitude, Abn – abnormal.
doi:10.1371/journal.pone.0052895.t002

Significant correlations were noted between Visual Acuity and VEP latency of the right eye ($p = 0.003$) and VEP latency of the left eye ($p = 0.03$,) but not with VEP amplitude (Table 3). When BCVA was abnormal 17/24 (70.8%) and 15/21 (71.4%) of VEP latency was abnormal in the right and left eyes respectively. When BCVA was normal, 13/40 (32.5%) and 19/45 (42.2%) of subclinical VEP latency abnormality was detected. VEP amplitude however did not have a similar relationship, being normal in 19/24 (79.2%) and 18/21 (85.7%) of right and left eyes respectively, when BCVA was abnormal. Subclinical detection of VEP amplitude abnormality was detected in 10/40 (25%) and 10/45 (22.2%) of the right and left eyes respectively.

Swollen optic disc was correlated with VEP P100 latency for the right and left eyes ($p = 0.02$, 0.047 resp.) but not with VEP amplitude. No significant correlations were noted between CSF pressure and CD4 count with VEP latency and amplitude (Table 3).

Table 4 demonstrates significant correlation between VEP latency and HVF in both eyes ($p = 0.001$, 0.0049). BCVA is correlated with HVF of the right eye, but not the left ($p = 0.03$ vs $p = 0.5$). Whilst this may reflect the impact of central scotomata on visual acuity testing, figure 1 shows equal frequency of central scotomata in the right and left eyes. Therefore subclinical and asymmetrical optic nerve dysfunction is a possible explanation. When BCVA was abnormal, 17/36 (47.2%) and 10/32 (31.2%) of the right and left HVF were abnormal. Subclinical HVF abnormality was only detected in 1/11 (9.1%) and 2/13 (15.4%) of right and left eyes respectively.

Discussion

Cryptococcal induced visual loss can be devastating and, if neglected, irreversible [21]. Despite the easy availability of antiretroviral therapy in some developing countries, the neuro-opthalmological complications of HIV infection and cryptococcal meningitis are still encountered. Studies have shown that early and intensive management of raised intracranial pressure in CM can reverse the visual loss associated with the disease [8,9]. Unfortunately, due to the encephalopathic state of most patients with CM and the lack of vigilance by medical personnel in emergency departments visual acuity is not tested or crude testing is done on admission. Early detection of visual impairment is therefore missed and the window of opportunity to reverse optic nerve damage is often lost.

The first aim of this study was to detect the frequency of VEP and HVF abnormalities in patients with CM, correlate these findings with visual acuity, thereby determining the presence of clinical and subclinical disease. The second aim was to determine if this unique VEP and HVF data could contribute to the optic

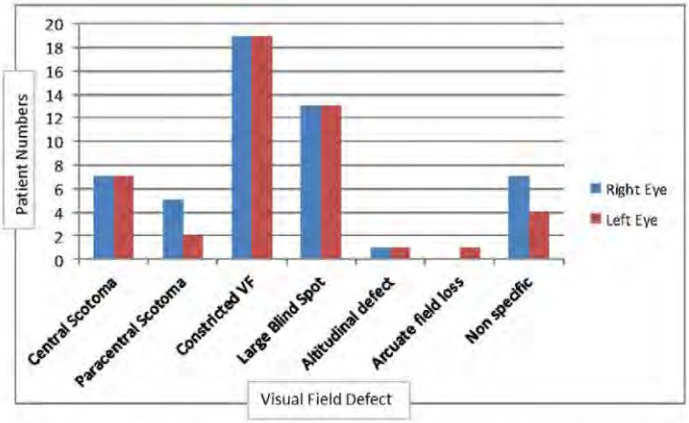

Figure 1. Frequencies of Visual Field Defects. Constricted VF – Constricted Visual Field.
doi:10.1371/journal.pone.0052895.g001

Table 3. Correlation between VEP and VA, CSF Pressure, Swollen optic disc and CD4 count in 66 patients.

		VEP Latency of Right Eye		p value	VEP Latency of Left Eye		p value	VEP Amplitude of Right Eye		P value	VEP amplitude of Left eye		P value
		n = 64			n = 66			n = 64			n = 66		
		Normal	Abnormal		Normal	Abnormal		Normal	Abnormal		Normal	Abnormal	
Visual Acuity	Normal	27	13	**0.003**	26	19	**0.03**	30	10	**0.7**	35	10	**0.5**
		(67.5%)	(32.5%)		(57.8%)	(42.2%)		(75%)	(25%)		(77.8%)	(22.2%)	
	Abnormal	7	17		6	15		19	5		18	3	
		(29.2%)	(70.8%)		(28.6%)	(71.4%)		(79.2%)	(20.8%)		(85.7%)	(14.3%)	
CSF Pressure	Normal	11	9	**0.9**	10	9	**0.6**	17	3	**0.3**	15	4	**0.9**
	Elevated	21	18		19	22		28	11		33	8	
Swollen optic disc	No	29	18	**0.02**	26	21	**0.047**	36	11	**0.9**	37	10	**0.7**
	Yes	5	12		5	13		13	4		15	3	
CD4 count	<50	19	17	**0.6**	16	22	**0.6**	28	8	**0.2**	30	8	**0.9**
	50–100	10	6		9	7		12	4		13	3	
	101–199	1	2		1	1		3	0		2	0	
	>200	1	0		1	0		0	1		1	0	

VEP – Visual Evoked Potential, Visual Acuity refers to Best Corrected Visual Acuity.
doi:10.1371/journal.pone.0052895.t003

Table 4. Correlation between HVF and VA, CSF Pressure, Swollen optic disc, CD4 count and VEP in 47 patients.

		HVF of Right Eye		p value	HVF of Left Eye		P value
		n = 47			n = 45		
		Normal	Abnormal		Normal	Abnormal	
Visual Acuity	Normal	10	1	**0.03**	11	2	**0.5**
		(90.9%)	(9.1%)		(84.6%)	(15.4%)	
	Abnormal	19	17		22	10	
		(52.8%)	(47.2%)		(68.8%)	(31.2%)	
CSF Pressure	Normal	2	9	**0.9**	4	8	**0.4**
	Elevated	8	25		6	24	
Swollen optic disc	No	7	4	**0.9**	9	4	**0.8**
	Yes	22	13		20	11	
CD4 count	<50	4	19	**0.7**	4	18	**0.14**
	50–100	3	9		5	6	
	101–199	0	2		0	2	
	>200	1	0		1	0	
VEP latency	Normal	10	10	**0.001**	9	10	**0.0049**
	Abnormal	1	20		4	19	
VEP amplitude	Normal	5	6	**0.1**	3	6	**0.1**
	Abnormal	6	24		10	23	

HVF – Humphrey's visual field, VEP – Visual evoked potential, Visual Acuity refers to Best Corrected Visual Acuity.
doi:10.1371/journal.pone.0052895.t004

neuritis vs. papilloedema vs. compartment syndrome debate surrounding the pathogenesis of cryptococcal induced visual loss.

Visual impairment was detected in 40/86 (46.5%) of patients with CM, and 16/40 (40%) had profound visual loss of <6/60 (19% in total). VEP abnormalities were detected more frequently, occurring in 68.9% of right eyes and 67.6% of left eyes and subclinical disease in 56.5% (Tables 1 and 2). The predominant abnormal VEP parameter was prolongation of the P100 latency occurring in 42.3% of all eyes (table 2). The mean P100 latency values were 118.9 (±16.5) ms and 119.8 (±15.7) ms for the right and left eyes respectively, mildly prolonged when compared to our laboratory references of 104 (±10) ms but still significant ($p<0.001$). Prolonged P100 latencies suggest demyelination or conduction block (focal demyelination), as occurs in acute optic neuritis which in the case of CM, a non-demyelinating disorder, will suggest focal pressure effects on the optic nerve. Conceivably the most likely sites of optic nerve compression will be at the optic canal or at sites of dense subarachnoid trabeculae within the optic nerve sheath, providing soft evidence for the compartment syndrome in cryptococcal induced visual loss.

VEP latency strongly correlated with visual acuity and swollen optic disc; when VEP latency was prolonged, visual acuity was reduced and optic disc swelling occurred (Table 3). Such abnormal parameters provide strong clinical and electrophysiological evidence for optic nerve dysfunction in cryptococcal induced visual loss. The fact that 32.5% and 42.2% of right and left eyes respectively with normal acuity had prolonged VEP latency is good evidence for subclinical optic nerve dysfunction. The contribution to prolonged VEP latency made by the HIV virus in advanced HIV infection requires further evaluation. Claims of subclinical VEP abnormalities in 3–49% of HIV infected patients due to retro-chiasmic or occipital cortical neuron loss have not been verified [19,22]. Mwanza's group did not exclude cryptococcal meningitis and it is likely that the 49% includes patients with cryptococcal meningitis. In Malessa's group of asymptomatic HIV-infected patients, 3% had VEP latency prolongation and 33% had VEP amplitude reduction when CD4 counts were below 100. However in the setting of co-infection with CM, and noting the prominence played by the fungus in visual loss, one has to presume that a large amount of the 56.5% of overall VEP abnormality (latency and amplitude) in our patients was due to cryptococcal co-infection rather than HIV alone (Table 2). A limitation of this study is the failure of comparison to an asymptomatic HIV positive group without CM to determine the impact if any of HIV infection itself. No significant correlations were noted between VEP latency and CSF pressure or CD4 counts (Table 3), possibly due to the relatively small number of patients recruited or that VEP and CSF pressure measurements were not always done at the same time.

VEP amplitude changes occurred less frequently and this was the abnormality in only 14.6% of eyes suggesting that secondary axonal changes were not frequent despite the low mean amplitude of 7.4 (±3.9) μV and 7.0 (±3.7) μV for the right and left eyes respectively.(Table 2). The low frequency of amplitude changes may be a reflection of the somewhat early recruitment of patients from symptom onset (4 weeks). Perhaps repeat testing later in the disease may reveal more secondary axonal change, which is a late phenomenon. Consequently, no significant correlations were noted between VEP amplitude and visual acuity, CSF pressure, optic disc swelling or CD4 counts in early CM. (Table 2).

HVF abnormalities were very frequent in patients who could be tested, occurring in 76.6% of right eyes and 71.1% of left eyes. (Table 1) A major limitation of HVF testing was that patients with profound visual loss (VA <6/60) could not be tested. The predominant field defects were peripheral constriction with large blind spots followed by central and paracentral field defects.

(Figure 1) As peripheral constriction with large blind spots is associated with papilloedema-related optic nerve dysfunction, HVF supports raised intracranial pressure being an important cause of optic nerve dysfunction in cryptococcal induced visual loss. The central field defects found suggest intrinsic optic nerve disease or secondary macular dysfunction from severe papilloedema; however an inability to test patients with profound visual loss suggests that the central field defect was probably underestimated in this patient cohort.

HVF is also strongly correlated with VEP latency prolongation ($p = 0.001$ right eyes and $p = 0.0049$ for left eyes) (Table 4). Subclinical HVF abnormalities were not as frequent as VEP latency abnormalities and are therefore less sensitive in detecting optic nerve dysfunction in patients with normal visual acuity in CM. No significant correlations were noted between HVF and CSF pressure, optic disc swelling, CD4 counts or VEP amplitude.

The VEP P100 wave is easily recognized on VEP testing and reproducible. Testing of encephalopathic patients was challenging in our cohort of patients with CM. In patients who could be tested, VEP P100 latency was the predominant abnormality and most strongly correlated with decreased visual acuity and optic disc swelling. Furthermore, an appreciable number of patients with normal visual acuity demonstrated P100 latency prolongation suggesting subclinical disease and perhaps a cohort that require close monitoring and aggressive management of raised intracranial pressure to prevent visual loss. The contribution to the P100 latency prolongation made by HIV infection alone needs further investigation. HVF defects were mostly consistent with raised intracranial pressure, even though patients with profound visual loss were unable to be tested.

Prolongation of the P100 latency in early CM lends some support for focal conduction block and hence the compartment syndrome from raised intracranial pressure as a cause for visual loss in these patients. Papilloedema alone which occurs less frequently than visual loss does not account for most cases of visual loss, neither does optic neuritis which is uncommon in the pauci-inflammatory state of CM in HIV infected patients [12]. The neurapraxia caused by the compression at the optic canal or orbital segment of the nerve is potentially reversible by lowering of intracranial pressure rather than immunosuppressant therapy as is used for idiopathic optic neuritis [8,23].

While this study does demonstrate appreciable P100 latency prolongation even in asymptomatic CM patients, the long term implication of this result can only be answered by longitudinal studies. VEP as a tool to predict visual loss in CM is conceivable and worth further investigation. Furthermore, VEP and HVF provide clinical and subclinical evidence for raised intracranial pressure causing a possible compartment syndrome and optic nerve dysfunction. So can CSF pressure lowering measures in addition to offering an improved overall prognosis prevent blindness in CM by prevention of the optic nerve compartment syndrome rather than merely preventing papilloedema?

Acknowledgments

We are most grateful to Miss N Hlatshwayo for her contribution to the testing of VEP and HVF on our patients.

Author Contributions

Conceived and designed the experiments: A. Moodley WR AB TH AL. Performed the experiments: A. Moodley ND A. Michowicz. Analyzed the data: A. Moodley WR AB CC ND A. Michowicz TH. Wrote the paper: A. Moodley WR.

References

1. Lighiowler JV, Cooke GS, Mutevedzi P, Lessells RJ, Newell ML, et al. (2010) Treatment of cryptococcal meningitis in KwaZulu-Natal, South Africa. PLoS One 5: e8630.
2. Moosa MY, Cooyadia YM (1997) Cryptococcal meningitis in Durban, South Africa: a comparison of clinical features, laboratory findings, and outcome for human immunodeficiency virus (HIV)-positive and HIV-negative patients. Clin Infect Dis 24: 131–134.
3. Seaton RA, Verma N, Naraqi S, Wembri JP, Warrell DA (1997) Visual loss in immunocompetent patients with Cryptococcus neoformans var. gattii meningitis. Trans R Soc Trop Med Hyg 91: 44–49.
4. Cohen DB, Glasgow BJ (1993) Bilateral optic nerve cryptococcosis in sudden blindness in patients with acquired immune deficiency syndrome. Ophthalmology 100: 1689–1694.
5. Lipson BK, Freeman WR, Beniz J, Goldbaum MH, Hesselink JR, et al. (1989) Optic neuropathy associated with cryptococcal arachnoiditis in AIDS patients. Am J Ophthalmol 107: 523–527.
6. Jabs DA (1995) Ocular manifestations of HIV infection. Trans Am Ophthalmol Soc 93: 623–683.
7. Rex JH, Larsen RA, Dismukes WE, Cloud GA, Bennett JE (1993) Catastrophic visual loss due to Cryptococcus neoformans meningitis. Medicine (Baltimore) 72: 207–224.
8. Claus JJ, Portegies P (1998) Reversible blindness in AIDS-related cryptococcal meningitis. Clin Neurol Neurosurg 100: 51–52.
9. Ferreira RC, Phan G, Bateman JB (1997) Favorable visual outcome in cryptococcal meningitis. Am J Ophthalmol 124: 558–560.
10. Kestelyn P, Taelman H (1997) Visual loss and cryptococcal meningitis. Trans R Soc Trop Med Hyg 91: 727–728.
11. Seaton RA, Verma N, Naraqi S, Wembri JP, Warrell DA (1997) The effect of corticosteroids on visual loss in Cryptococcus neoformans var. gattii meningitis. Trans R Soc Trop Med Hyg 91: 50–52.
12. Moodley A, Rae W, Bhigjee A, Loubser N, Michowicz A (2012) New Insights into the Pathogenesis of Cryptococcal Induced Visual Loss Using Diffusion-Weighted Imaging of the Optic Nerve. Neuro-ophthalmology 36(5): 186–192.
13. Killer HE, Jaggi GP, Miller NR (2011) Optic nerve compartment syndrome. Acta Ophthalmol 89: e472; author reply e472–473.
14. Orem J, Tindyebwa L, Twinoweitu O, Mukasa B, Tomberland M, et al. (2005) Feasibility study of serial lumbar puncture and acetazolamide combination in the management of elevated cerebrospinal fluid pressure in AIDS patients with cryptococcal meningitis in Uganda. Trop Doct 35: 19–21.
15. Milman T, Mirani N, Turbin RE (2008) Optic nerve sheath fenestration in cryptococcal meningitis. Clin Ophthalmol 2: 637–639.
16. Johnston SR, Corbett EL, Foster O, Ash S, Cohen J (1992) Raised intracranial pressure and visual complications in AIDS patients with cryptococcal meningitis. J Infect 24: 185–189.
17. Corti M, Solari R, Cangelosi D, Dominguez C, Yampolsky C, et al. (2010) Sudden blindness due to bilateral optic neuropathy associated with cryptococcal meningitis in an AIDS patient. Rev Iberoam Micol 27: 207–209.
18. De Schacht C, Smets RM, Callens S, Colebunders R (2005) Bilateral blindness after starting highly active antiretroviral treatment in a patient with HIV infection and cryptococcal meningitis. Acta Clin Belg 60: 10–12.
19. Mwanza JC, Nyamabo LK, Tylleskar T, Plant GT (2004) Neuro-ophthalmological disorders in HIV infected subjects with neurological manifestations. Br J Ophthalmol 88: 1455–1459.
20. Odom JV, Bach M, Brigell M, Holder GE, McCulloch DL, et al. (2010) ISCEV standard for clinical visual evoked potentials (2009 update). Doc Ophthalmol 120: 111–119.
21. Ng CW, Lam MS, Paton NI (2000) Cryptococcal meningitis resulting in irreversible visual impairment in AIDS patients–a report of two cases. Singapore Med J 41: 80–82.
22. Malessa R, Agelink MW, Diener HC (1995) Dysfunction of visual pathways in HIV-1 infection. J Neurol Sci 130: 82–87.
23. Torres OH, Negredo E, Ris J, Domingo P, Catafau AM (1999) Visual loss due to cryptococcal meningitis in AIDS patients. AIDS 13: 530–532.

CHAPTER 8 PAPER 5

Optic nerve and Peri-optic CSF diffusion in Cryptococcal Meningitis, Optic Neuritis and Papilloedema:

- This paper addresses aim 3.4 (especially 3.4.3)
- A Moodley is the main author
- The paper has been submitted to *Journal of Neurological Sciences*, and is awaiting review

Twenty-nine healthy controls, 59 culture confirmed CM patients, 14 patients with papilloedema and 14 patients with optic neuritis from causes other than CM underwent magnetic resonance diffusion-weighted imaging and diffusion tensor imaging of the optic nerve and the peri-optic CSF. The apparent diffusion coefficient (ADC), fractional anisotropy (FA) and anisotropic index (AI) were compared among all 4 groups.

Results:

The AI of the peri-optic space (mean of 1.25) while less than that of the optic nerve (mean of 1.85) was greater than that of the nearby vitreous (mean of 0.99) suggesting anisotropic diffusion within the peri-optic CSF. Hence, laminar rather than turbulent flow occurs within the peri-optic subarachnoid space (SAS). The papilloedema group alone showed lower AI of the peri-optic CSF than normal controls (1.3 vs. 1.1, and 1.2 vs. 1.1; p= 0.02 and 0.046 for the right and left eyes respectively). The optic neuritis group alone showed lower FA of the optic nerve than the control group (0.25 vs.0.41 respectively, p = 0.02) on the left side only. The FA in the peri-optic space was lower in the CM group with decreased vision than the control group (p = 0.03).

Optic nerve diffusion could not draw similarities between CM and papilloedema or optic neuritis regardless of CSF pressure or vision.

Optic nerve and Peri-optic CSF diffusion in Cryptococcal Meningitis, Optic Neuritis and Papilloedema

Anand A Moodley[1,3], William ID Rae[2] , Ahmed I Bhigjee[3] ,Cathy Connolly[4] ,Andrew Michowicz[5]

[1] *Department of Neurology, Greys Hospital, Pietermaritzburg, South Africa*

[2] *Department of Medical Physics, University of the Free State, South Africa*

[3] *Department of Neurology, University of KwaZulu Natal, South Africa*

[4] *Biostatistics Unit, Medical Research Council of South Africa, Durban, South Africa*

[5] *Department of Medicine, Edendale Hospital, Pietermaritzburg, South Africa*

Corresponding author: AA Moodley, Department of Neurology, Greys Hospital, Pietermaritzburg, South Africa.

Postal Address: PO Box 13833, Cascades, 3202, South Africa.
Email: anand.moodley@kznhealth.gov.za Tel: +2733 897 3298 Fax: +2733 8973409
Mobile: +2784 5955077

Word Count (excluding abstract, tables, figures and references) : 3434

Number of References: 27

Keywords: Cryptococcal meningitis; Optic nerve diffusion; Optic neuritis, Papilloedema; Peri-optic subarachnoid space; Apparent diffusion coefficient; Fractional anisotropy; Anisotropic index

Abstract

Background:

Cryptococcal-induced visual loss is a devastating complication of cryptococcal meningitis (CM) despite antifungal therapy. There is no consensus regarding its pathogenesis and evidence for and against the optic neuritis and papilloedema theories abound in the literature.

Method:

Twenty-nine healthy controls, 59 culture confirmed CM patients, 14 patients with papilloedema and 14 patients with inflammatory/infective optic neuropathy (IION) from causes other than CM underwent magnetic resonance diffusion weighted imaging and diffusion tensor imaging of the optic nerve and the peri-optic CSF. The apparent diffusion coefficient (ADC), fractional anisotropy (FA) and anisotropic index (AI) were compared among all 4 groups.

Results:

The AI of the peri-optic space (mean of 1.25) while less than that of the optic nerve (mean of 1.85) was greater than that of the nearby vitreous (mean of 0.99) suggesting anisotropic diffusion within the peri-optic CSF. Hence, laminar rather than turbulent flow occurs within the peri-optic SAS. The papilloedema group alone showed lower AI of the peri-optic CSF than normal controls (1.3 vs. 1.1, and 1.2 vs. 1.1; p= 0.02 and 0.046 for the right and left eyes respectively). The IION group alone showed lower FA of the optic nerve than the control group (0.25 vs.0.41 respectively, p = 0.02) on the left side only. The FA in the peri-optic space was lower in the CM group with decreased vision than the control group (p = 0.03).

Conclusion:

Optic nerve diffusion could not draw similarities between CM and papilloedema or optic neuritis regardless of CSF pressure or vision.

Introduction

Cryptococcal meningitis (CM), and its devastating complication of visual loss, continues to be a scourge in developing countries during the HIV pandemic [1,2]. Prevention of cryptococcal induced visual loss is a challenge to primary care physicians. Early subclinical detection by visual evoked potential is possible at tertiary level care [3], but the foremost problem is consensus on its pathogenesis so that interventional strategies can be formally investigated and adopted. Ever since Rex et al proposed 2 principal mechanisms of early optic neuritis and late papilloedema, several reports have been published supporting or refuting those claims [4-12]. Most studies are case reports and anecdotal. Pathological studies are few and they still fail to address the conundrum [8].

Isotropic diffusion within a fluid such as CSF or intracellular fluid refers to the random diffusion of molecules which is equal in all directions whereas anisotropy refers to preferential diffusion in a particular direction. Diffusion of water molecules within the optic nerve is anisotropic [13,14]. Restriction of radial diffusion is offered by the 1.2 million longitudinally arranged axons and thus preference is given to diffusion along the longitudinal axis. The relationship between longitudinal and radial diffusion on diffusion weighted imaging (DWI) and diffusion tensor imaging (DTI) can be quantified by various parameters as indices of anisotropy. Firstly on DWI, the Apparent Diffusion Coefficient (ADC) in the longitudinal direction can be expressed as a ratio to that in the radial direction of the optic nerve as an Anisotropic Index (AI) and secondly on DTI, the Fractional Anisotropy (FA). An FA map is determined by solving the diffusion tensor. FA is computed from the eigenvalues of the tensor. FA values are obtained from the signal intensity on the FA maps [15]. An AI obtained as >1.0 is indicative of greater longitudinal to radial diffusion of water molecules within the optic nerve. FA ranges from 0 to 1 where 0 represents isotropic diffusion and 1

represents perfectly anisotropic diffusion. The normal FA for the optic nerve is quoted as 0.4-0.5 and the AI as 1.81-1.88 [16,17]. The impact of CM and optic neuritis on optic nerve diffusion has been described, but the effect of papilloedema from raised intracranial pressure has not [13,17,18].

Optic nerve diffusion obtained from DWI and DTI is well described in optic neuritis and indices have been derived for assessment of the optic nerve microstructure [18-21]. The diffusion of CSF in the peri-optic subarachnoid space (SAS) however, has not been examined in previous studies. There is free communication between the intracranial SAS and the peri-optic SAS along the optic nerve sheath and CSF that is produced intracranially is transported to the peri-optic SAS. Intracranial pressure is also transmitted along this pathway such that raised intracranial pressure results in elevated peri-optic CSF pressure. The raised pressure applied at the lamina cribrosa is responsible for axoplasmic stasis and axonal swelling at the optic nerve head which is visualized as optic disc oedema (papilloedema) [22]. CSF flow within the peri-optic space conceivably is bidirectional towards the globe and back intracranially [23,24]. This process is slower than the flow intracranially due largely to the smaller size of the optic nerve sheath and the presence of septae and trabeculae within the peri-optic SAS [25]. Presumably, laminar flow of CSF within this space occurs which is necessary to allow for CSF exchange between the intracranial SAS and peri-optic SAS, albeit a slow and partially compartmentalized process [24]. Even so the diffusion of water molecules within this peri-optic space is influenced by this CSF flow and if anisotropic diffusion is demonstrated, it will be evidence of laminar flow. It is intuitively expected that fungal loading within the peri-optic SAS in CM will impact on CSF flow producing less laminar and more turbulent flow with resultant less anisotropic (i.e. isotropic) diffusion. Diffusion of water molecules in the SAS of the optic nerve has not been measured. Intuitively, one can predict anisotropic diffusion in view of the CSF circulation from the

intracranial SAS to the SAS of the optic nerve and a return path along some parallel channels. The impact of meningitic disease processes such as CM on this diffusion has not been investigated. The extent to which this diffusion is affected and how it relates to visual loss and elevated CSF pressure in CM patients is unknown.

The first aim of the study was to obtain the ADC, FA and anisotropic index of the peri-optic SAS and compare that to the optic nerve in the normal control group. The second aim was to determine diffusion parameters in the optic nerve and peri-optic SAS in patients with papilloedema from causes of raised intracranial pressure other than CM. The third aim of this study was to compare the ADC, FA and anisotropic index of the optic nerve and peri-optic SAS among normal healthy controls, patients with CM, patients with optic neuritis and those with papilloedema from various causes. Could shared characteristics point to a possible pathogenesis?

Method

This study forms part of an ongoing investigation into the pathogenesis of cryptococcal induced visual loss. Patients and controls were recruited from Greys and Edendale Hospitals, KwaZulu-Natal South Africa, from October 2008 to February 2011. Informed written consent was obtained from subjects and controls and for encephalopathic patients, from their next of kin. Ethical approval for the study was obtained from the Greys and University of KwaZulu-Natal human ethics committees. Patients underwent full neuro-ophthalmological evaluation, examination of immune status and were subjected to MRI, DWI and DTI of the brain, orbits and optic nerves, using standard and modified imaging protocols on a Phillips 1.5 Tesla Gyroscan Magnetic Resonance Scanner. Parameters used for magnetic resonance (MR) diffusion-weighted imaging (DWI) and diffusion-tensor imaging (DTI) of the brain and optic nerves using the coronal oblique technique for each nerve have been reported previously [17].

Diffusion gradient of b = 1000 s/mm^2 was selected and fat saturated (SPIR) single shot EPI using SENSE without cardiac gating was used. EPI was acquired using echo time (TE) = 93 ms, relaxation time (TR) = 3000 ms, 180 mm field of view (FOV), matrix = 112 x 128 and 4 mm slice thickness. DTI was obtained in 15 directions and longitudinal, axial and mean diffusivity values were selected for analysis.

Subjects were asked to breathe normally, relax and fixate on an orange target (placed above their heads) during the study to avoid excessive eye movement. ADC using DWI, FA using DTI and an Anisotropic index of axial diffusion to radial diffusion were done on the optic nerves and peri-optic CSF space of 29 normal controls, 59 culture confirmed cryptococcal meningitis patients, 14 patients with papilloedema and 14 patients with optic neuritis from causes other than CM. The ADC, FA and Anisotropic index were also done on the ipsilateral vitreous and frontal lobe white matter of the normal controls for verification of the diffusion method. Patients with cryptococcal meningitis were excluded if they had overt evidence of other CNS opportunistic infections.

The coronal oblique imaging of each optic nerve has been previously reported [17]. Data from the peri-optic space was obtained using the same technique. A 2x2 pixel region of interest (ROI) was placed on the peri-optic CSF and on the optic nerve that was most easily recognised on the B0 image, usually on slices 2 or 3 (Figure 1). Optic nerve movement during the B0 and B1000 images resulted in inaccurate placement of the ROI in some patients as the ROI was copied from B0 to B1000 as demonstrated in Figure 1. This was corrected for where possible. While fat saturation was essential FLAIR was avoided since the fluid signal in the peri-optic space was needed for analysis. The ADC was obtained in the axial and radial planes for the optic nerve and peri-optic CSF space. In addition to the FA obtained from DTI, an anisotropic index was calculated from the DWI using the formula;

Anisotropic Index (AI) = $2\lambda_1/(\lambda_2 + \lambda_3)$, where λ_1 = axial diffusion and λ_2, λ_3 = radial diffusion in the other two orthogonal axes.

Optic nerve and peri-optic CSF diffusion data obtained from the controls, CM patients,

papilloedema and optic neuritis patients will be presented. The CM patient group was further subdivided into those with normal and abnormal visual acuity (visual acuity < 6/6 on Snellen chart) and those with normal and elevated CSF pressure (CSF pressure > 20cmCSF). Further comparisons were made between these groups.

Statistical Methods

Demographic characteristics were compared among the four groups using analysis of variance for age and chi square for sex. Means and standard deviations were reported for normally distributed parameters and medians and interquartile ranges otherwise. Pairwise comparisons between independent groups were done using Mann and Whitney Rank Sum tests and Wilcoxon signed-rank test for paired comparisons. Data were displayed using scatter plots for individual data points and box plots for summary statistics. Data were analysed in Stata v12.1, StataCorp College Station TX.

Results

There was a discrepancy between the number of subjects scanned and the number of optic nerve images analysed, especially so for the optic neuritis cohort (Table 1). Identification of the nerve was particularly difficult, due mostly to involuntary movement of the nerve and its size. Only those eyes that were most readily identified were recruited for analysis. The optic neuritis group had the worst visual acuity and was therefore least likely to fixate on the target given to them during the study which probably accounts for the reduced number analysed. The unequal left and right eyes analysed was due mostly to poor visualization of the nerve on imaging rather than asymmetrical nerve involvement and might account for some inclusion

bias. The mean age of the four groups was comparable, however the papilloedema and optic neuritis group were predominantly females as they constituted mostly patients with Idiopathic Intracranial Hypertension and HIV associated acute disseminated encephalomyelitis (ADEM). All patients in the papilloedema group had elevated intracranial pressure as cause for the optic disc swelling as documented by CSF pressure measurement (> 20cmH_2O) or where contra-indicated by neuro-imaging evidence of raised intracranial pressure. None of the optic neuritis patients had elevated intracranial pressure by CSF pressure measurement or evidence on neuro-imaging. The control group comprised 9 HIV positive and 20 HIV negative individuals with normal visual acuity and mentation. No differences were noted between these 2 groups so their parameters are combined and presented as a mean.

Figure 2 shows no significant difference in the ADC and Anisotropic Index of the optic nerve among the Control, CM, papilloedema and optic neuritis groups. A significant difference was noted in the FA of the optic nerve between the control and optic neuritis group on the left side only (0.41 vs. 0.25, $p = 0.02$) (Table 3). Similar low FA has been previously documented in optic neuritis due to disruption of the myelin and axons producing greater isotropic diffusion [14,18,26]. This finding was however, not supported by the anisotropic index.

In Figure 3, the scatter plots of the Anisotropic index in the peri-optic CSF space show a significant difference between the control and papilloedema groups for the right eye (1.3 vs. 1.1, $p = 0.02$) and the left eye (1.2 vs. 1.1, $p = 0.046$). No significant differences were noted in the ADC and FA of the peri-optic SAS among the control, CM, papilloedema and optic neuritis groups.

In Figure 4, the box and whisker plot of anisotropy index among the 4 groups shows lower values in the peri-optic space compared to the optic nerve. Greater anisotropy is expected in the optic nerve where the axons and myelin limit radial diffusion and give preference to longitudinal diffusion along the nerve. The anisotropic index in the peri-optic space in

papilloedema is significantly lower than the control group (Right eye, $p = 0.02$ and Left eye, $p = 0.046$), suggesting that the higher pressure results in more random molecular diffusion of the CSF. Such findings should have been mirrored in the CM group where one would expect the elevated pressure in the peri-optic space to result in lower anisotropic index and more random diffusion.

Table 2 shows the comparison between the ADC, FA and anisotropic indices of the optic nerve, peri-optic SAS, vitreous and frontal lobe white matter in normal controls. An anisotropic index in the vitreous of approximately 1.0 confirms the isotropic diffusion within the vitreous and hence the reliability of our diffusion method. Tables 3 and 4 present the ADC and anisotropic indices data of the optic nerve and peri-optic SAS among the normal controls, CM, optic neuritis and papilloedema groups.

Discussion

The ADC of the peri-optic space is as expected much higher than that within the optic nerve due to the higher water content (Table 2). The FA and anisotropic index of the optic nerve is greater than that of the peri-optic SAS due to the longitudinal orientation of the axons in the nerve that promote longitudinal diffusion in preference to radial diffusion. Not surprisingly, the peri-optic SAS too has an anisotropic index > 1.0 and mean FA of 0.29 (both more than vitreous, $p < 0.001$), suggesting that the flow of CSF within this space is greater in the longitudinal rather than the radial plane. Hence the suggestion of laminar rather than turbulent flow is demonstrated by this data. Laminar flow results from either the septae and trabeculae within the peri-optic space which provide some directionality to the flow of CSF or from the pressure gradient between the intracranial SAS and the peri-optic SAS or flow follows virtual channels created and obliterated as the nerve moves within its sheath as part

of the physiological function of the moving eye. Figure 3 and Table 4 show a significant lowering of the anisotropic index of the peri-optic CSF space in the papilloedema group when compared to the normal controls (1.3 vs. 1.1, and 1.2 vs. 1.1; p= 0.02 and 0.046 for the right and left eyes respectively). The lesser anisotropic (greater isotropic) diffusion in the setting of raised intracranial pressure suggests more turbulent flow of CSF in the peri-optic SAS. In the setting of raised intracranial pressure from CM, a similar lowering of the anisotropic index in the peri-optic SAS would be expected, but was not demonstrated in our cohort. The implication would be that the compartmentalization of the intracranial SAS from the peri-optic SAS was significant enough to prevent this effect. Killer et al have shown this compartmentalization to be both biochemical and pressure related.[24] Furthermore, fungal loading or even an excess of inflammatory cells within the peri-optic SAS would be expected to lower the anisotropic index in patients with CM and raised intracranial pressure, but this too did not occur. This finding together with the lack of dilatation of the peri-optic SAS in CM provides additional evidence for the compartment syndrome at the optic canal being the vital link between raised intracranial pressure and visual loss in CM [17].

Optic nerve diffusion in raised intracranial pressure has not previously been reported. Our data shows no differences in ADC, FA and anisotropic index between the normal controls and the papilloedema group. Figure 2 and Table 3 show significant difference between optic nerve FA in the normal controls and optic neuritis (0.41 vs.0.25 respectively, p = 0.02) on the left side only. As similar lowered FA values in optic neuritis have been previously reported this data is noteworthy [14,18]. The rather small optic neuritis group might account for the asymmetrical results. There were no other significant differences noted among the groups for ADC, FA and anisotropic index especially so when compared to the normal control group. The similarities between the CM and papilloedema groups cannot therefore be of significance. Even the subgroups of CM, viz. CM with decreased vision and CM with

elevated pressure whilst similar to papilloedema with regard to ADC, FA and anisotropic index were also similar to the normal controls and thus of no relevance. Consequently optic nerve diffusion could not draw similarities between CM and papilloedema or CM and optic neuritis in this study.

Table 4 shows a significant difference in FA in the peri-optic space between the control group and CM group with decreased vision ($p = 0.03$). The lack of correlation with papilloedema and optic neuritis however suggests that vision loss is perhaps not directly due to optic neuritis or papilloedema and that another mechanism is in existence, such as the compartment syndrome we have previously postulated [17].

The pathogenesis of cryptococcal- induced visual loss continues to be an enigma. Rex et al proposed 2 pathogenic mechanisms to explain visual loss in cryptococcal meningitis [4]. They identified rapid visual loss that occurred within 3 days which they attributed to optic neuritis and slow visual loss that occurred after the first week and progressed for up to 7 months due to chronic papilloedema. The rapid visual loss group had elevated CSF pressure in over 90 % of patients, thickened optic nerves on CT scan in 22% and symmetrical visual loss in 93%. The visual loss occurred before or soon after initiation of antifungal therapy and was severe and permanent. The slow visual loss group did not differ much, having elevated CSF pressure in 83%, thickened optic nerves in 22% and symmetrical visual loss in 93%. As to whether there was dilatation of the peri-optic CSF space or thickening of the optic nerve itself was not defined on CT scan for both groups. Therefore, apart from the tempo of presentation, a clear distinction between these groups does seem artificial. We have previously shown that raised intracranial pressure is common in CM induced visual loss (69%) but that papilloedema was present in only 25% [17]. The significance of raised intracranial pressure cannot be underestimated in visual loss and perhaps optic disc swelling and optic nerve infiltration/inflammation are secondary and co-occurrences.

The possibility that underlying optic nerve inflammation co-exists with raised intracranial pressure is difficult to prove in the same patient. Optic nerve infiltration which has been described in pathology specimens is an infrequent presentation and may simply be a manifestation of the meningoencephalitis involving the optic nerve. This assertion is supported by the infrequent occurrence of asymmetrical visual loss [4,7,27]. Papilloedema from raised intracranial pressure plays a prominent but not exclusive role. The role of a compartment syndrome at the level of the optic canal seems very plausible and this too might not be entirely exclusive. The fact that the intra-orbital optic nerve sheath is not dilated in patients with papilloedema and those without, regardless of visual loss is supportive of compression at the level of the optic canal [17].

We have been able to demonstrate for the first time using DWI and DTI that CSF flow in the peri-optic SAS is laminar. CSF flow in the longitudinal plane was in preference to that in the radial plane. Such anisotropy would be expected to be lost in the setting of CSF loading by cryptococcal fungi and inflammatory cells. We were unable to confirm this regardless of whether patients had normal or elevated CSF pressure, normal or decreased vision. Blockage of CSF flow upstream is likely. Turbulent peri-optic CSF flow in the papilloedema group was not demonstrated in CM further suggesting that the pressure in the peri-optic SAS is not elevated. The compartmentalization described by Killer et al between the intracranial SAS and peri-optic SAS is possibly exacerbated by the fungal loading at the optic canal level resulting in a compartment syndrome.

A limitation of the study was prevention of eye movement when scanning from B0 to B1000. Despite attempts made to limit eye movements and correction of movement where possible

we feel that the impact of movement may have resulted in some mis-registration of diffusion volumes. Hence future studies need to address this impact of movement.

Patients with CM did not demonstrate similar optic nerve or peri-optic SAS diffusion findings to that of optic neuritis or papilloedema regardless of their intracranial pressure and visual acuity. Raised intracranial pressure from causes other than CM does result in less anisotropic diffusion and more random diffusion of water molecules within the peri-optic SAS. The likelihood of greater compartmentalization between the intracranial SAS and peri-optic SAS exists in CM that prevents the transmission of pressure to the peri-optic space with blockage perhaps from fungal entrapment at the optic canal. There is however sufficient pressure transmitted to result in papilloedema in 25% of patients but insufficient to result in turbulent flow. Raised intracranial pressure (69 -90%) is far more common than papilloedema [4,17] and possibly results in visual loss from compartmentalization of the peri-optic SAS from the intracranial SAS rather than papilloedema itself.

Table 1. Demographic Data and Diagnosis of Study Groups

	Control	Cryptococcal Meningitis	Papilloedema	Optic Neuritis
Total Number Scanned	29	59	14	14
Number analysed	26 right eyes 26 left eyes	51 right eyes 52 left eyes	13 right eyes 11 left eyes	6 right eyes 5 left eyes
Mean Age (Range)	30 (21-46)	33 (21-49)	30 (21-66)	32 (19-51)
Female% **Male%**	14 (54%) 12 (46%)	27 (52%) 25 (48%)	10 (77%) 3 (23%)	4 (67%) 2 (33%)
Diagnosis	All Normal Visual Acuity and asymptomatic	All CM	9 IIH 2 Venous Sinus Thrombosis 1 Glioblastoma Multiforme 1 Toxoplasmosis	3 ADEM 1 NMO 1 Syphilitic ON 1 VZV ON

CM – Cryptococcal meningitis, IIH – Idiopathic Intracranial Hypertension, ADEM – Acute disseminated encephalomyelitis, NMO- Neuromyelitis Optica, ON – Optic neuritis, VZV – Varicella Zoster Virus

Table 2: Comparison of Apparent Diffusion Coefficient, Fractional Anisotropy and Anisotropic Index between the Optic Nerve, Peri-optic Subarachnoid Space, Vitreous and Frontal lobe white matter in normal controls

	ADC x 10^{-6} mm^2/s Mean (SD)		Fractional Anisotropy Mean (SD)		Anisotropy Index Median (IQR)	
	Right	Left	Right	Left	Right	Left
Optic Nerve	1320 (463)	1380 (547)	0.46 (0.13)	0.41 (0.12)	2.0 (1.5;2.7)	1.7 (1.4;2.0)
Peri-optic SAS	2193 (344)	2130 (400)	0.29 (0.09)†	0.29 (0.1)	1.3 (1.2;1.4)*	1.2 (1.1;1.4)‡
Vitreous	2932 (305)	2970 (235)	0.19 (0.04)	0.19 (0.06)	0.99(0.95;1.02)	0.98(0.94;1.03)
Frontal lobe WM	788 (49)	757 (54)	0.33 (0.05)†	0.34 (0.07)	1.17(1;1.3)*	1.16(0.96;1.4)‡

ADC – Apparent diffusion coefficient, SD – Standard Deviation, IQR – Interquartile range, CM – Cryptococcal meningitis, Peri-optic SAS – Peri-optic Subarachnoid Space, WM – White matter. The ADC represents the average for axial and radial diffusion. Significant differences were noted between the optic nerve, peri-optic SAS, vitreous and frontal white matter for ADC, FA and Anisotropy index ($p < 0.001$) except for * - $p = 0.01$, † - $p = 0.057$, ‡ - $p = 0.13$

Figure 1. Region of interest (ROI) on the coronal images of the optic nerve and perioptic CSF space

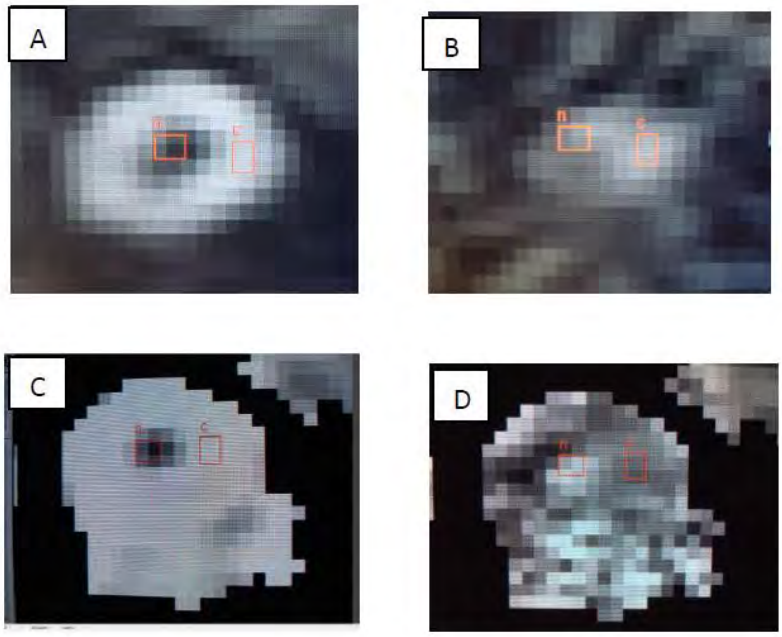

A – B0 image, B – B1000 image, C- Apparent Diffusion Coefficient (ADC) map representing an average of axial and radial diffusion, D – Fractional Anisotropy (FA) image

Figure 2. Scatter Plots of ADC, AI and FA of the optic nerves

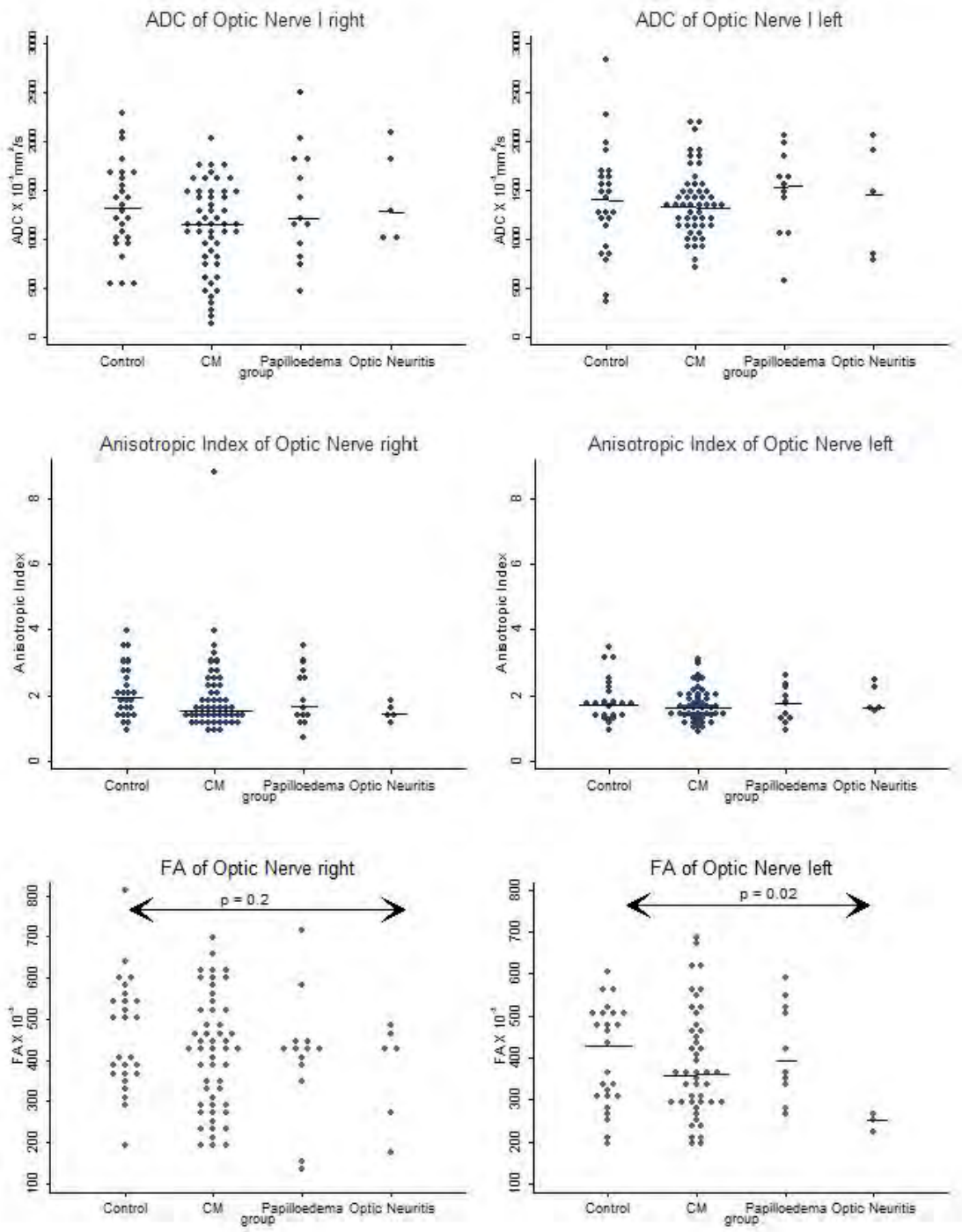

ADC – Apparent Diffusion Coefficient, I – represents the eigenvector of diffusion along the nerve, FA – Fractional Anisotropy, For ADC scatter plots Y axis is ADC x 10^{-3} mm^2/s, For FA scatter plots Y-axis is FA x 10^{-3}

Figure 3 Scatter Plots of ADC, AI and FA of the peri-optic CSF

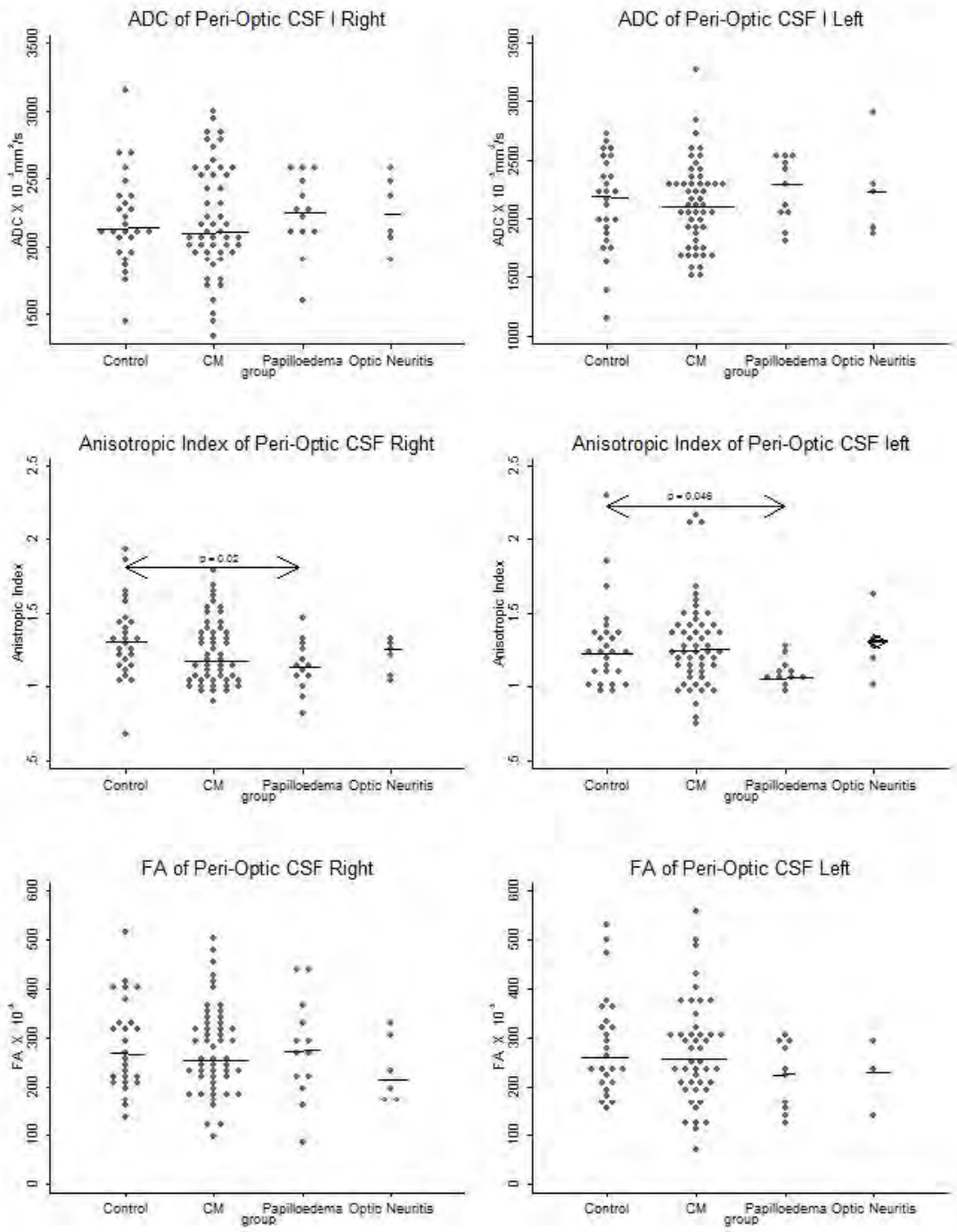

ADC – Apparent Diffusion Coefficient, I – represents the eigenvector of diffusion along the nerve, FA – Fractional Anisotropy, For ADC scatter plots Y axis is ADC x 10^{-3} mm^2/s, For FA scatter plots Y-axis is FA x 10^{-3}

Figure 4. Comparison of Anisotropic Index between the Study Groups

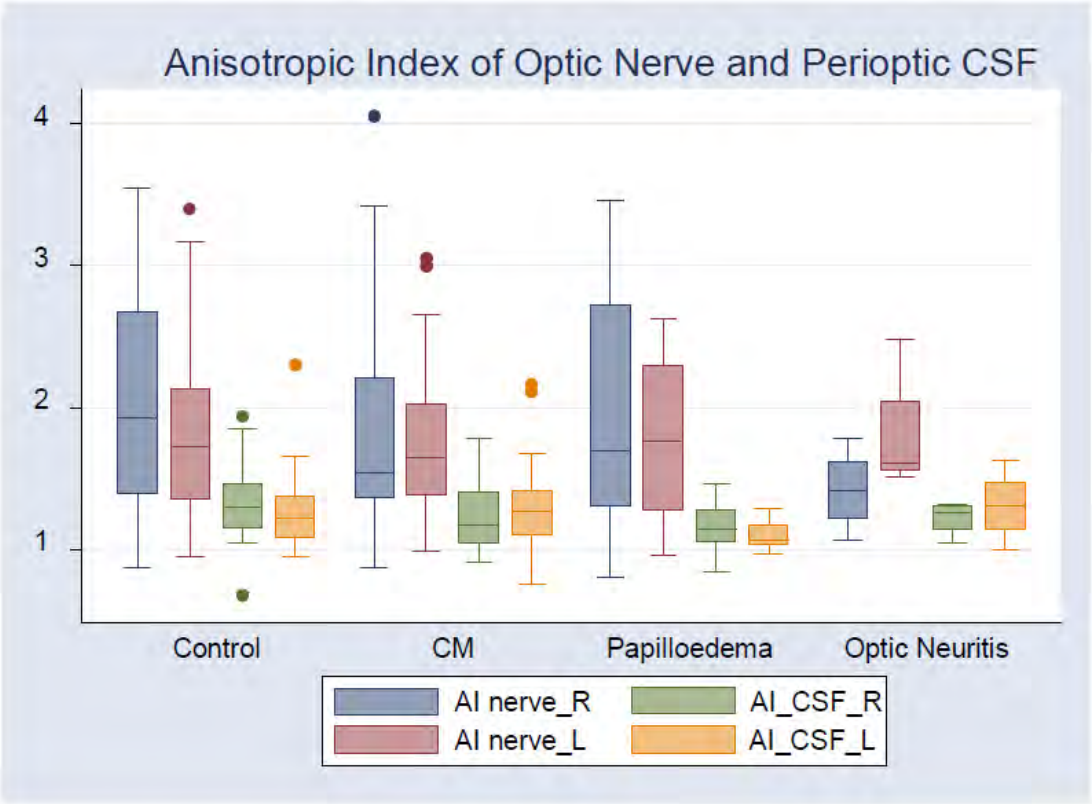

AI – Anisotropic Index, CM – Cryptococcal Meningitis, R – right optic nerve, L – left optic nerve

Table 3. ADC, Anisotropic Index and Fractional Anisotropy of the Optic Nerve

	ADC x 10^{-3} mm^2/s Mean (SD)		Fractional Anisotropy Mean (SD)		Anisotropy Index Median (IQR)	
	Right	Left	Right	Left	Right	Left
Normal Control	1320 (463)	1380 (547)	0.46 (0.13)	0.41 (0.12)[a]	2.0 (1.5;2.7)	1.7 (1.4;2.0)
CM with normal vision	1207 (412)	1387 (316)	0.41 (0.16)	0.42 (0.15)	1.5 (1.2;1.8)	1.6 (1.4;2.0)
CM with decreased vision	976 (513)	1382 (359)	0.44 (0.11)	0.34 (0.08)	2.2 (1.4;2.6)	1.7 (1.4;2.0)
CM with normal CSF pressure	1117 (418)	1229 (239)	0.39 (0.17)	0.45 (0.16)	1.5 (1.4;2.3)	2.0 (1.6;2.6)
CM with elevated CSF pressure	1118 (498)	1407 (357)	0.43 (0.14)	0.38 (0.12)	1.5 (1.2;2.3)	1.6 (1.3;2.0)
All CM patients	1116 (461)	1365 (339)	0.42 (0.14)	0.39 (0.13)	1.6 (1.4;2.3)	1.6 (1.4;2.0)
Papilloedema	1354 (575)	1471 (433)	0.41 (0.15)	0.42 (0.11)	1.7 (1.3;2.7)	1.8 (1.3;2.3)
Optic Neuritis	1451 (487)	1419 (589)	0.38 (0.13)	0.25 (0.02)[a]	1.5 (1.4;1.7)	1.6 (1.6;2.3)

ADC – Apparent diffusion coefficient, SD – Standard Deviation, IQR – Interquartile range, CM – Cryptococcal meningitis. [a] Significant difference between FA of normal controls and optic neuritis ($p = 0.02$)

Table 4: ADC, Anisotropic Index and Fractional Anisotropy of the Peri-optic SAS (CSF)

	ADC x 10^{-3} mm^2/s Mean (SD)		Fractional Anisotropy Mean (SD)		Anisotropy Index Median (IQR)	
	Right	Left	Right	Left	Right	Left
Normal Control	2193 (344)	2130 (400)	0.29 (0.09)[a]	0.29 (0.1)[a]	1.3 (1.2;1.4)[b]	1.2 (1.1;1.4)[b]
CM with normal vision	2118 (356)	2081 (358)	0.30 (0.08)	0.32 (0.1)	1.2 (1.1;1.4)	1.3 (1.1;1.5)
CM with decreased vision	2315 (411)	2183 (364)	0.24 (0.09)[a]	0.21 (0.08)[a]	1.2 (1.1;1.5)	1.3 (1.1;1.4)
CM with normal CSF pressure	2078 (352)	2057 (248)	0.3 (0.12)	0.29 (0.13)	1.3 (1.0;1.4)	1.2 (1.1;1.4)
CM with elevated CSF pressure	2190 (378)	2073 (356)	0.27 (0.08)	0.28 (0.11)	1.2 (1.1;1.4)	1.3 (1.1;1.5)
All CM patients	2196 (400)	2127 (360)	0.28 (0.09)	0.27 (0.11)	1.2 (1.1;1.4)	1.3 (1.1;1.4)
Papilloedema	2250 (283)	2248 (271)	0.28 (0.11)	0.22 (0.07)	1.1 (1.1;1.3)[b]	1.1 (1.0;1.2)[b]
Optic Neuritis	2260 (267)	2236 (417)	0.23 (0.07)	0.22 (0.07)	1.3 (1.1;1.3)	1.3 (1.2;1.3)

ADC – Apparent diffusion coefficient, SD – Standard Deviation, IQR – Interquartile range, CM – Cryptococcal meningitis. [a] Significant difference between FA in Normal Control and CM with decreased vision (p=0.03). [b] Significant difference between Anisotropic index in Normal Control and Papilloedema groups.

References

1. Lightowler JV, Cooke GS, Mutevedzi P, Lessells RJ, Newell ML, et al. (2010) Treatment of cryptococcal meningitis in KwaZulu-Natal, South Africa. PLoS One 5: e8630.
2. Park B.J WK, Marston BJ (2009) Estimation of the global burden of cryptococcal meningitis among persons living with HIV/AIDS. AIDS 23: 525-530.
3. Moodley A, Rae W, Bhigjee A, Connolly C, Devparsad N, Michowicz A, Harrison T, Loyse A Early Clinical and Subclinical Visual Evoked Potential and Humphrey's Visual Field Defects in Cryptococcal Meningitis. PLoS ONE 7(12): e52895. doi:10.1371/journal.pone.005.
4. Rex JH, Larsen RA, Dismukes WE, Cloud GA, Bennett JE (1993) Catastrophic visual loss due to Cryptococcus neoformans meningitis. Medicine (Baltimore) 72: 207-224.
5. Chan KH, Mak W, Ho SL (2007) Cryptococcal meningitis with raised intracranial pressure masquerading as malignant hypertension. Int J Infect Dis 11: 366-367.
6. Claus JJ, Portegies P (1998) Reversible blindness in AIDS-related cryptococcal meningitis. Clin Neurol Neurosurg 100: 51-52.
7. Cohen DB, Glasgow BJ (1993) Bilateral optic nerve cryptococcosis in sudden blindness in patients with acquired immune deficiency syndrome. Ophthalmology 100: 1689-1694.
8. Corti M, Solari R, Cangelosi D, Dominguez C, Yampolsky C, et al. (2010) Sudden blindness due to bilateral optic neuropathy associated with cryptococcal meningitis in an AIDS patient. Rev Iberoam Micol 27: 207-209.
9. Johnston SR, Corbett EL, Foster O, Ash S, Cohen J (1992) Raised intracranial pressure and visual complications in AIDS patients with cryptococcal meningitis. J Infect 24: 185-189.
10. Kestelyn P, Taelman H (1997) Visual loss and cryptococcal meningitis. Trans R Soc Trop Med Hyg 91: 727-728.

11. Lipson BK, Freeman WR, Beniz J, Goldbaum MH, Hesselink JR, et al. (1989) Optic neuropathy associated with cryptococcal arachnoiditis in AIDS patients. Am J Ophthalmol 107: 523-527.

12. Seaton RA, Verma N, Naraqi S, Wembri JP, Warrell DA (1997) The effect of corticosteroids on visual loss in Cryptococcus neoformans var. gattii meningitis. Trans R Soc Trop Med Hyg 91: 50-52.

13. Trip SA, Wheeler-Kingshott C, Jones SJ, Li WY, Barker GJ, et al. (2006) Optic nerve diffusion tensor imaging in optic neuritis. Neuroimage 30: 498-505.

14. Kolbe S, Chapman C, Nguyen T, Bajraszewski C, Johnston L, et al. (2009) Optic nerve diffusion changes and atrophy jointly predict visual dysfunction after optic neuritis. Neuroimage 45: 679-686.

15. Hagmann P, Jonasson L, Maeder P, Thiran JP, Wedeen VJ, et al. (2006) Understanding diffusion MR imaging techniques: from scalar diffusion-weighted imaging to diffusion tensor imaging and beyond. Radiographics 26 Suppl 1: S205-223.

16. Naismith RT, Xu J, Tutlam NT, Trinkaus K, Cross AH, et al. (2010) Radial diffusivity in remote optic neuritis discriminates visual outcomes. Neurology 74: 1702-1710.

17. Moodley A, Rae W, Bhigjee A, Loubser N., Michowicz A (2012) New Insights into the Pathogenesis of Cryptococococcal Induced Visual Loss Using Diffusion-Weighted Imaging of the Optic Nerve. Neuro-ophthalmology 36: 186-192.

18. Hickman SJ, Wheeler-Kingshott CA, Jones SJ, Miszkiel KA, Barker GJ, et al. (2005) Optic nerve diffusion measurement from diffusion-weighted imaging in optic neuritis. AJNR Am J Neuroradiol 26: 951-956.

19. Iwasawa T, Matoba H, Ogi A, Kurihara H, Saito K, et al. (1997) Diffusion-weighted imaging of the human optic nerve: a new approach to evaluate optic neuritis in multiple sclerosis. Magn Reson Med 38: 484-491.

20. Wheeler-Kingshott CA, Trip SA, Symms MR, Parker GJ, Barker GJ, et al. (2006) In vivo diffusion tensor imaging of the human optic nerve: pilot study in normal controls. Magn Reson Med 56: 446-451.

21. Chabert S, Molko N, Cointepas Y, Le Roux P, Le Bihan D (2005) Diffusion tensor imaging of the human optic nerve using a non-CPMG fast spin echo sequence. J Magn Reson Imaging 22: 307-310.

22. Schirmer CM, Hedges TR, 3rd (2007) Mechanisms of visual loss in papilledema. Neurosurg Focus 23: E5.

23. Killer HE, Jaggi GP, Miller NR, Huber AR, Landolt H, et al. (2011) Cerebrospinal fluid dynamics between the basal cisterns and the subarachnoid space of the optic nerve in patients with papilloedema. Br J Ophthalmol 95: 822-827.

24. Killer HE, Jaggi GP, Flammer J, Miller NR, Huber AR, et al. (2007) Cerebrospinal fluid dynamics between the intracranial and the subarachnoid space of the optic nerve. Is it always bidirectional? Brain 130: 514-520.

25. Killer HE, Laeng HR, Flammer J, Groscurth P (2003) Architecture of arachnoid trabeculae, pillars, and septa in the subarachnoid space of the human optic nerve: anatomy and clinical considerations. Br J Ophthalmol 87: 777-781.

26. Naismith RT, Xu J, Tutlam NT, Snyder A, Benzinger T, et al. (2009) Disability in optic neuritis correlates with diffusion tensor-derived directional diffusivities. Neurology 72: 589-594.

27. De Schacht C, Smets RM, Callens S, Colebunders R (2005) Bilateral blindness after starting highly active antiretroviral treatment in a patient with HIV infection and cryptococcal meningitis. Acta Clin Belg 60: 10-12.

CHAPTER 9 PAPER 6

The Optic Nerve Compartment Syndrome in Cryptococcal-induced Visual Loss:

- This case report provides clinical support for the optic nerve compartment syndrome in CM induced visual loss
- A Moodley is the main author
- Published in *Neuro-ophthalmology* June 2013

Visual loss in cryptococcal meningitis (CM) has been postulated to be due to papilloedema and/or optic neuritis. A 28 yr. old HIV positive female presented with visual loss, swollen optic discs and elevated CSF pressure due to CM. CT cisternography and T2 MRI showed occlusion of the peri-optic CSF space and re-opening after serial lumbar punctures. Presumably lowering of the intracranial pressure resulted in equalization of pressure across the pressure gradient created by the fungal block. This case supports a third mechanism of visual loss in CM viz. an optic nerve compartment syndrome which seems more plausible as the principal mechanism.

The Optic Nerve Compartment Syndrome in Cryptococcal-induced Visual Loss

Anand Moodley[1], Neil Naidoo[1], Deneys Reitz[2], Naren Chetty[3], William Rae[4]

[1] *Department of Neurology, Greys Hospital, Pietermaritzburg, South Africa*

[2] *Department of Radiology, Greys Hospital, Pietermaritzburg, South Africa*

[3] *Department of Ophthalmology, Greys Hospital, Pietermaritzburg, South Africa*

[4] *Department of Medical Physics, University of the Free State, Bloemfontein, South Africa*

Corresponding author: A Moodley, Department of Neurology, Greys Hospital, Pietermaritzburg, South Africa.

Postal Address: PO Box 13833, Cascades, 3202, South Africa.

Email: anand.moodley@kznhealth.gov.za Tel: +2733 897 3298 Fax: +2733 8973409

Mobile: +2784 5955077

Word Count (excluding abstract, figures and references): 1068

Number of References: 10

Keywords: cryptococcal meningitis, optic nerve, compartment syndrome, papilloedema, optic neuritis

Abstract

Visual loss in cryptococcal meningitis (CM) has been postulated to be due to papilloedema and/or optic neuritis. A 28 yr. old HIV positive female presented with visual loss, swollen optic discs and elevated CSF pressure due to CM. CT cisternography and T2 MRI showed occlusion of the peri-optic CSF space and re-opening after serial lumbar punctures. Presumably lowering of the intracranial pressure resulted in equalization of pressure across the pressure gradient created by the fungal block. This case supports a third mechanism of visual loss in CM viz. an optic nerve compartment syndrome which seems more plausible as the principal mechanism.

Case Report

Visual loss in cryptococcal meningitis (CM) occurs in 35% of patients [1]. The landmark study by Rex et al proposed 2 mechanisms of visual loss, an early optic neuritis model that occurs within 6 days of disease onset and a late papilloedema model that occurs after 4 weeks [2]. Since then, there have been many case reports supporting or contesting those claims [3-6]. The overwhelming evidence is that raised intracranial pressure, which occurs in up to 67% of patients, plays a role [1,2]. Measures to lower intracranial pressure, such as serial lumbar punctures, ventriculoperitoneal shunts, lumbo-peritoneal shunts and optic nerve sheath fenestrations are all associated with improved visual outcome [7-9]. However, papilloedema in patients with raised intracranial pressure occurs in only 22% of patients [1,2]. So papilloedema alone cannot be entirely responsible for the visual loss. While optic neuritis has been documented in histopathological cases, its occurrence too is infrequent. We have suggested the possibility of a compartment syndrome as being more common and the more likely mechanism responsible for visual loss in the setting of raised intracranial pressure by using diffusion weighted imaging of the optic nerve [1]. We postulate that the compartment syndrome develops from plugging of the peri-optic CSF space by fungal elements at the optic canal level or within the orbital segment of the nerve. The nerve compression at these sites probably results in axoplasmic stasis and optic nerve dysfunction.

Plugging of the peri-optic space by fungi and polysaccharide remnants is facilitated by the presence of septae, trabeculae and pillars within this space. Killer et al have demonstrated the presence of these anatomical structures within the peri-optic space which are responsible for the compartmentalization of the peri-optic CSF space from the intracranial subarachnoid space (SAS) [10]. They have postulated that these structures may account for idiopathic intracranial hypertension (IIH) without papilloedema or asymmetrical papilloedema. We present a case that supports such a theory in CM, which shares similar characteristics to IIH as regards raised intracranial pressure, impaired CSF re-absorption and the lack of hydrocephalus.

A 28 year old HIV positive black female, on antiretroviral therapy presented with culture confirmed CM. Her symptoms included headaches, blurred vision, neck pain and fever. Of note was that she had no pain on eye movements and no diplopia. She was awake, alert and co-operative with minimal neck stiffness. Fundoscopy revealed bilateral swollen optic discs with peripapillary subretinal haemorrhages (Figure 1). Her best corrected visual acuity (BCVA) was 6/18 OD and 6/12 OS, colour vision on Ishihara pseudoisochromatic plates was 15/15 OU and her pupils were 3mm OU in ambient light and reactive to direct and consensual reflexes. Humphrey's visual fields demonstrated enlarged blind spots OU and nasal constriction OD (Figure 2). The rest of her cranial nerves, motor, sensory and co-ordination assessment were normal. Visual evoked potential (VEP) P100 latencies were normal bilaterally (111ms OD and 108ms OS).

MRI brain was normal and MRI orbits showed no signal change within the optic nerve on high resolution 3D T2 imaging (Figure 3, A and B). The peri-optic CSF signal was absent bilaterally on the T2 imaging. There was flattening of the posterior pole of the globe and optic disc elevation bilaterally indicative of raised intracranial pressure. Post contrast T1 SPIR (FAT Saturation) imaging showed optic nerve sheath enhancement (Figure 4). Her CD4 count was 181, CSF was acellular with normal biochemistry, CSF pressure was elevated at 37cmH_2O and cryptococcal antigen and India ink were positive. She had a macrocytic anaemia of 10.2 g/dl. Her vitamin B12 levels were normal suggesting that the macrocytosis was due to antiretroviral therapy.

CT cisternography, performed via lumbar puncture, showed good contrast filling of the basal cisterns but stasis of the contrast loaded CSF at the distal optic nerve sheath before the optic canal (Figure 5). No contrast filling was noted to proceed beyond this block despite having the patient in a Trendelenburg position. She was managed with intravenous Amphotericin B (0.7mg/kg/d) for 2 weeks followed by consolidation therapy with oral Fluconazole 400mg daily. Serial lumbar punctures were offered to relieve the intracranial pressure which was normalized after 3 lumbar punctures. At 8 weeks follow up, her headaches had completely cleared and BCVA improved to 6/12 OD and 6/7.5 OS. CSF pressure was noted to be normal before the repeat MRI which showed unblocking and re-filling of the peri-optic CSF space (Figure 3).

The patient's clinical presentation is consistent with raised intracranial pressure from CM. Her swollen optic discs, subretinal haemorrhages and visual field defects are consistent with raised intracranial pressure whereas the intact pupillary reflexes, colour vision, VEP and absence of optic nerve signal change on MRI make optic neuritis very unlikely. MRI brain showed no other cause for raised intracranial pressure apart from CM. The absence of CSF signal surrounding the optic nerve on T2 weighted imaging (Figure 2) and the stasis of contrast filled CSF at the orbital segment of the optic nerve (Figure 5) suggest complete plugging of the peri-optic space by cryptococcal fungal elements. The result would be a large pressure gradient created by this blockage between the significantly elevated intracranial pressure within the intracranial subarachnoid space (SAS) and the pressure of the proximal peri-optic CSF space. A compartment syndrome would thus follow causing optic nerve compression, axoplasmic stasis and optic nerve dysfunction that manifests with visual blurring. Seemingly, the extent of axoplasmic stasis determines the presence of papilloedema which develops when stasis reaches the optic nerve head; a phenomenon that will explain the disparity between the frequencies of elevated intracranial pressure, visual loss and papilloedema in CM.

This case provides good support for the compartment syndrome of the optic nerve in CM and needs further study. The optic nerve compartment syndrome addresses many deficiencies of the papilloedema and optic neuritis models. Papilloedema is partly responsible for visual loss but nerve compression downstream resulting in large pressure gradients and a compartment syndrome seems to explain the optic nerve dysfunction on Diffusion Weighted Imaging and the absence of signal changes on T2 imaging [1]. The absence of optic nerve sheath dilatation and surrounding CSF signal is perhaps due to fungal loading in the peri-optic CSF space. Optic neuritis as a cause for visual loss in CM is well documented but rare and possibly develops from a perineuritis. The pauci-inflammatory state of CM in HIV infected immunosuppressed patients is further support for the infrequent occurrence of optic neuritis in CM.

References

1. Moodley A, Rae W, Bhigjee A, Loubser N, Michowicz A (2012) New Insights into the Pathogenesis of Cryptococcal Induced Visual Loss Using Diffusion-Weighted Imaging of the Optic Nerve. Neuro-ophthalmology 36: 186-192.
2. Rex JH, Larsen RA, Dismukes WE, Cloud GA, Bennett JE (1993) Catastrophic visual loss due to Cryptococcus neoformans meningitis. Medicine (Baltimore) 72: 207-224.
3. Claus JJ, Portegies P (1998) Reversible blindness in AIDS-related cryptococcal meningitis. Clin Neurol Neurosurg 100: 51-52.
4. Graybill JR, Sobel J, Saag M, van Der Horst C, Powderly W, et al. (2000) Diagnosis and management of increased intracranial pressure in patients with AIDS and cryptococcal meningitis. The NIAID Mycoses Study Group and AIDS Cooperative Treatment Groups. Clin Infect Dis 30: 47-54.
5. Kestelyn P, Taelman H (1997) Visual loss and cryptococcal meningitis. Trans R Soc Trop Med Hyg 91: 727-728.
6. Corti M, Solari R, Cangelosi D, Dominguez C, Yampolsky C, et al. (2010) Sudden blindness due to bilateral optic neuropathy associated with cryptococcal meningitis in an AIDS patient. Rev Iberoam Micol 27: 207-209.
7. Macsween KF, Bicanic T, Brouwer AE, Marsh H, Macallan DC, et al. (2005) Lumbar drainage for control of raised cerebrospinal fluid pressure in cryptococcal meningitis: case report and review. J Infect 51: e221-224.
8. Petrou P, Moscovici S, Leker RR, Itshayek E, Gomori JM, et al. (2012) Ventriculoperitoneal shunt for intracranial hypertension in cryptococcal meningitis without hydrocephalus. J Clin Neurosci 19: 1175-1176.
9. Milman T, Mirani N, Turbin RE (2008) Optic nerve sheath fenestration in cryptococcal meningitis. Clin Ophthalmol 2: 637-639.
10. Killer HE, Jaggi GP, Flammer J, Miller NR, Huber AR, et al. (2007) Cerebrospinal fluid dynamics between the intracranial and the subarachnoid space of the optic nerve. Is it always bidirectional? Brain 130: 514-520.

Figure 1: **Bilateral severe papilloedema with subretinal haemorrhages**

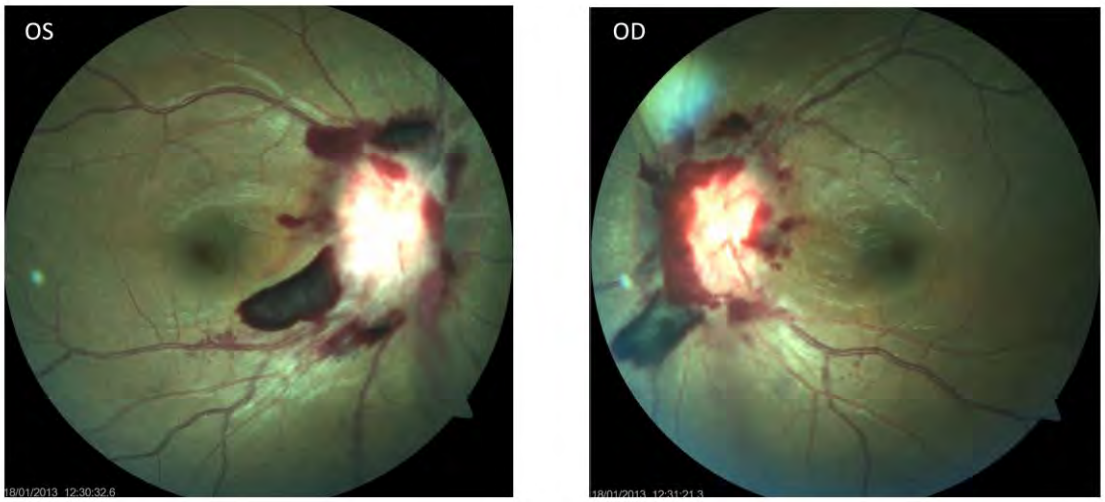

Figure 2: Humphrey's Visual Fields consistent with raised intracranial pressure bilaterally.

Large blind spots noted bilaterally and nasal field constriction noted on the right.

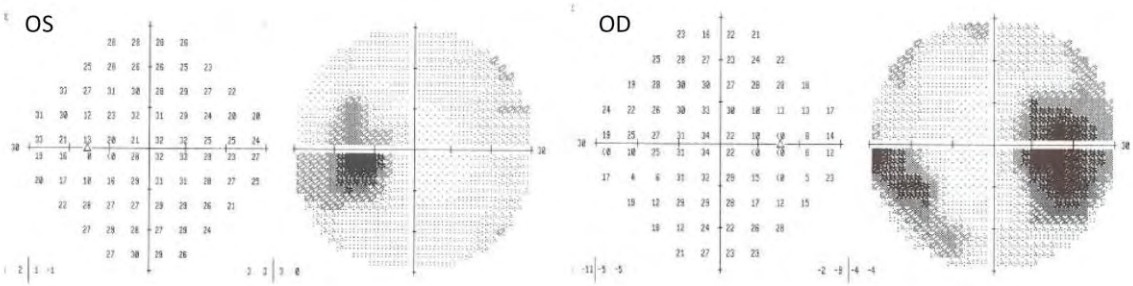

Figure 3: Axial T2 High Resolution 3D images of the orbit. There is loss of peri-optic CSF signal on A and B – Pre Serial Lumbar Punctures, and present on C and D (8 weeks later) – Post Serial Lumbar Punctures. B- shows a sleeve of CSF entering the optic canal with no continuation into the orbital segment of the optic nerve. D – shows re-opening of the peri-optic CSF space with narrowing and filling defects noted at the distal part of the orbital segment of the optic nerve.

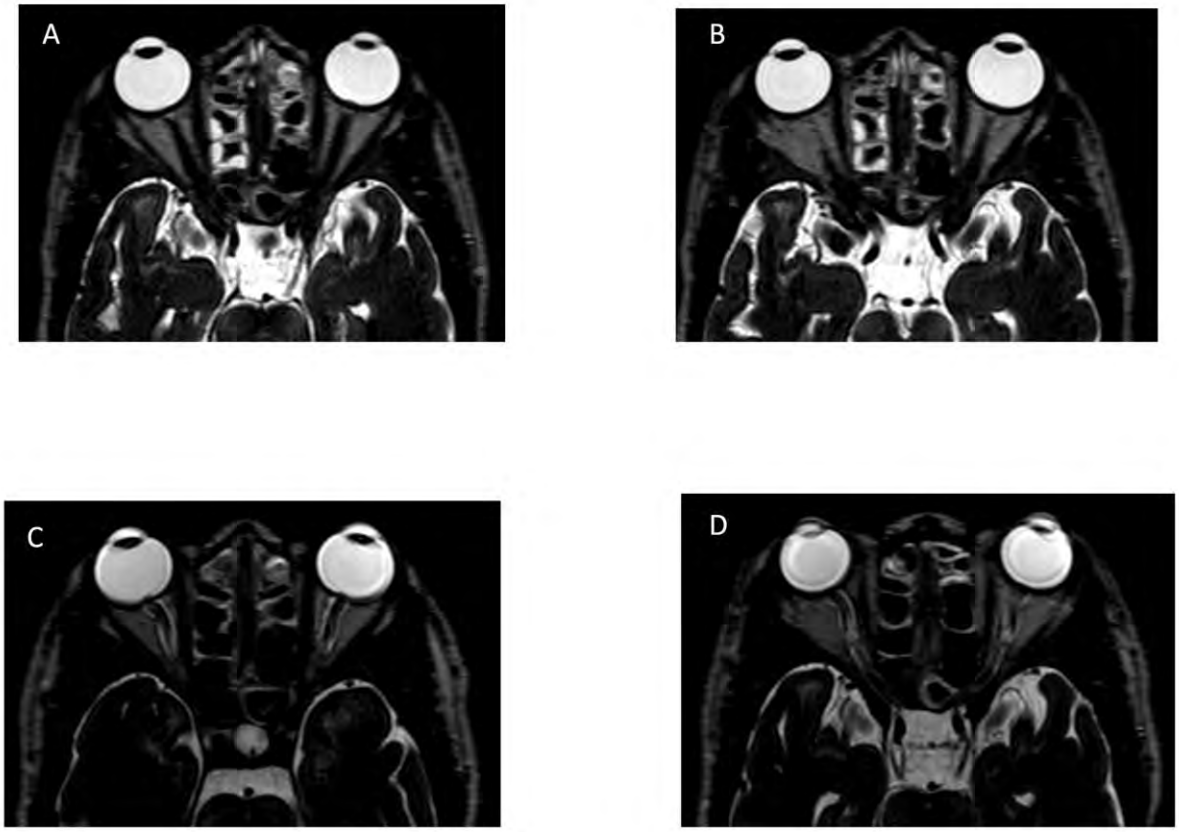

Figure 4: Pre (A) and Post (B) contrast T1 SPIR (Fat Saturation) images of the orbit showing only optic nerve sheath enhancement

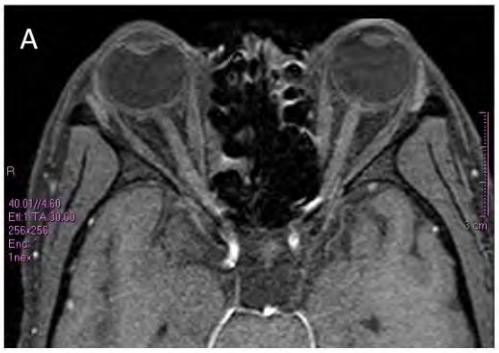

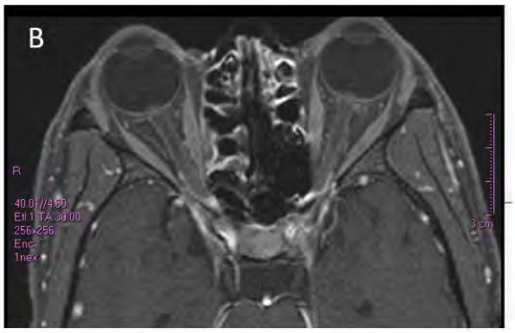

Figure 5: CT Cisternography. A, C show no contrast loaded CSF in the peri-optic CSF space. B, D show bilateral stasis of contrast loaded CSF at the distal part of the optic nerve sheath before the optic canal.

CHAPTER 10 DISCUSSION

The qualitative and quantitative diffusion imaging of the optic nerve has proven to be a significant investigational tool in the imaging of optic nerve microstructure. In disease processes, most advances have been made in the imaging of chronic optic neuritis in multiple sclerosis and latterly in the imaging of acute optic neuritis [21, 22, 79, 112], ischaemic optic neuropathy [24] and glaucoma [86]. Hitherto, optic nerve diffusion imaging has never been applied to neuro-infectious disorders. With cryptococcal-induced visual loss being common in developing countries and noting that reversibility of blindness is possible with early intervention, we opted to use optic nerve diffusion to investigate the pathogenesis of CM induced visual loss. Consensus regarding the pathogenesis of CM induced visual loss has been lacking with good evidence for both the optic neuritis and papilloedema models reported in the literature. The likelihood of a dual mechanism has also been entertained but never demonstrated. The possibility of a third mechanism viz. the optic nerve compartment syndrome is also conceivable. Hence the motivation for this study was to establish if optic nerve diffusion imaging could provide new insights into the pathogenesis of CM induced visual loss.

Testing of visual acuity is difficult in patients presenting acutely with CM for various reasons. Patients are confused, poorly attentive, systemically unwell, have raised intracranial pressure and frequently have 6th nerve palsies as false localizing signs. Despite these setbacks, we were able to demonstrate visual loss as a complication in 34.6% (18/52) of patients (reported in Chapter 4, Paper 1), similar to the incidence previously reported by Moosa et al [6]. All cases occurred within 4 weeks of disease onset and none after commencement of treatment. Severe visual loss occurred in 5 patients (9.6%), but none developed catastrophically within 12 hours as described by Rex et al in their series [10]. Such

visual loss was due to optic nerve infiltration/ neuritis. None of our patients complicated with optic nerve infiltration as demonstrated by clinical, radiological and electrophysiological means. Optic nerve infiltration as reported by Rex et al occurs early, so imaging within 4 weeks of symptom onset was sufficient time to detect nerve infiltration [10].

Raised intracranial pressure was common, occurring in 69% (36/52) at an average of 34cmCSF whereas disc swelling was noted in 25% of patients. Extremely high CSF pressures were noted in 7 patients at levels greater than 50cmCSF. Patients with decreased vision were more likely to have elevated CSF pressure and swollen discs; however only 44% had both, suggesting that elevated CSF pressure impairs optic nerve functioning, not predominantly at the optic nerve head, but somewhere between the lamina cribrosa and the optic canal. Despite elevated CSF pressure being common in CM, swollen optic discs is not as common (Figure 4, Chapter 4 Paper 1). Only twenty-three percent of all patients had both elevated pressure and swollen discs. The possibility of pressure related effects on the optic nerve exists, but not only at the optic nerve head. Whilst not entirely supporting the papilloedema model for vision loss this lends support for the compartment syndrome occurring somewhere along the nerve, either at the optic canal or the intra-orbital segment of the nerve.

None of the CM patients scanned showed any optic nerve signal change on T1, T2, T2 FLAIR or T1 post contrast image. The absence of signal change reflects a paucity of inflammatory reaction had there been any optic nerve infiltration by the organism, a situation that is reflected by minimal CSF changes in CM [6]. Conversely, the absence of signal change suggests that no infiltration of the optic nerve occurs by the organism or inflammatory cells and that an optic neuritis model does not occur in early CM to explain visual loss. Optic nerve infiltration by the organism does occur and is well documented but is not an early feature and not as frequent as reported by Rex et al [10, 11, 13].

The lack of any significant difference between the optic nerve sheath diameter in the cryptococcal meningitis patients with and without elevated CSF pressure also supports the likelihood of a compartment syndrome (Table 2, Chapter 4 Paper 1). The lack of appreciable swelling of the optic nerve sheath in the presence of elevated CSF pressure as confirmed on lumbar puncture is possibly due to a blockage proximally at the rigid optic canal or somewhere along the intra-orbital optic nerve where septae in the subarachnoid space have created a blockage to CSF flow.

In Paper 3, Chapter 6 MRI scanning has again been demonstrated to be an extremely sensitive imaging modality in the setting of central nervous system (CNS) cryptococcosis [48]. The overall percentage of presumptive cryptococcosis-related lesions on radiological findings is in line with results from the French case series [63% (55/87) vs. 79% (19/24) presumed cryptoccosis-related lesions, respectively] [48]. We detected significant numbers of patients with focal cerebral oedema [16% (14/87)]. No patients with generalised cerebral oedema were detected in the French series. 2% (2/87) patients had hydrocephalus versus 0% (0/24) in the French series, and we detected more cases of pseudocysts/cryptococcomas, radiological meningitis and infarcts [48].

In the case series of 87 patients, 20 (23%) patients had either cortical or lacunar infarcts that were presumed to be CNS cryptococcosis-related. This finding is in keeping with recent Taiwanese data from immunocompetent patients where acute/subacute cerebral infarction (ASCI) occurred in 7/37 (20%) of patients [113]. Cerebral infarction, presumably related to some vascular, or perivascular inflammation, may not be uncommon in CM even in profoundly immunosuppressed patients with low CD4 cell counts.

In this dataset, visual loss significantly correlated with the presence of presumed cryptococcosis-related lesions. Dilated VRS may indicate elevated CSF pressure. It is

difficult to determine the presence of brain swelling on a single brain scan in the context of late stage HIV-disease when significant but variable degrees of cerebral atrophy are present. We were particularly interested to see if paired initial and follow up scans suggested the presence of initial relative brain swelling in the first few days after presentation when any inflammatory response is likely to be maximal [114]. However, initial brain swelling was only identified in one patient on this basis. Brain swelling may not be a common or significant factor in explaining the raised CSF pressure or abnormal mental status associated with CM. However, in the study initial MRI scanning was carried out a median of seven days from patients starting antifungal therapy and it is conceivable that this was perhaps too late to detect early brain swelling that may have improved after initial antifungal therapy and appropriate management of CM complications such as raised ICP.

In Chapter 7, paper 4 we report on 90 patients who were recruited for the electrophysiological study of CM induced visual loss. Visual impairment was detected in 40/86 (46.5%) of patients with CM, and 16/40 (40%) had profound visual loss of < 6/60 (19% in total). VEP abnormalities were detected more frequently, occurring in 68.9% of right eyes and 67.6% of left eyes and subclinical disease in 56.5% (Tables 1 and 2, Chapter 7 Paper 4). The predominant abnormal VEP parameter was prolongation of the P100 latency occurring in 42.3% of all eyes (Table 2, Paper 4). The mean P100 latency values were 118.9 (±16.5) ms and 119.8 (±15.7) ms for the right and left eyes respectively, mildly prolonged when compared to our laboratory references of 104 (±10) ms, but still significant ($p<0.001$). Prolonged P100 latencies suggest demyelination or conduction block (focal demyelination), as occurs in acute optic neuritis which in the case of CM, a non-demyelinating disorder, will suggest focal pressure effects on the optic nerve. Conceivably the most likely sites of optic nerve compression will be at the optic canal or at sites of dense subarachnoid trabeculae

within the optic nerve sheath, providing soft evidence for the compartment syndrome in cryptococcal induced visual loss.

VEP latency strongly correlated with visual acuity and swollen optic disc; when VEP latency was prolonged, visual acuity was reduced and optic disc swelling occurred (Table 3, Chapter 7 Paper 4). Such abnormal parameters provide strong clinical and electrophysiological evidence for optic nerve dysfunction in cryptococcal induced visual loss. The fact that 32.5% and 42.2% of right and left eyes respectively with normal acuity had prolonged VEP latency is good evidence for subclinical optic nerve dysfunction. The contribution to prolonged VEP latency made by the HIV virus in advanced HIV infection requires further evaluation. Claims of subclinical VEP abnormalities in 3-49% of HIV infected patients due to retro-chiasmic or occipital cortical neuron loss have not been verified [115, 116]. Mwanza's group did not exclude cryptococcal meningitis and it is likely that the 49% includes patients with cryptococcal meningitis. In Malessa's group of asymptomatic HIV-infected patients, 3% had VEP latency prolongation and 33% had VEP amplitude reduction when CD4 counts were below 100. However in the setting of co-infection with CM, and noting the prominence played by the fungus in visual loss, one has to presume that a large amount of the 56.5% of overall VEP abnormality (latency and amplitude) in our patients was due to cryptococcal co-infection rather than HIV alone (Table 2, Chapter 7 Paper 4). A limitation of this study is the failure of comparison to an asymptomatic HIV positive group without CM to determine the impact if any of HIV infection itself.

VEP amplitude changes occurred less frequently and this was the abnormality in only 14.6% of eyes suggesting that secondary axonal changes were not frequent despite the low mean amplitude of 7.4 (±3.9) μV and 7.0 (±3.7) μV for the right and left eyes respectively (Table 2, Chapter 7 Paper 4). The low frequency of amplitude changes may be a reflection of the

somewhat early recruitment of patients from symptom onset (4 weeks). Perhaps repeat testing later in the disease may reveal more secondary axonal change, which is a late phenomenon. Consequently, no significant correlations were noted between VEP amplitude and visual acuity, CSF pressure, optic disc swelling or CD4 counts in early CM (Table 2, Chapter 7 Paper 4).

HVF abnormalities were very frequent in patients who could be tested, occurring in 76.6% of right eyes and 71.1% of left eyes (Table 1, Chapter 7 Paper 4). A major limitation of HVF testing was that patients with profound visual loss (VA < 6/60) could not be tested. The predominant field defects were peripheral constriction with large blind spots followed by central and paracentral field defects (Figure 1, Chapter 7 Paper 4). As peripheral constriction with large blind spots is associated with papilloedema-related optic nerve dysfunction, HVF supports raised intracranial pressure being an important cause of optic nerve dysfunction in cryptococcal induced visual loss. The central field defects found suggest intrinsic optic nerve disease or secondary macular dysfunction from severe papilloedema; however an inability to test patients with profound visual loss suggests that the central field defect was probably underestimated in this patient cohort.

Subclinical HVF abnormalities were not as frequent as VEP latency abnormalities and are therefore less sensitive in detecting optic nerve dysfunction in patients with normal visual acuity in CM. No significant correlations were noted between HVF and CSF pressure, optic disc swelling, CD4 counts or VEP amplitude.

Optic nerve diffusion imaging has gained prominence as a useful investigational tool of optic nerve microstructure and pathology [22, 81, 85]. We have opted to use both DWI and DTI to objectively examine the microstructure of the optic nerve in CM induced visual loss to obtain insights into its pathogenesis.

The technique used to scan the optic nerve was different to that of Wheeler- Kingshott's zonal oblique multislice echo planar imaging (ZOOM-EPI) [33], Iwasawa's IVIM [32] and Chabert's non-CPMG FSE [34]. We used a higher B1000 gradient to eliminate CSF artifact rather than FLAIR, single shot fast spin echo to limit the effect of motion and a coronal oblique slice to image the optic nerves individually. By not using FLAIR, identification of the optic nerve on B0 images was made much simpler. The MD values reported for healthy optic nerves in the studies of Wheeler-Kingshott et al [33], Iwasawa et al [32] and Chabert et al [34] range between 1.0 and 1.3 x 10^{-3} mm^2/s and FA range between 0.4 and 0.6. The method we used revealed comparable values of 1.2 ± 0.34 x 10^{-3} mm^2/s for MD and 0.4 ± 0.12 for FA of healthy optic nerves.

Optic nerve movement and CSF signal artifact still posed challenges to reliable imaging. In Chapter 5 Paper 2, we report on 29 healthy volunteers with intact visual acuity and eye movements that were subjected to DWI and DTI of the optic nerves. Optic nerve tracking was also done on 26 right eyes using single shot EPI FSE over a 3 minute period. Twenty still shots from nerve tracking were analysed and compared to diffusion data.

Optic nerve movement distorts diffusion imaging of the optic nerve. Six eyes had to be excluded from analysis due to poor visualization as a result of eye movement. Where analysis was possible, table 1 (Chapter 5 Paper 2) shows us that the results obtained were reliable. The ADC, MD, FA and AI of the optic nerve obtained in this study are comparable to those of Wheeler-Kingshott et al [33], Iwasawa et al [32]and Chabert et al [34](Table 1, Chapter 5 Paper 2). The values for the peri-optic CSF space however are novel. The peri-optic CSF has a higher ADC and MD, and lower FA and AI indicative of the higher water content of the space. The greater isotropic diffusion is expected, but the AI > 1.0 seems to indicate laminar rather than turbulent flow of CSF in this space. As to whether there is bidirectional flow of

CSF within this space to allow return of the CSF back towards the brain [66] or unidirectional flow to the optic sheath cul-de-sac and extravasation into the orbit and optic nerve sheath lymphatics [111], cannot be determined from these data.

Despite attempts at limiting optic nerve movement both voluntary and involuntary saccadic movements are unavoidable during a 3-5 minute DWI or DTI recording. Macroscopically, the optic nerve moves appreciably during a 3 minute recording. We recorded for our normal control group a mean of 11.8 mm (range 5.7 – 23.7) over a mean area of 5.2 mm^2 (range 0.6-22.1). Fortunately, our data shows that optic nerve movement has no significant impact on optic nerve and peri-optic CSF diffusion parameters (Table 2, Chapter 5 Paper 2). Even more pleasing is the result that not suppressing the peri-optic CSF has no significant impact on optic nerve diffusion parameters on DWI and DTI. The advantage of not suppressing the CSF signal is better identification of the nerve on B0 images and the benefit of recording peri-optic CSF diffusion parameters which can be applied to disorders such as papilloedema.

Axonal disruption within the optic nerve following chronic optic neuritis is associated with an increase in ADC and a decrease in FA [22]. Whilst no significant difference in MD or FA was found between the elevated and normal CSF pressure groups in cryptococcal meningitis (graphs 1, 2 and table 3, Chapter 4 Paper 1), the tendency towards an elevated ADC and reduced FA suggests either axonal disruption in the elevated CSF pressure group or papilloedema related changes. In the acute setting where axonal degeneration is not expected, the latter seems more plausible. These findings lend support to the role played by elevated CSF pressure and papilloedema in early vision loss in CM.

The similar anisotropy index in all pressure groups (Table 3, Chapter 4 Paper 1) and all vision groups (Table 4, Chapter 4 Paper 1) suggests that axial diffusion along the nerve is not preferentially affected in CM. Optic nerve infiltration therefore seems unlikely as a plausible

explanation for visual loss in early CM, contrary to the widely accepted theory of Rex et al [10]. This tendency towards increased ADC and reduced FA needs to be confirmed in future studies by recruiting larger number of patients, using 3T MRI which would offer higher resolution and by comparison to other causes of papilloedema.

From 29 normal controls, 59 culture confirmed CM patients, 14 patients with papilloedema and 14 patients with optic neuritis (from causes other than CM) we were able to compare ADC, FA and AI obtained from the optic nerves and peri-optic CSF space. Paper 5 reports on their results. The numbers analysed were reduced due to movement artifact and difficulty encountered in identifying the optic nerve on DWI and DTI (Table 1, Chapter 8 Paper 5).

The ADC of the peri-optic space is as expected much higher than that within the optic nerve due to the higher water content (Table 2, Chapter 8 Paper 5). The FA and anisotropic index of the optic nerve is greater than that of the peri-optic SAS due to the longitudinal orientation of the axons in the nerve that promote longitudinal diffusion in preference to radial diffusion. Not surprisingly, the peri-optic SAS too has an anisotropic index > 1.0 and mean FA of 0.29 (both more than vitreous, $p < 0.001$), suggesting that the flow of CSF within this space is greater in the axial rather than the radial axis. Hence the suggestion of laminar rather than turbulent flow is demonstrated by this data. Laminar flow results from either the septae and trabeculae within the peri-optic space which provide some directionality to the flow of CSF or from the pressure gradient between the intracranial SAS and the peri-optic SAS or flow follows virtual channels created and obliterated as the nerve moves within its sheath as part of the physiological function of the moving eye.

Figure 3 and Table 4 (Chapter 8 Paper 5) show a significant lowering of the anisotropic index of the peri-optic CSF space in the papilloedema group when compared to the normal controls (1.3 vs. 1.1, and 1.2 vs. 1.1; $p= 0.02$ and 0.046 for the right and left eyes respectively). The

lesser anisotropic (greater isotropic) diffusion in the setting of raised intracranial pressure suggests more turbulent flow of CSF in the peri-optic SAS. In the setting of raised intracranial pressure from CM, a similar lowering of the anisotropic index in the peri-optic SAS would be expected, but was not demonstrated in our cohort. The implication would be that the compartmentalization of the intracranial SAS from the peri-optic SAS was significant enough to prevent this effect. Fungal loading or even an excess of inflammatory cells within the peri-optic SAS would be expected to lower the anisotropic index in patients with CM and raised intracranial pressure, but this too did not occur. This finding together with the lack of dilatation of the peri-optic SAS in CM provides additional evidence for the compartment syndrome at the optic canal being the vital link between raised intracranial pressure and visual loss in CM.

We have been able to demonstrate for the first time using DWI and DTI that CSF flow in the peri-optic SAS is laminar. CSF flow in the longitudinal plane was in preference to that in the radial plane. Such anisotropy would be expected to be lost in the setting of CSF loading by cryptococcal fungi and inflammatory cells. We were unable to confirm this regardless of whether patients had normal or elevated CSF pressure, normal or decreased vision. The likelihood of blockage upstream to prevent this cannot be refuted. Turbulent peri-optic CSF flow in the papilloedema group was not demonstrated in CM further suggesting that the pressure in the peri-optic SAS is not elevated. The compartmentalization described by Killer et al between the intracranial SAS and peri-optic SAS is possibly exacerbated by the fungal loading at the optic canal level resulting in a compartment syndrome. Unlike the hypothesis proposed by Killer et al of compartmentalization without blockage, we propose that with blockage created by fungal loading trapped between the trabeculae, there is a greater pressure gradient, lack of elevation of pressure beyond and perhaps lack of dilatation of the peri-optic

space beyond the blockage due to fungal loading in that space and drainage of whatever CSF remains into the surrounding lymphatics.

Patients with CM did not demonstrate similar optic nerve or peri-optic SAS diffusion findings to that of optic neuritis or papilloedema regardless of their intracranial pressure and visual acuity. Raised intracranial pressure from causes other than CM does result in less anisotropic diffusion and more random diffusion of water molecules within the peri-optic SAS. The likelihood of greater compartmentalization between the intracranial SAS and peri-optic SAS exists in CM that prevents the transmission of pressure to the peri-optic space with blockage perhaps from fungal entrapment at the optic canal. There is however sufficient pressure transmitted to result in papilloedema in 25% of patients, but insufficient to result in turbulent flow. Raised intracranial pressure (69 -90%) is far more common than papilloedema [10, 49] and possibly results in optic nerve dysfunction and visual loss from compartmentalization of the peri-optic SAS from the intracranial SAS rather than papilloedema itself.

In Chapter 9 Paper 6, we present the case report of a 28 year old HIV positive female with CM induced visual loss. This case provides strong support for the optic nerve compartment syndrome as the mechanism underlying her visual loss. She presented with papilloedema and raised intracranial pressure from CM. There was complete obliteration of the peri-optic CSF space on MRI and CT cisternography showed blockage of flow of contrast loaded CSF into the distal orbital segment of the optic nerve. Lowering of intracranial CSF pressure and treatment with antifungal therapy resulted in re-opening of the peri-optic CSF space on MRI.

A large pressure gradient was created by the blockage between the significantly elevated intracranial pressure within the intracranial SAS and the pressure of the proximal peri-optic SAS. A compartment syndrome thus followed causing optic nerve compression, axoplasmic

stasis and optic nerve dysfunction that manifest with visual blurring. Seemingly, the extent of axoplasmic stasis determines the presence of papilloedema which develops when stasis reaches the optic nerve head; a phenomenon that will explain the disparity between the frequencies of elevated intracranial pressure, visual loss and papilloedema in CM.

This case provides good support for the compartment syndrome of the optic nerve in CM and needs further study.

Summary Points

- Visual loss is common in CM and occurs in 34.6 – 48% of patients
- Raised intracranial pressure occurs in 69-71% of patients and the average intracranial pressure in CM was 34cmCSF (range 21-50)
- Swollen optic discs occur in 25% of CM patients but 23% have swollen discs and raised intracranial pressure
- No signal changes or contrast enhancement were noted in any of the optic nerves in patients with CM induced visual loss
- Neither the optic nerve sheath nor the optic nerves were dilated in CM regardless of intracranial pressure

- Single shot EPI FSE, a b1000 gradient and lack of FLAIR are useful for limiting movement artifact and optic nerve identification on DWI and DTI
- The coronal oblique method of separate nerve imaging on DWI and DTI is a reliable and reproducible diffusion technique
- No significant correlation was noted between optic nerve movement parameters and diffusion parameters (ADC, MD, FA and AI)
- The non-suppressed CSF signal on DWI and DTI has minimal impact on diffusion parameters of the optic nerve but none translates to practical or clinical significance. No mathematical model is required for correction as reflected by low R^2 values on linear regression
- 63% of CM patients have neuroradiological lesions presumed to be cryptococcosis-related.
- 21% of CM patients have additional treatable diagnoses on imaging
- Visual loss correlated significantly with the presence of cryptococossis-related lesions on imaging
- Paired imaging shows that brain swelling is not a common or significant factor in explaining the raised CSF pressure associated with CM
- Subclinical VEP P100 latency prolongation occurs in 56.5% of CM patients
- In patients with impaired vision, abnormal HVF is common (76% right eye, 71% left eye) and the predominant field defects are large blind spots with peripheral field constriction, consistent with raised intracranial pressure.

- VEP P100 latency is a useful screening test of subclinical optic nerve dysfunction. Subclinical HVF abnormalities are minimal and therefore HVF is a poor screening test
- The ADC and MD of the peri-optic CSF space is higher and FA and AI of the peri-optic CSF space is lower than that of the optic nerve
- Laminar rather than turbulent flow exists within the peri-optic CSF space as suggested by an AI of 1.25. The AI of the optic globe is 0.99 suggesting isotropic diffusion and that of the optic nerve is 1.85 indicative of anisotropic diffusion.
- Lower AI of the peri-optic CSF in papilloedema from other causes suggests decreased axial diffusion and perhaps increased turbulent flow. This was not reflected in CM patients with elevated intracranial pressure with papilloedema possibly due to compartmentalization of the peri-optic CSF space from the intracranial space
- Optic nerve diffusion imaging could not draw similarities between CM and papilloedema or between CM and optic neuritis regardless of CSF pressure or vision
- The evidence from the various papers presented suggests that optic neuritis in CM is uncommon and papilloedema does not correlate with visual loss. Raised intracranial pressure is common and visual loss is perhaps due to an optic nerve compartment syndrome.
- The case report documents reversal of peri-optic CSF occlusion by lowering of intracranial pressure and 8 weeks of antifungal therapy is strong evidence for the optic nerve compartment syndrome in CM induced visual loss

CHAPTER 11 CONCLUSION

Optic nerve diffusion imaging and electrophysiological testing of the optic nerve provide good evidence for an optic nerve compartment syndrome as the principal pathogenic mechanism of cryptococcal-induced visual loss. Fungal loading of the peri-optic CSF space cause plugging and blockage of the spaces between the trabeculae, septae and pillars of the subarachnoid space. A steep pressure gradient develops between the high pressure of the intracranial SAS and the peri-optic SAS which results in optic nerve compression, axoplasmic stasis and axonal disruption. Our case report shows this site of compression to be the distal orbital segment of the optic nerve; however the optic canal is another likely site due to its small diameter. Papilloedema is probably a secondary event that develops when axoplasmic stasis reaches the optic nerve head. Optic neuritis develops from a perineuritis or optic nerve extension of the cryptococcal meningo-encephalitis, but is an infrequent occurrence.

We therefore recommend vigilant CSF pressure monitoring early during CM and alleviation of elevated CSF pressure to prevent blindness. Optic nerve sheath fenestration has been shown to be useful but is not readily available in most developing countries and rural areas. Lumbar peritoneal shunts and ventriculoperitoneal shunts are prone to displacement and secondary infection. Serial lumbar puncture while uncomfortable to the patient remains a useful and universally available procedure to decrease CSF pressure in CM.

CHAPTER 12: LIMITATIONS AND FUTURE RESEARCH

Limitations of the Study

1. Patients recruited had to be co-operative for electrophysiological testing and MRI scanning (which took about an hour). Selection bias might have been introduced as comatose patients were excluded.

2. It was not possible to do CSF pressure measurement and MRI scanning on all patients on the same day. However correlations were made between them.

3. Eye and optic nerve movement could not be avoided in all cases between B0 and B1000 diffusion gradients.

4. MRI scanning was done within 2 weeks of treatment commencement which might have influenced imaging features such as cerebral oedema.

5. Even though 14 patients with optic neuritis were recruited, diffusion data could only be analysed in 6 patients due to movement artifact and difficulty in locating the nerve on DWI and DTI.

6. Visual field testing was not done on HIV positive patients without CM for comparison. Such data was relied upon from the literature.

7. Optic nerve tracking was not done at the same time as DWI and DTI but immediately thereafter. The imaging sequences were different and therefore could not be done simultaneously.

Future Research

1. The possibility of the compartment syndrome needs to be explored further. A CT cisternography study comparing the peri-optic CSF filling of contrast loaded CSF in CM patients with normal and elevated CSF pressure needs to be investigated.

2. Study a larger cohort of CM patients using 3T MRI to determine if the higher ADC and reduced FA is verifiable in CM with elevated CSF pressure

3. An Optical Coherence Tomography Study that documents the degree of optic disc oedema in CM patients and follow up during treatment with comparison of CSF pressure. LP's (CSF pressure measurement) and optical coherence tomography can be done pre-treatment, at 4 weeks and at 10 weeks.

4. A long term follow-up study of survivors to determine visual outcome in patients treated with pressure lowering measures and those without.

5. A study to determine the incidence of hearing loss in CM and an MR imaging study of the vestibulo-cochlear nerve.

CHAPTER 13 REFERENCES

1. Park B.J, W.K., Marston BJ, *Estimation of the global burden of cryptococcal meningitis among persons living with HIV/AIDS.* AIDS, 2009. **23**: p. 525-530.
2. Lightowler, J.V., et al., *Treatment of cryptococcal meningitis in KwaZulu-Natal, South Africa.* PLoS One, 2010. **5**(1): p. e8630.
3. Jarvis, J. and G. Meintjes, *Cryptococcal meningitis--a neglected killer.* S Afr Med J, 2011. **101**(4): p. 244-5.
4. Lessells, R.J., et al., *Poor long-term outcomes for cryptococcal meningitis in rural South Africa.* S Afr Med J, 2011. **101**(4): p. 251-2.
5. Graybill, J.R., et al., *Diagnosis and management of increased intracranial pressure in patients with AIDS and cryptococcal meningitis. The NIAID Mycoses Study Group and AIDS Cooperative Treatment Groups.* Clin Infect Dis, 2000. **30**(1): p. 47-54.
6. Moosa, M.Y. and Y.M. Coovadia, *Cryptococcal meningitis in Durban, South Africa: a comparison of clinical features, laboratory findings, and outcome for human immunodeficiency virus (HIV)-positive and HIV-negative patients.* Clin Infect Dis, 1997. **24**(2): p. 131-4.
7. Schirmer, C.M. and T.R. Hedges, 3rd, *Mechanisms of visual loss in papilledema.* Neurosurg Focus, 2007. **23**(5): p. E5.
8. Kestelyn, P. and H. Taelman, *Visual loss and cryptococcal meningitis.* Trans R Soc Trop Med Hyg, 1997. **91**(6): p. 727-8.
9. Seaton, R.A., et al., *Visual loss in immunocompetent patients with Cryptococcus neoformans var. gattii meningitis.* Trans R Soc Trop Med Hyg, 1997. **91**(1): p. 44-9.
10. Rex, J.H., et al., *Catastrophic visual loss due to Cryptococcus neoformans meningitis.* Medicine (Baltimore), 1993. **72**(4): p. 207-24.

11. Seaton, R.A., et al., *The effect of corticosteroids on visual loss in Cryptococcus neoformans var. gattii meningitis.* Trans R Soc Trop Med Hyg, 1997. **91**(1): p. 50-2.

12. Cohen, D.B. and B.J. Glasgow, *Bilateral optic nerve cryptococcosis in sudden blindness in patients with acquired immune deficiency syndrome.* Ophthalmology, 1993. **100**(11): p. 1689-94.

13. Lipson, B.K., et al., *Optic neuropathy associated with cryptococcal arachnoiditis in AIDS patients.* Am J Ophthalmol, 1989. **107**(5): p. 523-7.

14. Ferreira, R.C., G. Phan, and J.B. Bateman, *Favorable visual outcome in cryptococcal meningitis.* Am J Ophthalmol, 1997. **124**(4): p. 558-60.

15. Claus, J.J. and P. Portegies, *Reversible blindness in AIDS-related cryptococcal meningitis.* Clin Neurol Neurosurg, 1998. **100**(1): p. 51-2.

16. Wijewardana, I., et al., *Large volume lumbar punctures in cryptococcal meningitis clear cryptococcal antigen as well as lowering pressure.* J Infect, 2011. **63**(6): p. 484-6.

17. Macsween, K.F., et al., *Lumbar drainage for control of raised cerebrospinal fluid pressure in cryptococcal meningitis: case report and review.* J Infect, 2005. **51**(4): p. e221-4.

18. Milman, T., N. Mirani, and R.E. Turbin, *Optic nerve sheath fenestration in cryptococcal meningitis.* Clin Ophthalmol, 2008. **2**(3): p. 637-9.

19. Loyse, A., et al., *Histopathology of the arachnoid granulations and brain in HIV-associated cryptococcal meningitis: correlation with cerebrospinal fluid pressure.* AIDS, 2010. **24**(3): p. 405-10.

20. Naismith, R.T., et al., *Radial diffusivity in remote optic neuritis discriminates visual outcomes.* Neurology, 2010. **74**(21): p. 1702-10.

21. Hickman, S.J., et al., *Optic nerve diffusion measurement from diffusion-weighted imaging in optic neuritis.* AJNR Am J Neuroradiol, 2005. **26**(4): p. 951-6.

22. Trip, S.A., et al., *Optic nerve diffusion tensor imaging in optic neuritis.* Neuroimage, 2006. **30**(2): p. 498-505.

23. Kolbe, S., et al., *Optic nerve diffusion changes and atrophy jointly predict visual dysfunction after optic neuritis.* Neuroimage, 2009. **45**(3): p. 679-86.

24. Cauquil, C., et al., *Diffusion MRI and tensor tractography in ischemic optic neuropathy.* Acta Neurol Belg, 2012. **112**(2): p. 209-11.

25. Dai, H., et al., *Whole-brain voxel-based analysis of diffusion tensor MRI parameters in patients with primary open angle glaucoma and correlation with clinical glaucoma stage.* Neuroradiology, 2012.

26. Le Bihan, D., *Diffusion/perfusion MR imaging of the brain: from structure to function.* Radiology, 1990. **177**(2): p. 328-9.

27. Mori, S. and P.B. Barker, *Diffusion magnetic resonance imaging: its principle and applications.* Anat Rec, 1999. **257**(3): p. 102-9.

28. Takahashi, M., et al., *Diffusional anisotropy in cranial nerves with maturation: quantitative evaluation with diffusion MR imaging in rats.* Radiology, 2000. **216**(3): p. 881-5.

29. Horsfield, M.A. and D.K. Jones, *Applications of diffusion-weighted and diffusion tensor MRI to white matter diseases - a review.* NMR Biomed, 2002. **15**(7-8): p. 570-7.

30. Ergene, E., et al., *Acute optic neuritis: association with paranasal sinus inflammatory changes on magnetic resonance imaging.* J Neuroimaging, 2000. **10**(4): p. 209-15.

31. Trobe, J.D., *Papilledema: the vexing issues.* J Neuroophthalmol, 2011. **31**(2): p. 175-86.

32. Iwasawa, T., et al., *Diffusion-weighted imaging of the human optic nerve: a new approach to evaluate optic neuritis in multiple sclerosis.* Magn Reson Med, 1997. **38**(3): p. 484-91.

33. Wheeler-Kingshott, C.A., et al., *ADC mapping of the human optic nerve: increased resolution, coverage, and reliability with CSF-suppressed ZOOM-EPI.* Magn Reson Med, 2002. **47**(1): p. 24-31.

34. Chabert, S., et al., *Diffusion tensor imaging of the human optic nerve using a non-CPMG fast spin echo sequence.* J Magn Reson Imaging, 2005. **22**(2): p. 307-10.

35. Bicanic, T., et al., *Antiretroviral roll-out, antifungal roll-back: access to treatment for cryptococcal meningitis.* Lancet Infect Dis, 2005. **5**(9): p. 530-1.

36. Jarvis, J.N. and T.S. Harrison, *HIV-associated cryptococcal meningitis.* AIDS, 2007. **21**(16): p. 2119-29.

37. Perfect, J.R., et al., *Clinical practice guidelines for the management of cryptococcal disease: 2010 update by the infectious diseases society of america.* Clin Infect Dis, 2010. **50**(3): p. 291-322.

38. Saag, M.S., et al., *Practice guidelines for the management of cryptococcal disease. Infectious Diseases Society of America.* Clin Infect Dis, 2000. **30**(4): p. 710-8.

39. van der Horst, C.M., et al., *Treatment of cryptococcal meningitis associated with the acquired immunodeficiency syndrome. National Institute of Allergy and Infectious Diseases Mycoses Study Group and AIDS Clinical Trials Group.* N Engl J Med, 1997. **337**(1): p. 15-21.

40. Chetchotisakd, P., et al., *Rapid Advice Diagnosis, Prevention and Management of Cryptococc al Disease in HIV -infected Adults, Adolescents and Children*, in *WHO Guideline*2011.

41. Gordon, S.B., et al., *Bacterial meningitis in Malawian adults: pneumococcal disease is common, severe, and seasonal.* Clin Infect Dis, 2000. **31**(1): p. 53-7.

42. Bekondi, C., et al., *Primary and opportunistic pathogens associated with meningitis in adults in Bangui, Central African Republic, in relation to human immunodeficiency virus serostatus.* Int J Infect Dis, 2006. **10**(5): p. 387-95.

43. Hakim, J.G., et al., *Impact of HIV infection on meningitis in Harare, Zimbabwe: a prospective study of 406 predominantly adult patients.* AIDS, 2000. **14**(10): p. 1401-7.

44. Okongo, M., et al., *Causes of death in a rural, population-based human immunodeficiency virus type 1 (HIV-1) natural history cohort in Uganda.* Int J Epidemiol, 1998. **27**(4): p. 698-702.

45. Corbett, E.L., et al., *Morbidity and mortality in South African gold miners: impact of untreated disease due to human immunodeficiency virus.* Clin Infect Dis, 2002. **34**(9): p. 1251-8.

46. Schaars, C.F., et al., *Outcome of AIDS-associated cryptococcal meningitis initially treated with 200 mg/day or 400 mg/day of fluconazole.* BMC Infect Dis, 2006. **6**: p. 118.

47. Mwaba, P., et al., *Clinical presentation, natural history, and cumulative death rates of 230 adults with primary cryptococcal meningitis in Zambian AIDS patients treated under local conditions.* Postgrad Med J, 2001. **77**(914): p. 769-73.

48. Charlier, C., et al., *Cryptococcal neuroradiological lesions correlate with severity during cryptococcal meningoencephalitis in HIV-positive patients in the HAART era.* PLoS One, 2008. **3**(4): p. e1950.

49. Moodley, A., et al., *New Insights into the Pathogenesis of Cryptococcal Induced Visual Loss Using Diffusion-Weighted Imaging of the Optic Nerve.* Neuro-ophthalmology, 2012. **36**(5): p. 186-192.

50. Torres, O.H., et al., *Visual loss due to cryptococcal meningitis in AIDS patients.* AIDS, 1999. **13**(4): p. 530-2.

51. Denning, D.W., et al., *Elevated cerebrospinal fluid pressures in patients with cryptococcal meningitis and acquired immunodeficiency syndrome.* Am J Med, 1991. **91**(3): p. 267-72.

52. Bicanic, T., et al., *Relationship of cerebrospinal fluid pressure, fungal burden and outcome in patients with cryptococcal meningitis undergoing serial lumbar punctures.* AIDS, 2009. **23**(6): p. 701-6.

53. Garrity, J.A., et al., *Optic nerve sheath decompression for visual loss in patients with acquired immunodeficiency syndrome and cryptococcal meningitis with papilledema.* Am J Ophthalmol, 1993. **116**(4): p. 472-8.

54. Orem, J., et al., *Feasibility study of serial lumbar puncture and acetazolamide combination in the management of elevated cerebrospinal fluid pressure in AIDS patients with cryptococcal meningitis in Uganda.* Trop Doct, 2005. **35**(1): p. 19-21.

55. Johnston, S.R., et al., *Raised intracranial pressure and visual complications in AIDS patients with cryptococcal meningitis.* J Infect, 1992. **24**(2): p. 185-9.

56. Ng, C.W., M.S. Lam, and N.I. Paton, *Cryptococcal meningitis resulting in irreversible visual impairment in AIDS patients--a report of two cases.* Singapore Med J, 2000. **41**(2): p. 80-2.

57. Petrou, P., et al., *Ventriculoperitoneal shunt for intracranial hypertension in cryptococcal meningitis without hydrocephalus.* J Clin Neurosci, 2012. **19**(8): p. 1175-6.

58. York, J., et al., *Raised intracranial pressure complicating cryptococcal meningitis: immune reconstitution inflammatory syndrome or recurrent cryptococcal disease?* J Infect, 2005. **51**(2): p. 165-71.

59. Chan, K.H., W. Mak, and S.L. Ho, *Cryptococcal meningitis with raised intracranial pressure masquerading as malignant hypertension.* Int J Infect Dis, 2007. **11**(4): p. 366-7.

60. Ofner, S. and R.S. Baker, *Visual loss in cryptococcal meningitis.* J Clin Neuroophthalmol, 1987. **7**(1): p. 45-8.

61. Corti, M., et al., *Sudden blindness due to bilateral optic neuropathy associated with cryptococcal meningitis in an AIDS patient.* Rev Iberoam Micol, 2010. **27**(4): p. 207-9.

62. Hoepelman, A.I., M. Van der Flier, and F.E. Coenjaerts, *Dexamethasone downregulates Cryptococcus neoformans-induced vascular endothelial growth factor production: a role for corticosteroids in cryptococcal meningitis?* J Acquir Immune Defic Syndr, 2004. **37**(3): p. 1431-2.

63. De Schacht, C., et al., *Bilateral blindness after starting highly active antiretroviral treatment in a patient with HIV infection and cryptococcal meningitis.* Acta Clin Belg, 2005. **60**(1): p. 10-2.

64. Cox, J.A., et al., *Autopsy causes of death in HIV-positive individuals in sub-Saharan Africa and correlation with clinical diagnoses.* AIDS Rev, 2010. **12**(4): p. 183-94.

65. Killer, H.E., et al., *Cerebrospinal fluid dynamics between the basal cisterns and the subarachnoid space of the optic nerve in patients with papilloedema.* Br J Ophthalmol, 2011. **95**(6): p. 822-7.

66. Killer, H.E., et al., *Cerebrospinal fluid dynamics between the intracranial and the subarachnoid space of the optic nerve. Is it always bidirectional?* Brain, 2007. **130**(Pt 2): p. 514-20.

67. Killer, H.E., et al., *Architecture of arachnoid trabeculae, pillars, and septa in the subarachnoid space of the human optic nerve: anatomy and clinical considerations.* Br J Ophthalmol, 2003. **87**(6): p. 777-81.

68. Liu, D. and M. Kahn, *Measurement and relationship of subarachnoid pressure of the optic nerve to intracranial pressures in fresh cadavers.* Am J Ophthalmol, 1993. **116**(5): p. 548-56.

69. Killer, H.E., A. Mironov, and J. Flammer, *Optic neuritis with marked distension of the optic nerve sheath due to local fluid congestion.* Br J Ophthalmol, 2003. **87**(2): p. 249.

70. Plant G, A.J., Clarke C, Graham E, Howard R, Shorvon S, *Neurology: A Queen Square Textbook*, ed. H.R. Clarke C, Rossor M, Shorvon S2009: Blackwell Publishing Ltd.

71. Balcer, L.J., et al., *Contrast letter acuity as a visual component for the Multiple Sclerosis Functional Composite.* Neurology, 2003. **61**(10): p. 1367-73.

72. Odom, J.V., et al., *ISCEV standard for clinical visual evoked potentials (2009 update).* Doc Ophthalmol, 2010. **120**(1): p. 111-9.

73. Sample, P.A., et al., *Pattern of early visual field loss in HIV-infected patients.* Arch Ophthalmol, 1999. **117**(6): p. 755-60.

74. Kedar, S., D. Ghate, and J.J. Corbett, *Visual fields in neuro-ophthalmology.* Indian J Ophthalmol, 2011. **59**(2): p. 103-9.

75. Keltner, J.L., et al., *Quality control functions of the Visual Field Reading Center (VFRC) for the Optic Neuritis Treatment Trial (ONTT).* Control Clin Trials, 1993. **14**(2): p. 143-59.

76. Keltner, J.L., et al., *Baseline visual field profile of optic neuritis. The experience of the optic neuritis treatment trial. Optic Neuritis Study Group.* Arch Ophthalmol, 1993. **111**(2): p. 231-4.

77. Barker, G.J., *Technical issues for the study of the optic nerve with MRI.* J Neurol Sci, 2000. **172 Suppl 1**: p. S13-6.

78. Barker, G.J., *Diffusion-weighted imaging of the spinal cord and optic nerve.* J Neurol Sci, 2001. **186 Suppl 1**: p. S45-9.

79. Fatima, Z., et al., *Diffusion-weighted imaging in optic neuritis.* Can Assoc Radiol J, 2013. **64**(1): p. 51-5.

80. Hickman, S.J., *Optic nerve imaging in multiple sclerosis.* J Neuroimaging, 2007. **17 Suppl 1**: p. 42S-45S.

81. Zhang, Y., et al., *Magnetic resonance diffusion tensor imaging and diffusion tensor tractography of human visual pathway.* Int J Ophthalmol, 2012. **5**(4): p. 452-8.

82. Einstein, A., *Investigations on the theory of the brownian movement.*1956, New York, NY: Dover.

83. Hagmann, P., et al., *Understanding diffusion MR imaging techniques: from scalar diffusion-weighted imaging to diffusion tensor imaging and beyond.* Radiographics, 2006. **26 Suppl 1**: p. S205-23.

84. Le Bihan, D., et al., *Diffusion tensor imaging: concepts and applications.* J Magn Reson Imaging, 2001. **13**(4): p. 534-46.

85. Xu, J., et al., *Assessing optic nerve pathology with diffusion MRI: from mouse to human.* NMR Biomed, 2008. **21**(9): p. 928-40.

86. Chen, Z., et al., *Diffusion tensor magnetic resonance imaging reveals visual pathway damage that correlates with clinical severity in glaucoma.* Clin Experiment Ophthalmol, 2013. **41**(1): p. 43-49.

87. Wheeler-Kingshott, C.A., et al., *In vivo diffusion tensor imaging of the human optic nerve: pilot study in normal controls.* Magn Reson Med, 2006. **56**(2): p. 446-51.

88. Stejskal, E.O.T., J.E., *Spin diffusion measurement: Spin echoes in the presence of a time-dependent field gradient.* J. Chem. Phys, 1965. **42**: p. 288-292.

89. Hoorbakht, H. and F. Bagherkashi, *Optic neuritis, its differential diagnosis and management.* Open Ophthalmol J, 2012. **6**: p. 65-72.

90. Fazzone, H.E., D.R. Lefton, and M.J. Kupersmith, *Optic neuritis: correlation of pain and magnetic resonance imaging.* Ophthalmology, 2003. **110**(8): p. 1646-9.

91. Wender, M., *Acute disseminated encephalomyelitis (ADEM).* J Neuroimmunol, 2011. **231**(1-2): p. 92-9.

92. Bradl, M., et al., *Neuromyelitis optica: pathogenicity of patient immunoglobulin in vivo.* Ann Neurol, 2009. **66**(5): p. 630-43.

93. Bradl, M. and D.H. Lassmann, *Anti-aquaporin-4 antibodies in neuromyelitis optica: how to prove their pathogenetic relevance?* Int MS J, 2008. **15**(3): p. 75-8.

94. Park JY, L.I., Song CJ, Hwang HY., *Diffusion MR imaging of postoperative bilateral acute ischemic optic neuropathy.* Korean J Radiol., 2012. **13**(2): p. 237-9.

95. Verma A, J.K., Mohan S, Phadke RV., *Diffusion-weighted MR imaging in posterior ischemic optic neuropathy.* Am J Neuroradiol, 2007. **28**(10): p. 1839-40.

96. Chen, J.S., et al., *Restricted diffusion in bilateral optic nerves and retinas as an indicator of venous ischemia caused by cavernous sinus thrombophlebitis.* AJNR Am J Neuroradiol, 2006. **27**(9): p. 1815-6.

97. Al-Shafai, L.S. and D.J. Mikulis, *Diffusion MR imaging in a case of acute ischemic optic neuropathy.* AJNR Am J Neuroradiol, 2006. **27**(2): p. 255-7.

98. Hui, E.S., et al., *Diffusion tensor MR study of optic nerve degeneration in glaucoma.* Conf Proc IEEE Eng Med Biol Soc, 2007. **2007**: p. 4312-5.

99. Kelman, S.E., et al., *Modified optic nerve decompression in patients with functioning lumboperitoneal shunts and progressive visual loss.* Ophthalmology, 1991. **98**(9): p. 1449-53.

100. Killer, H.E., G.P. Jaggi, and N.R. Miller, *Progressive optic neuropathy in idiopathic intracranial hypertension after optic nerve sheath fenestration.* J Neuroophthalmol, 2010. **30**(2): p. 205.

101. Huna-Baron, R., et al., *Unilateral swollen disc due to increased intracranial pressure.* Neurology, 2001. **56**(11): p. 1588-90.

102. Killer, H.E., et al., *The optic nerve: a new window into cerebrospinal fluid composition?* Brain, 2006. **129**(Pt 4): p. 1027-30.

103. Killer, H.E., G.P. Jaggi, and N.R. Miller, *Optic nerve compartment syndrome.* Acta Ophthalmol, 2011. **89**(5): p. e472; author reply e472-3.

104. Hickman, S.J., et al., *The optic nerve sheath on MRI in acute optic neuritis.* Neuroradiology, 2005. **47**(1): p. 51-5.

105. Killer, H.E., et al., *Cerebrospinal fluid exchange in the optic nerve in normal-tension glaucoma.* Br J Ophthalmol, 2012. **96**(4): p. 544-8.

106. Orgul, S., *Compartment syndrome in the optic nerve: a new hypothesis in the pathogenesis of glaucoma.* Acta Ophthalmol, 2012. **90**(7): p. 686-9.

107. Kerr, N.M., S.S. Chew, and H.V. Danesh-Meyer, *Non-arteritic anterior ischaemic optic neuropathy: a review and update.* J Clin Neurosci, 2009. **16**(8): p. 994-1000.

108. Burde, R.M., *Optic disk risk factors for nonarteritic anterior ischemic optic neuropathy.* Am J Ophthalmol, 1993. **116**(6): p. 759-64.

109. Shen, J.Y., et al., *Intraorbital cerebrospinal fluid outflow and the posterior uveal compartment of the hamster eye.* Cell Tissue Res, 1985. **240**(1): p. 77-87.

110. Killer, H.E., H.R. Laeng, and P. Groscurth, *Lymphatic capillaries in the meninges of the human optic nerve.* J Neuroophthalmol, 1999. **19**(4): p. 222-8.

111. Ludemann, W., et al., *Ultrastructure of the cerebrospinal fluid outflow along the optic nerve into the lymphatic system.* Childs Nerv Syst, 2005. **21**(2): p. 96-103.

112. Naismith, R.T., et al., *Disability in optic neuritis correlates with diffusion tensor-derived directional diffusivities.* Neurology, 2009. **72**(7): p. 589-94.

113. Chen, S.F., et al., *Acute/subacute cerebral infarction (ASCI) in HIV-negative adults with cryptococcal meningoencephalitis (CM): a MRI-based follow-up study and a clinical comparison to HIV-negative CM adults without ASCI.* BMC Neurol, 2011. **11**: p. 12.

114. Siddiqui, A.A., et al., *IFN-gamma at the site of infection determines rate of clearance of infection in cryptococcal meningitis.* J Immunol, 2005. **174**(3): p. 1746-50.

115. Malessa, R., M.W. Agelink, and H.C. Diener, *Dysfunction of visual pathways in HIV-1 infection.* J Neurol Sci, 1995. **130**(1): p. 82-7.

116. Mwanza, J.C., et al., *Neuro-ophthalmological disorders in HIV infected subjects with neurological manifestations.* Br J Ophthalmol, 2004. **88**(11): p. 1455-9.

APPENDIX

A. STUDY PROPOSAL

A Qualitative and Quantitative Magnetic Resonance (MR) Diffusion study investigating the pathogenesis of Cryptococcal induced vision loss

Principal Investigator: Dr AA Moodley
Designation: Consultant Neurologist
Student Number: 853855571
Contact Details: anand.moodley@kznhealth.gov.za
Greys Hospital
Town Bush Road
Pietermaritzburg
Tel. 033 8973298
Fax. 033 8973409

Supervisor: Prof AI Bhigjee
Designation: Head of Neurology
Contact Details: ahmedbhi@ialch.co.za
Dept of Neurology
IALCH
Tel. 031 2402359
Fax. 031 2402358

Co-supervisor: Dr W Rae
Designation: Control Medical Physicist
Contact details: williamrae@ialch.co.za
Dept of Medical Physics
IALCH
Tel. 031 2401877
Fax. 031 2403519

Funding

The study can proceed without immediate funding.
Application for funding will be done in due course.
Funds will be required for

1. Salaries for radiographers (Estimated cost is R8000)
2. Contrast agents (Estimated cost for entire study is R6000)
3. Travelling Costs to Congresses for presentations and training (Estimated cost is R25000)

INTRODUCTION

In South Africa, Cryptococcal meningitis is a common opportunistic infection in severely immunocompromised HIV infected patients. The antiretroviral rollout program has not yet had an impact on the incidence of cryptococcal meningitis due to limited access to ARV rollout sites and restrictions imposed on the number of patients eligible for treatment. Cryptococcal meningitis presents as an AIDS - defining illness in 84% of patients and 50 % of patients present with neurological complications (Moosa YM et al). One such complication is visual loss due to optic nerve disease which is reported in 52.6% of patients with cryptococcal meningitis. Vision loss continues to deteriorate in 17.3% despite antifungal therapy and in 3.7% of patients follows commencement of antifungal therapy (Seaton et al, 1997). So despite antifungal therapy vision may continue to deteriorate and recovery is unpredictable. Early and effective adjunctive therapy is therefore of paramount importance to prevent or reverse the frequent and sometimes catastrophic loss of vision.

Appropriate interventional therapy can only be identified once the pathophysiology of vision loss in cryptococcal meningitis is well understood. Unfortunately, there are conflicting reports regarding its pathophysiology and standard treatment protocols are disappointingly lacking.

An inflammatory (optic neuritis) model is supported by visual improvement with corticosteroid therapy in cryptococcal induced vision loss (Seaton RA et al), the demonstration of active inflammation and necrosis of the optic nerve without vascular infiltration but florid infiltration of the surrounding meninges by the cryptococcal organism (Cohen DB, 1993) and centrocaecal scotomata on visual field testing (Lipson BK et al). On the other hand, a raised intracranial pressure (papilloedema) model is suggested by the beneficial response to serial lumbar punctures, ventriculoperitoneal shunts and lumbar

peritoneal shunts on cryptococcal induced vision loss (Ferreira RC et al 1997, Clauss JJ 1998) and the accompanying constricted visual fields and enlarged blind spot in these patients.

The mechanism by which patients with cryptococcal meningitis develop visual loss continues to be unclear with anecdotal evidence supporting opposing theories of papilloedema and optic neuritis. These theories may not be mutually exclusive and a mechanism that incorporates both theories is also conceivable. Pathological studies and *in vitro* studies (rat optic nerve) are scanty and can be misleading due to the loss of the effects of raised pressure on the optic nerves post mortem. An *in vivo* study that investigates the pathogenesis of optic nerve dysfunction in cryptococcal induced visual loss is therefore necessary.

Diffusion weighted imaging (DWI) of the optic nerve has been shown to be of benefit in differentiating acute from chronic neuritis in Multiple Sclerosis (Iwasawa T, 1997, Wheeler-Kingshott, 2002). Apparent diffusion coefficient (ADC) values are obtainable on normal optic nerves and can be compared to pathological conditions. Qualitative mapping and quantitative data can be obtained on diffusion imaging. Diffusion of protons within optic nerves is anisotropic due to the orientation of fibres. Hence diffusion that occurs parallel to the axons is greater than that which occurs perpendicular. This parallel to perpendicular ratio is disrupted in the presence of inflammation and demyelination and becomes less anisotropic or more isotropic. The demonstration of anisotropic diffusion is achieved with DWI obtained separately in orthogonal directions or by Diffusion tensor imaging (DTI).
ADC values from DWI can be obtained in different orthogonal directions and compared. Such comparison will allow for an evaluation of the degree of anisotropic diffusion. Fractional Anisotropy obtained from DTI also provides a quantitative assessment of anisotropic diffusion. Comparative assessments of anisotropy as established by DWI and DTI can be done between patients with cryptococcal induced visual loss and control subjects.

In optic neuritis, there is perivascular lymphocytic infiltration, multifocal demyelination, and reactive astrocytosis (Ergene E, 2004). Iwasawa T et al have demonstrated decreased diffusion in acutely inflamed optic nerves with reduced ADC values but no comparisons were made between perpendicular and parallel diffusion. One may hypothesize a similar diffusion abnormality of the optic nerves in cryptococcal induced visual loss if the predominant disorder is optic nerve infiltration. In the optic neuritis model, the ADC values along the parallel plane will be decreased and Fractional Anisotropy values will also be reduced due to the presence of inflammatory cells and fungi. One may also expect a decrease in the parallel to perpendicular diffusion ratios and Fractional Anisotropy should decrease due to greater isotropic diffusion.

In papilloedema from any cause of elevated intracranial pressure, disc swelling results from axoplasmic flow stasis. There is entrapment of the optic nerve axons at the lamina cribrosa due to elevated intracranial pressure transmitted along the subarachnoid space to the junction of the globe and retrobulbar optic nerve. Axoplasm and metabolic products accumulate at the optic disc resulting in hyperaemia and elevation of the disc. The retrobulbar optic nerve is structurally normal in papilloedema but little is known about its functional status. In any liquid medium, diffusion of molecules is dependent on the thermal energy of the medium. When thermal energy increases, there is increased kinetic energy and increased diffusion of molecules. Therefore one may speculate that the effect of elevated pressure on the optic nerve as occurs in papilloedema, will result in increased thermal motion of the water molecules and

therefore increased diffusion. Higher ADC values will occur in both the parallel and perpendicular directions. The ratio of parallel to perpendicular diffusion should be maintained since diffusion will be increased in both planes. One may also speculate that the Fractional Anisotropy of diffusion along the optic nerve should be unchanged.

Hence, DWI and DTI could theoretically be useful measuring instruments to differentiate between the effects of raised pressure and infiltration on optic nerve functioning. The possibility of dual mechanisms will also be entertained and explored.

The aim of the study is to investigate the pathogenesis of cryptococcal induced visual loss by the use of DWI *in vivo.* The initial goal will be to clinically and electrophysiologically describe visual loss in patients with cryptococcal meningitis. Concurrently, the techniques of Diffusion and Diffusion Tensor imaging of the optic nerve will be optimized and made reproducible for reliable testing of subjects and controls. Techniques that have already been employed (Iwasawa T 1997, Wheeler-Kingshott 2002) will need modification to accommodate the restricted resources available and imaging of mildly confused patients. The modifiable parameters that will be considered are movement artifact, fat suppression, fluid attenuation, 'b' values etc to optimize signal to noise ratio (SNR).

Comparisons will be made to normal controls, patients without visual loss, and to patients with pathophysiologically established causes of papilloedema and optic neuritis. Such comparisons will support either a papilloedema or optic neuritis model. The benefit of such information will be realized in guiding appropriate treatment strategies to either lower intracranial pressure or institute anti-inflammatory therapy on an empirical basis.

References

Clauss JJ, Portegies P. Reversible blindness in AIDS-related cryptococcal meningitis. Clin Neurol Neurosurg. 1998 Mar; 100(1):51-2.

Cohen DB, Glasgow BJ. Bilateral optic nerve cryptococcosis in sudden blindness in patients with acquired immune deficiency syndrome. Ophthalmology.1993 Nov;100(11):1689-94.

Ergene E, Rupp FW, Qualls CR, Ford CC. Acute optic neuritis. Association with paranasal sinus inflammatory changes on magnetic resonance imaging. J Neuroimaging 2000 Oct; 10(4): 209-15

Ferreira RC, Phan G, Bateman JB. Favorable visual outcome in cryptococcal meningitis. Am J Ophthalmol. 1997 Oct;124(4):558-60.

Iwasawa T, Matoba H, Ogi A, Kurihara H, Saito K, Yoshida T, Matsubara S, Nozaki

A. Diffusion–Weighted Imaging of the Human Optic Nerve: A New Approach to Evaluate Optic Neuritis in Multiple Sclerosis. Magn Reson Med. 1997 Sep; 38(3)484-91

Lipson BK, Freeman WR, Beniz J, Goldbaum MH, Hesselink JR, Weinreb RN, Sadun AA. Optic Neuropathy associated with cryptococcal arachnoiditis in AIDS patients. Am J Ophthalmol. 1989 May 15;107(5):523-7.

Moosa MY, Coovadia YM. Cryptococococcal meningitis in Durban, South Africa: a comparison of clinical features, laboratory findings, and outcome for human immunodeficiency virus (HIV) – positive and HIV – negative patients. Clin Infect Dis. 1997 Feb; 24(2):131-4.

Seaton RA, Verma N, Naraqi S, Wembri JP, Warrell DA. Visual loss in immunocompetent patients with Cryptococcal neoformans var. gatti meningitis. Trans R Soc Trop Med Hyg. 1997 Nov-Dec;91(6)727-8.

Wheeler-Kingshott CAM, Parker GJM, Symms MR, Hickman SJ, Tofts PS, Miller DH, Barker GJ. ADC Mapping of the Human Optic Nerve: Increased Resolution, Coverage, and Reliability with CSF-Suppressed ZOOM-EPI. Magn Reson Med. 2002 47: 24-31

AIMS

1. To clinically, electrophysiologically and biochemically describe optic nerve dysfunction in cryptococcal induced visual loss according to
    - 1.1 Frequency of visual disturbance
    - 1.2 Severity of visual disturbance
    - 1.3 Mode of onset of vision loss
    - 1.4 Relationship to degree of immunopsuppression and treatment
    - 1.5 CSF findings

2. To optimise Diffusion-weighted (DWI) and Diffusion tensor (DTI) imaging of the optic nerve and thereby obtain standard and reproducible imaging protocols.

3. To devise a mathematical model that separates optic nerve diffusion from surrounding CSF diffusion within the optic nerve sheath.

4. To propose a probable pathogenesis of Cryptococcal induced visual loss by investigating and comparing the following

Quantitative DWI and DTI of the optic nerves in patients with cryptococcal induced visual loss, using protocols obtained in Aims 2 and 3 above and comparing to normal controls.

Comparison of routine FSE, DWI and DTI of the optic nerves in patients with cryptococcal meningitis stratified into 2 groups with normal and abnormal visual acuity.

.

Comparison of FSE, DWI and DTI of the optic nerves in patients with cryptococcal induced visual loss, to patients with papilloedema (IIH, malignant HPT and RICP) and optic neuritis i.e. optic nerve disorders secondary to elevated CSF pressure and infiltration respectively.

Method

Informed consent will be obtained from all patients and controls included in the study. Patients will be recruited from Grey's Hospital, Edendale Hospital and Northdale Hospital. Prior ethics approval will be obtained from the University of Kwazulu Natal and support obtained from management and clinician heads at the above institutions as well as approval from the Department of Research and Knowledge Management, Kwazulu-Natal Department of Health

Aim 1

Sequentially select 100 patients with cryptococcal meningitis and normal mental state.
Conduct the following tests on these patients;
Visual Acuity testing
Visual Field testing
Fundal photography
Visual evoked potentials
Neurological Examination including pupillary reflexes
CD4 count and Viral load
CSF examination- MCCS, India Ink, Cryptococcal antigen, FTA, Cysticercosis Elisa, CSF opening pressure. These tests will be performed as routine investigations on patients. Patients will be excluded if these tests were not done as standard management.
FBC, U&E, LFT, BG and HIV

Aim 2

Perform the following MRI tests on 20 normal controls;

2.1 FSE of the optic nerves, pre and post contrast on coronal and axial planes
2.2 High resolution T2 W of optic nerve and measure optic nerve sheath diameter
2.3 DWI of the optic nerves on axial and coronal planes.
ADC values obtained at 3 sites along the Nerve and its surrounding CSF.
2.4 Three ‘ b values’ will be used and ADC values obtained in 6 directions
2.5 ADC values will be obtained from the basal cisterns and optic chiasma on both the axial and coronal planes

Aim 3

3.1 Devise a mathematical model using values obtained in 2.3, 2.4 and 2.5

Aim 4

Perform the following on 20 patients with cryptococcal meningitis without vision loss and 20 patients with vision loss;

4.1 FSE of the optic nerves, pre and post contrast on axial and coronal planes
4.2 High resolution T2 W axial imaging of the optic nerves and measure optic nerve sheath diameter

4.2 DWI and DTI of the optic nerves, optic chiasma and basal cisterns on axial and coronal planes. Obtain ADC values as previously outlined.

Perform the following on 10 patients with papilloedema and 10 patients with optic neuritis from any cause excluding cryptococcal meningitis,

4.3 FSE of the optic nerves, pre and post contrast on axial and coronal planes
4.4 High resolution T2 W axial imaging of the optic nerves and measure optic nerve sheath diameter.
4.5 DWI and DTI of the optic nerves, optic chiasma and basal cisterns on axial and coronal planes. Obtain ADC values as previously outlined

B. RESEARCH ETHICS APPROVAL

UNIVERSITY OF
KWAZULU-NATAL

Research Office
BIOMEDICAL RESEARCH ETHICS ADMINISTRATION
Nelson R Mandela School of Medicine
Private Bag 7, Congella 4013
KwaZulu-Natal, SOUTH AFRICA
Tel: 27 31 2604769
Fax: 27 31 2604609
Email: buccas@ukzn.ac.za
Website: www.ukzn.ac.za

27 September 2006

Dr A A Moodley
Dept of Neurology
Grey's Hospital
Private Bag X9001
Pietermaritzburg 3200

Dear Dr Moodley

PROTOCOL: A Qualitative and Quantitative Magnetic Resonance (MR) Diffusion study investigating the pathogenesis of Cryptococcal induced vision loss. Dr A A Moodley, Neurology. Ref: H100/06

The Biomedical Research Ethics Committee considered the abovementioned application and the protocol was approved at its meeting held on 15 August 2006 pending appropriate responses to queries raised. These conditions have now been met and the study is given full ethics approval and may begin as at **27 September 2006**.

This approval is valid for one year from **27 September 2006.** To ensure continuous approval, an application for recertification should be submitted a couple of months before the expiry date. In addition, when consent is a requirement, the consent process will need to be repeated annually.

I take this opportunity to wish you everything of the best with your study. Please send the Biomedical Research Ethics Committee a copy of your report once completed.

Yours sincerely

DR J MOODLEY
Chair: Biomedical Research Ethics Committee

UNIVERSITY OF
KWAZULU-NATAL

RESEARCH OFFICE
Biomedical Research Ethics Administration
Westville Campus, Govan Mbeki Building
Private Bag X 54001
Durban
4000
KwaZulu-Natal, SOUTH AFRICA
Tel: 27 31 2604769 - Fax: 27 31 2604609
Email: BREC@ukzn.ac.za
Website: http://research.ukzn.ac.za/ResearchEthics/BiomedicalResearchEthics.aspx

16 July 2010

Dr A A Moodley
Dept of Neurology
Grey's Hospital
Private Bag X9001
Pietermaritzburg, 3200

Dear Dr Moodley

PROTOCOL: A Qualitative and Quantitative Magnetic Resonance (MR) Diffusion study investigating the pathogenesis of Cryptococcal induced vision loss. Dr A A Moodley, Neurology. Ref: H100/06

RECERTIFICATION APPLICATION APPROVAL NOTICE

Approved:	27 September 2010
Expiration of Ethical Approval:	26 September 2011

I wish to advise you that your application for Recertification dated 01June 2010 for the above protocol has been noted and approved by a sub-committee of the Biomedical Research Ethics Committee (BREC) for another approval period. The start and end dates of this period are indicated above. The Lapsed recertification 2007-2008, 2008-2009 and 2009-2010 is condoned. Kindly ensure that recertification requests are submitted timorously in future.

If any modifications or adverse events occur in the project before your next scheduled review, you must submit them to BREC for review. Except in emergency situations, no change to the protocol may be implemented until you have received written BREC approval for the change.

The approval will be **ratified** by a full sitting of the Committee at a meeting to be held on **10 August 2010.**

Yours sincerely

Mrs A Marimuthu
Senior Administrator: Biomedical Research Ethics

UNIVERSITY OF
KWAZULU-NATAL
INYUVESI
YAKWAZULU-NATALI

RESEARCH OFFICE
Biomedical Research Ethics Administration
Westville Campus, Govan Mbeki Building
Private Bag X 54001
Durban
4000
KwaZulu-Natal, SOUTH AFRICA
Tel: 27 31 2604769 - Fax: 27 31 2604609
Email: BREC@ukzn.ac.za
Website: http://research.ukzn.ac.za/ResearchEthics/BiomedicalResearchEthics.aspx

29 September 2011

Dr A A Moodley
Dept of Neurology
Grey's Hospital
Private Bag X9001
Pietermaritzburg, 3200

Dear Dr Moodley

PROTOCOL: A Qualitative and Quantitative Magnetic Resonance (MR) Diffusion study investigating the pathogenesis of Cryptococcal induced vision loss. Dr A A Moodley, Neurology. Ref: H100/06

RECERTIFICATION APPLICATION APPROVAL NOTICE

Approved:	27 September 2011
Expiration of Ethical Approval:	26 September 2012

I wish to advise you that your application for Recertification received on 07 September 2011for the above protocol has been noted and approved by a sub-committee of the Biomedical Research Ethics Committee (BREC) for another approval period. The start and end dates of this period are indicated above.

If any modifications or adverse events occur in the project before your next scheduled review, you must submit them to BREC for review. Except in emergency situations, no change to the protocol may be implemented until you have received written BREC approval for the change.

This approval will be **ratified** by a full Committee at its next meeting taking place on **08 November 2011.**

Yours sincerely

Mrs A Marimuthu
Senior Administrator: Biomedical Research Ethics